ERDC/EL TR-09-21

US Army Corps of Engineers®
Engineer Research and Development Center

Preconstruction Biogeochemical Analysis of Mercury in Wetlands Bordering the Hamilton Army Airfield (HAAF) Wetlands Restoration Site

Part 3

E. P. H. Best, H. L. Fredrickson, H. Hintelmann, O. Clarisse, B. Dimock, G. R. Lotufo, W. A. Boyd, and G. A. Kiker

December 2009

Environmental Laboratory

ERDC/EL TR-09-21
December 2009

Preconstruction Biogeochemical Analysis of Mercury in Wetlands Bordering the Hamilton Army Airfield (HAAF) Wetlands Restoration Site

Part 3

Elly P. H. Best, Gui R. Lotufo, and William A. Boyd

Environmental Laboratory
U.S. Army Engineer Research and Development Center
3909 Halls Ferry Road
Vicksburg, MS 39180-6199

Holger Hintelmann, Olivier Clarisse, and Brian Dimock

Trent University
1600 West Bank Drive
Peterborough, ON K9J 7B8, Canada

Herbert L. Fredrickson

U.S. Environmental Protection Agency
National Risk Management Research Laboratory
26 West Martin Luther King Boulevard
Cincinnati, OH 45268

Gregory A. Kiker

University of Florida
Agricultural and Biological Engineering Department
PO Box 110570
Gainesville, FL 32611

Final report

Prepared for U.S. Army Engineer District, San Francisco
1455 Market Street, San Francisco, CA 94103-1398

Monitored by U.S. Army Engineer Research and Development Center
3909 Halls Ferry Road, Vicksburg, MS 39180-6199

Abstract: The U.S. Army Corps of Engineers (USACE) is working to reconstruct wetlands at the former Hamilton Army Airfield (HAAF) on San Pablo Bay (SPB). This 203-ha site will provide tidal habitat to endangered species such as the clapper rail and the saltmarsh harvest mouse. Means to mitigate MeHg magnification in bay aquatic food webs are needed not only for HAAF but for other Bay restoration sites as well. This interim technical report describes studies primarily performed in 2006.

A field study was conducted in San Pablo Bay focusing on site-specific rates of mercury methylation and demethylation, and biogeochemical parameters related to the mercury cycle as measured by both conventional and emerging methods, including Diffusive Gradient in Thin Film (DGT) and Diffusional Equilibration in Thin Film (DET) techniques. Experiments on MeHg accumulation by clams, fish, and DGTs were conducted under laboratory conditions to test the ability of the DGT technique to mimic MeHg bioaccumulation.

The multiple source mixing models SOURCE and STEP were used to quantify food web sources and trophic structure using multiple stable isotopes, and, thus, contribute to elucidating the trophic relationships leading to MeHg bioaccumulation. Use of these models showed that macrophytic primary producers of the salt marsh formed important food sources of consumers. Consumers in the nearshore bay were found to be largely benthivorous and fed partly on higher plant fragments and/or bay-POM, of which the relative contributions decreased with increasing trophic level.

The Questions and Decisions ™ (QnD) screening model system was developed as a framework to evaluate consequences of wetland restoration for MeHg emissions at the former Hamilton Army Air Field (HAAF).

A data gap exists on food chain structure, components, bioaugmentation mechanisms and MeHg accumulated in the biota associated with San Francisco Bay wetlands. Additional field, experimental, and modeling research was recommended to decrease the uncertainty of these early model outcomes.

Contents

Figures and Tables

Figures

Tables

Preface

The work reported herein was conducted by the Environmental Laboratory (EL) of the U.S. Army Engineer Research and Development Center (ERDC), Vicksburg, MS.

With funding from the Long Term Management Strategy research staff from the U.S. Army Corps of Engineers (USACE) ERDC-Vicksburg is working with the San Francisco Basin Regional Water Board, the California State Coastal Conservancy, and the San Francisco Bay Conservation and Development Commission to reconstruct wetlands at the former Hamilton Army Airfield (HAAF).

In March 2003, the U.S. Army Engineer District, San Francisco, requested that EL expand pre-construction monitoring of total mercury and methylmercury concentrations in sediments and soils of existing wetlands bordering the Hamilton Army Airfield (HAAF) Wetlands Restoration Site on San Pablo Bay, California. The purpose of the expanded activities was to gain site-specific knowledge of the geochemical/geophysical, microbial, and predominant plant- and animal-related interactions that affect the stabilization and mobilization of mercury and methylmercury in the sediments and soils of the area. Exploratory research data from 2003 resulted in a first-generation site-specific screening-level model created for estimating mercury and methylmercury mobility during wetlands reconstruction. Follow-up research in 2004-05 encompassed descriptions of (1) site-specific rates of methylation and demethylation, as well as characterizations of sedimentary microbial communities; (2) mercury dynamics in decomposing plant litter; (3) mercury dynamics in food webs; and (4) bioavailability of sediment-associated mercury to macrobenthos. In addition, in 2005 a new Diffusive Gradient in Thin Film (DGT) method for measuring and monitoring mercury cycle-related biogeochemical parameters in marshes was developed, and the role of marsh vegetation as a vector in mercury species transport was quantified.

The current report describes information generated primarily during 2006. Work during this period focused on

1. Site-specific rates of methylation and demethylation and mercury cycle related biogeochemical parameters measured by conventional methods and DGT and Diffusional Equilibration in Thin Film (DET) techniques.
2. A comparison between accumulation of water- and sediment-associated mercury in clams, fish, and DGT.
3. Exploring food web sources and pathways using multi-source mixing models.
4. Recalibration of a screening-level model integrating physical, chemical, and biological processes that drive mercury cycling in San Pablo Bay salt marshes.

The project leader of this work was Dr. Herbert L. Fredrickson, (U.S. Environmental Protection Agency, Cincinnati, OH), formerly of the Environmental Processes Branch (EPB), Environmental Processes and Engineering Division (EPED), Environmental Laboratory (EL). The multidisciplinary team was composed of multiple principal investigators. Dr. Holger Hintelmann, Dr. Olivier Clarisse, and Dr. Brian Dimock (Trent University, Department of Chemistry, Peterborough, Ontario, Canada); Dr. Elly P. H. Best (Environmental Risk Assessment Branch, EL); and Dr. Fredrickson conducted the work on mercury cycle-related dynamics in wetland sediments of San Pablo Bay. Dr. Clarisse, Dr. Gui R. Lotufo (EL), and Dr. Best conducted the study on comparing accumulation of water- and sediment-associated mercury species in bioassays and DGT. Dr. Best and W. A. Boyd (EPB), conducted the multi-source mixing model application to the China Camp food webs. Dr. Best, W. A. Boyd, and Dr. Gregory A. Kiker (University of Florida, Agricultural and Biological Engineering Department, Gainesville, FL) conducted the expansion and recalibration of the screening-level model.

The authors gratefully acknowledge the help provided by Dr. Susan Lubetkin, University of Washington, Quantitative Ecology and Resource Management, Seattle, WA, by running the multi-source mixing models originally developed by her.

The authors gratefully acknowledge the external reviews by staff at the San Francisco Estuary Institute, Oakland, CA.

Special thanks go to the following Corps of Engineers personnel who gave generously of their time and expertise to review the drafts of this report: Drs. Mark Chappell, John Nestler, Anthony Bednar, and David Smith.

This study was conducted under the general supervision of Dr. Robert P. Jones, Chief Ad Interim ERAB; Dr. Richard E. Price, Chief, EPED; Dr. Mike Passmore, Deputy Director, EL; and Dr. Beth Fleming, Director, EL.

COL Gary E. Johnston was Commander and Executive Director of ERDC. Dr. James R. Houston was Director.

1 Report Summary

Over 90% of the wetlands bordering San Francisco Bay were lost between 1850 and 1990 (U.S. Geological Survey (USGS) 2002); 80% between 1800 and 1988 according to Valiela et al. (2004). Habitats for wildlife and fish species are being threatened and coastal shore erosion mitigation is greatly diminished due to human activities and, possibly, sea level rise. Long-term goals for San Francisco Bay development, formulated in a report of habitat recommendations by the San Francisco Bay Area Habitat Ecosystem Goals Project, include extensive wetland restoration. The tidal marshes bordering San Francisco Bay are to be increased from 16,200 ha in 1999 to 42,525 ha by the year 2055 (Goals Project 1999). Dikes currently protect most of the areas targeted for restoration. Drying and oxidation of the soils on the landward side of the dikes have resulted in subsidence such that current soil elevations are often meters below the mean tide level. Simply breaching the dikes would result in lakes, not wetlands. Considerable amounts of fill material are required to raise the elevation of subsided areas to a level that would support aquatic macrophytes that would in turn trap sediments required to sustain the elevation of the wetland. Sediments derived from operations and maintenance of navigation channels in the San Francisco Bay could be used for this purpose. This beneficial use of locally dredged sediment would reduce the cost of obtaining other fill material or transporting the material to more distant disposal sites.

The elevated levels of mercury (Hg) currently present in the San Francisco Bay fishery constrain environmental management. The San Francisco Bay watershed is impacted by the legacy of mercury mines in the coastal range and placer style gold mining in parts of the Sierra Nevada watershed. Wetlands, particularly tidal wetlands, are recognized for their potential to convert mercury into monomethylmercury (CH_3Hg^+). Monomethylmercury is referred to as methylmercury (MeHg) in this report. MeHg is a potent toxin that efficiently biomagnifies in many aquatic food webs.

In this context, the immediate concern of the U.S. Army Corps of Engineers (USACE) focuses on the use of mercury containing dredged material for the restoration of wetlands. The larger environmental issue is the contribution of San Francisco Bay salt marshes to mercury

contamination in the San Francisco Bay fishery, regardless of the source of the mercury. For example, wetland restoration at the Hamilton Army Airfield (HAAF) site will require approximately 8.1 million m^3 of dredged material to attain an elevation of approximately 0.5 ft above mean sea level where the marsh macrophyte *Spartina foliosa* would colonize. The first 1.6 to 1.9 million m^3 of material came from the Oakland Harbor Navigation Improvement Project, was deposited in the HAAF site from spring 2006 onwards, and does not contain elevated mercury levels. Additional material will come from efforts to maintain existing shipping channels in San Francisco Bay, is expected to be in place by 2014, and may contain Hg levels typical of that found in the majority of San Francisco Bay sediment (300 ng g^{-1} dry weight, with MeHg typically being 1% of THg; Beijer and Jernelow 1979; Best et al. 2005, 2007; Regional Monitoring Program (RMP) 2006). HAAF represents only 203 ha of the additional 26,325 ha of wetlands to be established around the bay between 2005 and 2055. Means to mitigate MeHg magnification in bay aquatic food webs are needed not only for HAAF but other Bay restoration sites as well. Those means are currently unknown.

Most of the work in this interim report was designed to address consensus technical questions formulated at the CALFED Stakeholders' Workshop on Mercury in San Francisco Bay, held 8–9 October 2002 at Moss Landing Marine Laboratories (Wiener et al. 2003). These included the following:

- What are the present levels of MeHg in SF Bay wetlands with respect to biota, sub-habitats, and location within the Bay?
- What are the rates of MeHg production?
- What factors control MeHg production? Can these be managed?
- Are some wetlands larger mercury exporters than others?
- Can we model/predict the effects of wetland restoration on MeHg production and export?

In partial response to these questions, and building on prior research, the following 2005/2006 data were collected and analyzed in four major studies and presented in the current annual report.

A site map is provided in Figure 1-1.

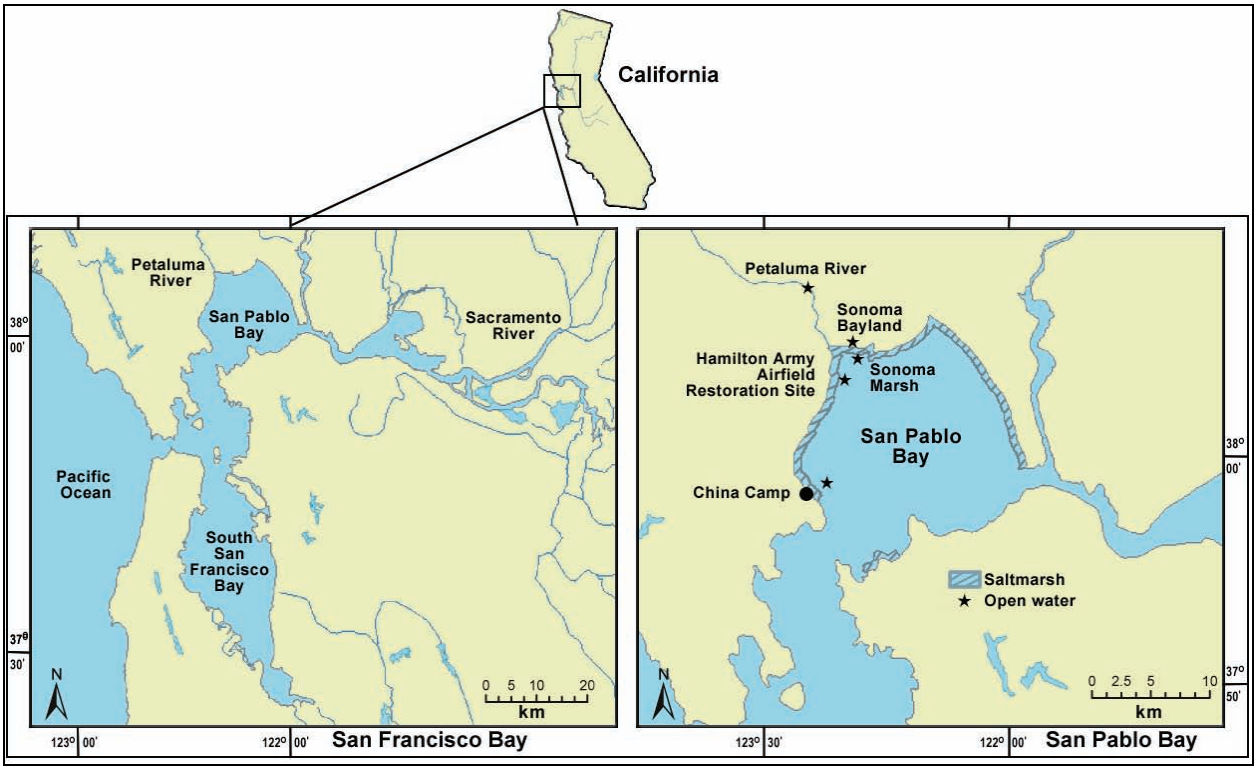

Figure 1-1. Location of San Pablo Bay within San Francisco Bay (left) and location of the Hamilton Army Airfield Restoration Site, China Camp reference, and other sites (right).

A field study was conducted in San Pablo Bay in July 2006 focusing on site-specific rates of mercury methylation and demethylation, and biogeochemical parameters related to the mercury cycle as measured by both conventional and emerging methods, including Diffusive Gradient in Thin Film (DGT) and Diffusional Equilibration in Thin Film (DET) techniques. Three tidal sites were included in the present study: the Hamilton Army Airfield (HAAF) restoration site, the China Camp State Park (CC; as a reference) and an upstream site in the Petaluma River (PR) with lower salinity than both other sites. A new strategy was developed to determine the net methylation profile with sediment depth at a far higher (cm) resolution than used before. This was expected to enable the calculation of MeHg diffusion from sediment, by which process a large part of the newly produced MeHg may become accessible to local and regional food webs. Net MeHg production is the result of methylation and demethylation rates in the sediment. In the present study, average net methylation rates of 1.3 (±0.5) and 0.7 (±0.3) ng g^{-1} DW d^{-1} were found in CC and HAAF sediments, which did not significantly differ from the rates measured previously (Best et al. 2005; 2007). The net methylation rate was greatest in PR sediment at 3.3 (± 2.2) ng g^{-1} DW d^{-1}, with a lower salinity and corresponding sulfate concentration. The MeHg profiles of CC and HAAF sediments

showed almost no concentration gradient, indicating that the diffusive MeHg flux from these sediments is expected to be close to zero. In contrast, MeHg production was greatest in the upper sediment layer at the PR site, favoring MeHg export from the sediment to the overlying water. A positive, linear, relationship between net methylation rate and MeHg concentration measured by DGT was found, which explained 79% of the variability in the data set. The latter illustrated that methylation, a biogeochemical process, strongly affected the quantity of MeHg accumulated by the DGT device in the sediment, and suggested that DGT measurements can be used to predict net methylation rates. DGT in contact with sediment mimics the main mechanism of metal uptake by organisms by lowering the concentration locally, which induces a diffusive supply and a release of metal from the solid phase. In the case of MeHg, DGT measurements also reflected the methylation process, which generates new MeHg. Therefore, the DGT device is a promising tool for assessing exposure of organisms to MeHg in sediments, as it provides an integrated value of all reactions involved in Hg biogeochemical cycling.

Experiments on MeHg uptake in clams and fish were conducted under laboratory conditions. These experiments had the objective to test the ability of the DGT technique to mimic MeHg bioaccumulation by a clam (*Macoma balthica,* Baltic clam) and a fish (*Cyprinodon variegatus,* sheepshead minnow), and, thus, provide the basis for application of the DGT device as a sentinel for monitoring bioavailable MeHg. The bioavailability of MeHg species was determined by measuring the uptake kinetics of stable MeHg isotopes in organisms and DGTs in time-series exposures. A novel double labelling technique was used whereby ^{199}Hg enriched MeHg was added to the water, while fish food was amended with ^{202}Hg enriched MeHg. By following these two tracers into the sentinels, the relative importance of MeHg uptake from water versus uptake through food could be established. Accumulation of MeHg from water by clams and DGTs was strongly correlated. MeHg accumulation was affected by changes in salinity and MeHg speciation equally in clams and DGTs. Both clams and DGTs can, therefore, be used to gauge MeHg exposure from water. A large part of the Hg burden in fish is methylated and thought to accumulate primarily from dietary sources, but direct accumulation from water can also contribute. In the fish experiment, both MeHg uptake routes were considered and investigated using two different MeHg isotopic tracers and environmentally relevant exposure concentrations. Over 97% of the MeHg accumulated in fish was attributed to food and 3% to water.

Accumulation of MeHg by fish and DGTs was strongly correlated for both MeHg isotopic tracers, which was attributed partly to the leaching of MeHg from food into water. Thus, DGTs can also mimic direct MeHg accumulation from water by fish. However, in the field the MeHg available in food depends on the local food web, and, therefore, the relative contributions of MeHg from food and from water may vary considerably with site.

The companion multiple source mixing models SOURCE and STEP were used to quantify food web sources and trophic structure using multiple stable isotopes, and, thus, contribute to elucidating the trophic relationships leading to MeHg bioaccumulation. The models were used with site-specific isotopic tracer values of primary producers and consumers relating to the China Camp salt marsh associated food web(s), to estimate fractional ranges of contributing food sources. Both models follow a mathematically simple first order approach. SOURCE estimates the mixture of autotrophic sources that have been assimilated, directly or indirectly, into a consumer's tissues and the consumer's trophic level. STEP estimates the mixture of autotrophic and heterotrophic sources that have been assimilated into a consumer's tissues and the consumer's trophic level. Based on their isotopic nearest neighbor distances, the producers were categorized in nine groups and the consumers in eight groups. SOURCE estimates, based on all three isotopes, indicated contributions to consumer diets > 5% of the producer groups: bay-POM, marsh-POM, *S. foliosa*+litter, *S. virginica*+litter, marsh-microalgae, marsh filamentous algae+*D. spicata*, and bay macroalgae. STEP characterized higher order consumers as directly consuming a smaller percentage of primary producers than lower order consumers, and included an increased number of potential food sources. STEP was used to estimate food source contributions to the consumers using all three isotopes, and to calculate the trophic levels. Based on STEP estimates and natural history information, a food web diagram was constructed for the China Camp salt marsh and adjacent San Pablo Bay area. Three main points became apparent:

- Macrophytic primary producers of the salt marsh formed important food sources of consumers: live plants were most important on the high marsh and dead plants contributed to the DOM pools in the nearshore bay.
- The bay-POM pool was likely dominated by detritus originating from marsh macrophytes, because bay phytoplankton production is low.

- Consumers in the nearshore bay were largely benthivorous and fed partly on higher plant fragments and/or bay-POM, of which the relative contributions decreased with increasing trophic level.

Higher order consumers were relatively more carnivorous than lower order consumers. The goby showed a considerable tendency to consume its own species. An evaluation of MeHg accumulation in consumers with the greatest MeHg levels following the pathways identified by this food web analysis suggested that consumption of amphipods, seeds from higher plants such as *S. virginica*, and consumption of selected higher trophic level organisms (shore crab, Baltic clam, Asian clam, shrimp, goby) may contribute the most, while the central role of detritus-associated MeHg has to be further explored.

The *Questions and Decisions* ™ (QnD) screening model system was created as a tool to incorporate ecosystem and management issues into a user-friendly framework to evaluate alterations in any of its components. QnD links the spatial components within GIS files to the climatic, abiotic, and biotic interactions in an ecosystem. QnD has a simple design and can be upgraded easily. QnD:HAAF was developed as a framework to evaluate consequences of wetland restoration for MeHg emissions at the former Hamilton Army Air Field (HAAF). The purpose of the present QnD application was to identify critical abiotic and biotic drivers of salt marsh mercury and MeHg cycling and guide subsequent work on HAAF and other San Francisco Bay salt marshes. QnD:HAAF encompasses four spatial areas (High *Salicornia*-vegetated Marsh, Mid *Spartina*-vegetated Marsh, Mud Flat, and Sub Tidal), three drivers (tide-dependent redox potential, wet and dry season, and daytime light), and two processes (methylation and demethylation). Biota are represented by typical plant and animal species. A new model version, QnD:HAAF V2, was developed in 2006-2007, based on QnD :HAAF V1. QnD:HAAF V2 differs from V1 by inclusion of a (1) HAAF base map containing 100x100-m grid-cells and digital elevation information; (2) verified, realistic elevation assignments to the spatial areas and tidal movements pertaining to 2005; (3) revised formulation of net methylmercury production matching field data collected after 2003; (4) MeHg diffusion from sediments; (5) Hg deposition and volatilization from the wetlands module. QnD:HAAF V2 has been recalibrated for the physico-chemical processes using more recent field data. Two 14-day scenarios were simulated, i.e., one scenario representing the wet season and one scenario representing the dry season. From

comparisons of simulated and measured data, the following became apparent. Simulated MeHg concentrations in the sediments of the spatial areas exceeded measured MeHg concentrations, potentially indicating either limitations to solubilities of Hg species and, therefore, limited export, or considerable transport with tidal waters. A data gap exists on the concentrations of Hg species and important electron donors and acceptors in sediments of various locations within the Bay and adjacent wetlands, impeding calculations of solubilities of Hg species. Simulated potential export of MeHg from wetlands exceeded MeHg export calculated from measured values, causing uncertainties in the contribution of wetlands to the MeHg TMDL of the Bay. A data gap exists on food chain structure, components, bioaugmentation mechanisms, and MeHg accumulated in the biota associated with San Francisco Bay wetlands. Recommendations for additional field, experimental, and modeling research were formulated to decrease the uncertainty of these early model outcomes.

2 Background Methylmercury Study

The potential for methylation of mercury in sediments and soils of tidal marsh and seasonal wetlands bordering the Hamilton Army Airfield (HAAF) Wetlands Restoration Site was assessed by same-sample analysis for total mercury (THg) and monomethylmercury (CH_3Hg^+, MMHg, or MeHg) during the dry season (McFarland and Lee 2002, and appendices therein) and during the wet season in 2002–2003 (McFarland and Lee 2002; McFarland et al. 2003). Surficial sediment samples of 1–2 cm at 60 sites were replicated five times from seven locations. Results served as the basis for selection of sites for subsequent intensive study.

In March 2003, the U.S. Army Engineer District, San Francisco (CESPN) requested an expansion of pre-construction monitoring of THg and MeHg concentrations in sediment and soils of existing wetlands bordering the Hamilton Army Airfield (HAAF) Wetlands Restoration Site at San Pablo Bay, California. Sampling locations are shown in Figure 2-1. The purpose of the expanded activities was to gain site-specific knowledge of the geochemical/geophysical, microbial, and predominantly plant- and animal related interactions that affect the stabilization and mobilization of THg and MeHg there.

Results of previous studies conducted in 2003 have been published (Best et al. 2005, 2007) and are summarized here.

The levels of THg in the surface sediments of wetlands bordering San Pablo Bay (SPB) average 0.3 µg g^{-1} dry weight and are comparable to those generally found in San Francisco Bay. No strong correlations were demonstrated between levels of THg and MeHg. Results of field studies using a heavy-labeled mercury isotope approach indicated that methylation and demethylation rates are rapid, and that current rates of methylation would double the standing pool size of MeHg within a day if this rate was not counter-balanced by demethylation. The current rates of demethylation would deplete the standing MeHg pool size to null within a few days if methylation ceased. This produces a dynamic MeHg pool with respect to time and space.

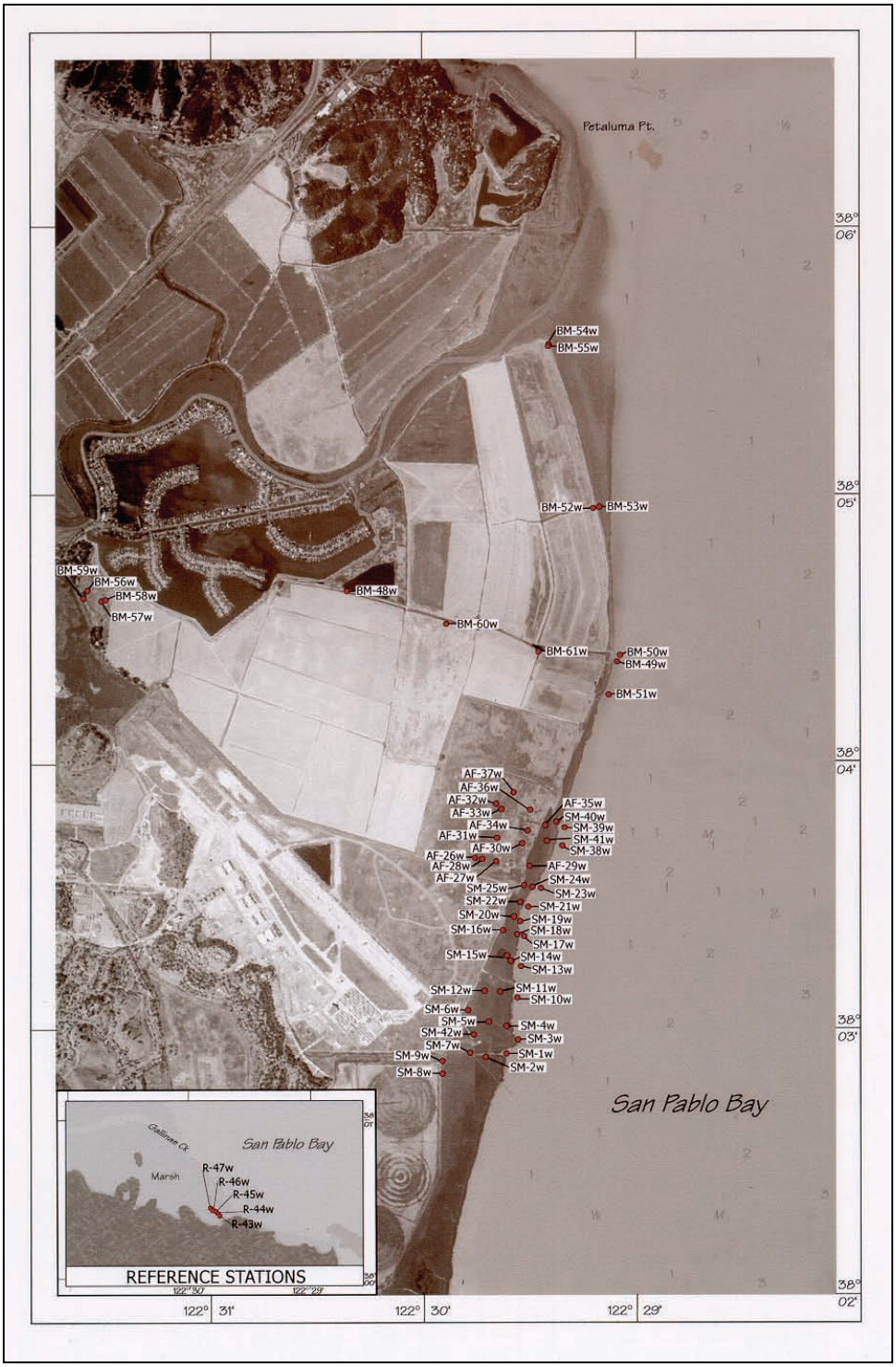

Figure 2-1. Sampling locations at HAAF and China Camp (inset).

No consistent trend in net MeHg production rates (methylation rate minus demethylation rate) was shown in Bay wetlands ranging from the China Camp (CC) State Park (24 ppt salinity) to the Petaluma River (7 ppt). However, net MeHg production was significantly lower in vegetated than

in bare sediments. A significant relationship between microbial biomass and relative abundances of the sulfate-reducing bacterial (SRB) genera *Desulfobacter* and *Desulfovibrio*, and MeHg pool size was found, but no significant relationships between THg and other sediment characteristics were demonstrated.

A new method, called DGT technique, was developed to monitor bio-available MeHg. This method uses 3−mercaptopropyl−functionalized silica gel to bind MeHg. The detection limit of the overall method, 1 pg of MeHg, corresponds approximately to 30 pg L^{-1} of MeHg in a water sample, when deployed for 24 hr. Field tests have shown that DGT measurements of dissolved MeHg provide comparable results to conventional methods of sample collection and measurement. The DGT technique provides an alternative in situ sampling method for MeHg with the added advantage that it integrates exposure levels over a time period. This may dampen the wide fluctuations in MeHg levels often observed and may provide more reliable data required for monitoring and management decisions. Early field verification of the method estimated a MeHg diffusion flux from sediment at 15 μg m^{-2} y^{-1}.

The role of marsh plants as vectors in the transport of mercury species was studied in the CC salt marsh. The fluxes of organic matter, THg and MeHg, were studied in natural stands of *S. foliosa* and *S. virginica*. Seasonal fluxes into aboveground biomass of live plants were measured, as was transfer to the dead plant community by mortality. Disappearance from the latter community through fragmentation, leaching, and excretion was calculated. Seasonal data were used to calculate annual input-output budgets. Based on data that covered a large part of a year, annual fluxes were estimated. In *S. foliosa*, annual net production was approximately 1,499 g dry weight (DW) m^{-2}, and the annual uptakes of THg and MeHg were, respectively, 34.897 μg m^{-2} and 0.784 μg m^{-2}. In *S. virginica*, annual net production was approximately 1,361 g DW m^{-2}, and the annual uptakes of THg and MeHg were, respectively, 9.422 μg m^{-2} and 0.018 μg m^{-2}. Because *S. foliosa* had a similar production rate and higher mercury species uptake and loss rates than *S. virginica*, *S. foliosa* matter is expected to affect the local and possibly the regional food web relatively more than *S. virginica* (Best et al. 2008).

Decomposition of *S. foliosa* and *S. virginica* plant litter, harvested in March 2004 from the CC salt marsh, was studied under laboratory

conditions. Dried plant materials were incubated in litter bags within vessels, filled with SPB water, and inoculated with local sediment, under aerobic or anaerobic conditions for up to 150-day periods. Mass loss, mercury species, and carbon, nitrogen, and sulfur stable isotopes were used to characterize the changes in the plant litter during the decomposition process. Total microbial biomass and the contributions of two SRB groups to the total microbial biomass, i.e., *Desulfobacter* sp. and *Desulfovibrio desulfuricans*, in the decomposing plant litter were determined using phospho lipid fatty acids (PLFA) to explore their involvement in the Hg dynamics. Plant materials decomposed with different rates, with a dry weight loss of maximally 66 percent in *S. foliosa* and 84 percent in *S. virginica*. Oxygen concentration affected decomposition rates differentially, in that aerobic conditions increased mass loss in *S. foliosa* litter, but decreased it in *S. virginica* litter. The THg concentration in the litter increased during the decomposition process, but the THg mass contained in the litter did not. The temporarily increased MeHg portion of THg in the decomposing plant litter, up to 17.9 ng g^{-1}, supports the hypothesis that THg in and on the surface of the plant litter is methylated during decomposition. In a later decomposition phase the MeHg concentration decreased, and, thus, demethylation of MeHg also occurred. This indicates that plant litter from coastal marshes can act as a transient source of MeHg. The $\delta^{13}C$ ratio proved to be a reliable indicator of plant material source. The C:N ratio generally decreased during decomposition and exceeded the value of 35 temporarily and only in *S. foliosa* litter. Because a C:N ratio of >35 is indicative of low food quality for animals, litter of *S. foliosa* may have a lower food quality than that of *S. virginica* during part of the decomposition process.

The food webs of the China Camp salt marsh and adjacent San Pablo Bay area were characterized using carbon, nitrogen, and sulfur stable isotopes. Producer groups were most clearly differentiated by carbon, followed by sulfur, and least clearly by nitrogen isotope values. Consumer ^{15}N isotopic enrichment suggested that four trophic levels exist in the China Camp marsh and adjacent San Pablo Bay area food web. Associations among sources and consumers indicated that a mixture of inputs from bay macroalgae, C_4-grasses (largely *S. foliosa*), marsh-diatoms and –cyanobacteria and marsh-pool filamentous algae may provide the organic matter that forms the base of the food web, supporting invertebrates, fishes, mammals (*R. raviventris* and *M. californicus*), and birds (*M. melodia samuelis* and *L. jamaicensis coturniculus*). C_3-marsh plants (largely

S. virginica) and bay-phytoplankton were expected to play a minimal role in food web support, due to their relative depletion of ^{13}C. Ranking consumers into their approximate trophic levels based on their $\delta^{15}N$-values did not correlate with their MeHg concentrations for most consumers. Fish ranked the highest or fourth trophic level and exhibited high MeHg levels. Although birds ranked below fish at the third trophic level, they demonstrated by far the highest MeHg concentrations. Mammals ranked lower than either other consumer group and exhibited low MeHg concentrations. MeHg concentrations and stable isotope ratios indicated that the associations between species are more defined by their diets than by habitat. Further analysis of the associations among producers and consumers using multiple-source mixing models to approximate the relative inputs of each source into the food web of the CC marsh and adjacent San Pablo Bay area is expected to elucidate these relationships. THg concentrations in all consumer samples were below the screening value of 230 ng g^{-1} wet weight as limit for human consumption.

Measures to decrease Hg bioavailability were explored as a management tool. The bioavailability characteristics of Hg species in sediments of HAAF and other marshes bordering SPB were evaluated experimentally. The bioaccumulation factor (BAF) values of MeHg exceeded those of THg. The THg and MeHg body burdens of *Nereis virens (*polychaete worm) experimentally exposed for 56 days were similar to body burdens determined in crabs and mussels field-collected from the HAAF and CC sites. The bioavailabilities of THg and MeHg to *N. virens* were not significantly decreased by sediment amendment with 3.4% granular activated carbon (GAC), in contrast to results obtained earlier where amendment decreased the bioavailability of spiked THg and MeHg on sediments to the clam *Macoma nasuta*.

Results of studies largely conducted in 2006 are described in this document.

3 Site-specific Mercury Cycle-related Dynamics in Wetland Sediments of San Pablo Bay: Methylation, Demethylation, and Environmental Factors

Introduction

Biogeochemical processes in sediments play an important role in the geochemistry of mercury (Hg), with sulfate reduction in sediments being thought to be the principal mechanism in the conversion of dissolved Hg to methylmercury (MeHg). The latter is a toxin and the main form in which Hg bioaccumulates. For decades geochemists have studied the chemistry of sediment pore water to investigate biogeochemical processes in sediments (Berner 1971, 1980). The enrichment or depletion of various chemical species in pore water may indicate the nature of ongoing biogeochemical processes in sediments, i.e., processes not readily apparent from studies of the solid phase geochemistry. Pore water chemical data also provide the basis for quantitative estimates of the rates of biogeochemical processes in the sediments (Berner 1980).

Most bacteria in marine sediments meet their energy needs by decomposing organic matter, a process that, in turn, drives many other geochemical processes in sediments. Bacteria chemically oxidize the organic matter (commonly written as CH_2O) to obtain energy

$$CH_2O + Oxidant^{microbes} \rightarrow CO_2 + Reductant + H_2O \qquad (3.1)$$

yielding carbon dioxide, water, and the conversion of the oxidant to a reduced form. Depending on the oxidant available, decomposition yields different amounts of energy for microbial growth and metabolism. The effects of utilizing different oxidants can be seen more clearly by dividing the reaction (Equation 3.1) into distinct oxidation and reduction steps. In the oxidation step, bacteria remove electrons shared by the carbon atoms in organic compounds, here referred to as CH_2O:

$$CH_2O + H_2O \rightarrow CO_2 + 4H^+ + 4e^- \quad (3.2)$$

The electrons produced by this process cannot be released into solution, but must be transferred to an available electron-poor molecule, termed the oxidant or electron acceptor. In marine sediments, the most important electron acceptors are oxygen (O_2), manganese oxide ($MnO_{2(s)}$), iron oxides ($Fe(OH)_{3(s)}$), and sulfate (SO_4^{2-}), which undergo the following reactions when supplied with electrons:

Aerobic respiration	$O_2 + 4H^+ + 4e^- \rightarrow 2H_2O$
Manganese reduction	$MnO_{2(s)} + 4H^+ + 2e^- \rightarrow Mn^{2+} + 2H_2O$
Iron reduction	$Fe(OH)_{3(s)} + 3H^+ + e^- \rightarrow Fe^{2+} + 3H_2O$
Sulfate reduction	$SO_4^{2-} + 10H^+ + 8e^- \rightarrow H_2S + 4H_2O$

(3.3)

These reduction reactions are listed in order of decreasing energy yield when coupled with the oxidation of organic matter. Oxygen, which yields the most energy by a large margin, is always consumed first and is generally not measurable below the first few millimeters to centimeters of sediment. At greater depth in the sediment, Mn-oxides, Fe-oxides, and then sulfate are utilized as oxidants, resulting in vertical segregation (with some blurring of boundaries) of these processes. Note that the reactions in Equation 3.3 are greatly simplified, since multiple steps, different minerals, and many different bacterial species may be involved. Reactions between the various end products of microbial processes also occur. For the purposes of this study, one of the most important is the precipitation of iron sulfide ($FeS_{(s)}$), which occurs in zones of sulfate reduction when sufficient Fe^{2+} is available, as is generally the case in this study.

$$Fe^{2+} + H_2S \leftrightarrow 2H^+ + FeS_{(s)} \quad (3.4)$$

Variations in these microbial processes influence sedimentary Hg methylation in several ways. One of the most important processes is the alteration of Hg solubility and bioavailability in environments where sulfate-reducing bacteria (SRB) produce hydrogen sulphide (H_2S) (Benoit et al. 1999). A second process is the associated change in microbial community composition, and consequent biochemical capability to methylate Hg. In particular, SRB are thought to be the main, if not sole, methylating bacteria in the environment. Both of these considerations highlight the central role of SRB in methylation and suggest the possibility of modeling Hg

methylation as a function of sulfate reduction, a process that can be modeled without reference to specific bacterial populations.

In previous work (Best et al. 2007), in order to examine Hg biogeochemistry, new gel techniques (DGT and DET) were developed to sample key parameters in sediment pore water and the results were compared with those obtained from conventional pore water sampling. DGT-based measurement methods have been developed by Davison and Zhang (1994). The DGT device is comprised of an ion-exchange resin immobilized in a gel (resin gel), which is separated from the test solution by an ion-permeable gel (diffusive gel). Concentration gradients develop across the diffusive gel and the contaminants are transported to the resin gel where they are fixed (in the case of MeHg by an ion-exchange reaction) and accumulate during the deployment time. The DGT approach has several advantages over other techniques proposed for measuring trace metals in natural waters:

1. The device can be mass produced and is easy to use;
2. The device can provide information about the actual MeHg species present in the water by varying the thickness and pore size of the diffusion gel layer;
3. The device concentrates MeHg in situ;
4. The device yields time-averaged concentrations over the length of the deployment period; the analysis of the devices can be optimized for high-throughput analyses.

DGT devices accumulate only certain forms of metal, i.e., mainly the labile metal species able to pass through the diffusion layer and bind with the resin layer. After the DGT device is removed from the sampling site, the mass of metal in the resin layer is determined analytically. The well-defined geometry of the DGT device enables quantitative interpretation of the mass accumulated, either in terms of dissolved concentrations or remobilization fluxes from sediments to pore waters. In waters that are reasonably well-mixed, the interpretation of DGT measured fluxes as labile metal concentrations in solution external to the DGT device is relatively straightforward (Zhang and Davison 1995). In sediments and saturated soils, interpretation is more complicated, due to the interaction of metal in solution with metal associated with the solid phase. Simple interpretations can provide estimates of a time-averaged remobilization flux from solid phase to solution and estimates of pore water concen-

trations (Zhang et al. 1995). A numerical modeling approach (Harper et al. 1998) is used to provide more quantitative interpretations in terms of the rate of supply from sediment to solution (i.e. the exchangeable metal fractions associated with sediment particles). The model enables the determination of the characteristic sorption-desorption reactions, together with information on the size of the exchangeable fraction associated with the solid phase. In the case of MeHg, methylation of proximate Hg as a source of MeHg also affects DGT measurements. Interpretation of such measurements is therefore not simple, but, if done correctly, it provides valuable data for the understanding of Hg biogeochemical cycles in sediments.

Objectives

The objectives of this study were as follows:

- Develop a new strategy to determine the net methylation rate profile with depth at a far higher (centimeters) resolution than used before. This was expected to enable the calculation of MeHg diffusion from sediment, by which process a large part of the newly produced MeHg may become accessible to local and regional food webs.
- Determine the significance of DGT for MeHg concentrations in sediments.
- Define the relationship between DGT for MeHg concentrations and net methylation rate.
- Expand the knowledge on the relationship between mercury cycling in sediments and environmental factors in San Pablo Bay sediments.

Study sites

The Hamilton Army Airfield (HAAF) on San Pablo Bay is part of the San Francisco Baylands. It is located in the North Bay Subregion. The Baylands ecosystem includes the shallow water habitats between the maximum and minimum tidal fluctuations, adjacent habitats, and their associated plants and animals. The boundaries of the ecosystem vary with the bayward and landward movements of fish and wildlife that depend upon the Baylands for survival. Many habitats of the Baylands are wetlands. Habitat goals selected for the restored HAAF include tidal marshes, with natural transitions into upland areas with seasonal wetlands. The restored HAAF area is expected to increase the habitat of the regionally rare clapper rail, because it will contain a large tidal wetland and is remote from predator outposts and corridors (Goals Project 1999). The test site representative

for the tidal part of HAAF was situated at the HAAF Bay Edge (38°02.908 N 122°29.576 W). The restored HAAF is expected to cover ca. 203 ha. The nearby tidal salt marsh at the China Camp State Park, chosen as a reference (CC; 38°00.428 N 122°28.762 W), covers ca. 45 ha (Hopkins and Parker 1984) and is frequently immersed by tidal waters (salinity 25-32 ‰). As net MeHg production is expected to reach an optimum at intermediate sulfate (SO_4^{2-}) concentrations that occur at intermediate salinities, a third site was chosen upstream in Petaluma River (PR; 38°13.767 N 122°36.854 W).

Materials and Methods

Redox potential and pH measurements

The redox potential (Eh) is a relative measure of oxidizing/reducing conditions in a soil. Eh depends on both the presence of electron acceptors (oxygen and other oxidizing agents) and pH. In a well-drained soil, the Eh is in the 400- to 700-mV range. In flooded conditions Eh values as low as −300 mV can be found. Microbial reaction rates in soils are strongly influenced by Eh.

Eh and pH were measured in two sediment cores at a 1-cm resolution. Eh was measured using an Orion® SP75B ORP Ag-AgCl referenced/Pt wire (Fisher Scientific, Nepean, ON, Canada) all-in-one waterproof glass probe attached to a Consort® C535 multi-meter (Fisher Scientific, Nepean, ON, Canada) analyzer. The multi-meter is compatible with the ORP probe with manual temperature setting and automatic temperature correction. Calibration for ORP was performed using a Zobel® (Fisher Scientific, Nepean, ON, Canada) solution at a standard 231 mV for the Ag-AgCl referenced probe. pH was measured using the same meter and a pH probe. To ensure proper function, Eh/pH probes and meters were checked frequently (~ hourly) using buffer and standard solutions. Eh values were calculated from measured mV readings of Pt-electrodes and corrected for the potential of the reference AgCl by adding 220 mV to the instrument reading.

Eh and pH probes were inserted horizontally through predrilled holes in the side of an acrylic tube, and the Eh and pH were recorded as soon as the meter stabilized (typically less than 3 minutes). In this manner, Eh and pH readings were taken at 1-cm intervals over the full length of the sample core (15 cm). Because redox conditions may change upon collection, Eh readings were taken as quickly as possible and always before pH readings.

This approach for measuring redox potential in freshly sampled cores is predicated on the assumption that such measurements would reasonably reflect the site condition.

DGT and methylmercury

DGT probes for sampling Hg species in pore water of marine sediments have been previously deployed for the measurement of Hg^{2+} (Divis et al. 2005). DGT probes for accumulating MeHg were constructed with standard filter membranes (cellulose nitrate), diffusive gels ($\Delta d = 0.013$ and 0.08 cm), and a binding resin consisting of mercapto-propyl functionalized silica gel embedded in a 0.05-cm-thick polyacrylamide gel. The probe was deployed after de-aeration and retrieved in the standard manner for DGT-sediment probes. The diffusive gel was removed from the binding resin, which was cut into 1-cm sections and placed in clean glass vials. The resin sections were preserved by refrigeration. In the laboratory, the resins were leached using a thiourea/HCl solution (0.005% in 0.1 M HCl) and analyzed by inductively coupled plasma/mass spectrometry (ICP/MS). Pore water MeHg concentrations were computed using the recorded incubation times of 24–30 hr. Calculated concentrations correspond to the interval from 5 mm above to 5 mm below the indicated nominal depth in the cores.

Stable Hg isotopic tracer studies

For each sampling site, methylation and demethylation rates were determined in three sediment cores based on a protocol described in the previous reports (Best et al. 2005, 2007). The methodology was slightly modified to determine methylation and demethylation rate at a far higher (cm) resolution than used before. This was expected to enable the calculation of MeHg diffusion from sediment, by which process a large part of the newly produced MeHg may become accessible to local and regional food webs. The following enriched Hg isotopes were used for the methylation assay: $^{199}HgCl_2$ (150 mg L^{-1}, 91.95%) and $^{202}HgCl_2$ (344 mg L^{-1}, 99.2 %). $CH_3{}^{198}HgCl$ (2.5 mg L^{-1}, 94.26%) was used for the demethylation assay. Two sets of spike solutions were prepared by dilution of the enriched isotopes stock solutions: the ‘odd’ spike solution was a mixture of $^{199}HgCl_2$ and $CH_3{}^{198}HgCl$ and the ‘even’ spike solution was a mixture of $^{202}HgCl_2$ and $CH_3{}^{198}HgCl$. Spike solutions (100 µL) were injected through predrilled ports in the acrylic tube into 15 sediment layers (1 cm thick) of each core. The ‘odd’ spike solution was injected into the odd sediment

layers and the even spike solution was injected into the even sediment layer. After injection of the isotopes, all cores were set back into their original location and incubated in place for 24 hr. Sediment cores were sliced at a 1-cm resolution and incubation was terminated by quick-freezing the sediment slices with dry ice in the field (Figure 3-1).

Samples remained frozen until analysis in the laboratory. Sediment samples were homogenized and subsamples were taken for the various measurements. Wet sediment was dried at 50 °C overnight or until weight consistency was obtained to determine the dry/wet weight ratio (percent solids).

Total Hg determination

About 0.2 g of sample was weighed into 40-mL acid-washed glass vials. Then 12.2 ng of $^{201}HgCl_2$ was added as an internal standard. After addition of 5 mL of concentrated 3:7 (v:v) H_2SO_4/HNO_3, the mixture was left to react for 1 hr at room temperature. Digestion was completed by heating vials in an Al block at 120 °C on a hot plate for 3 hr or until formation of brown nitrous gases had ceased. The digest was diluted with Milli-Q water to approximately 40 mL. The concentration of Hg isotopes in the digest was quantified using continuous-flow cold-vapor generation with ICP/MS detection (Finnigan MAT, Model Element 2). The acidified sample was continuously mixed with a solution of stannous chloride using a peristaltic pump. The formed Hg vapor was separated from the liquid in a gas-liquid separator (Model L1-2) and the elemental Hg swept into the plasma of the ICP/MS. The following isotopes of Hg were measured: ^{199}Hg, ^{202}Hg (added isotopes for the methylation assay), ^{198}Hg (added isotope for the demethylation assay), ^{201}Hg (internal standard), and ^{200}Hg (to calculate ambient total Hg). Concentrations of individual isotopes were calculated using an Excel spreadsheet, employing matrix algebra, as described in Hintelmann and Ogrinc (2003).

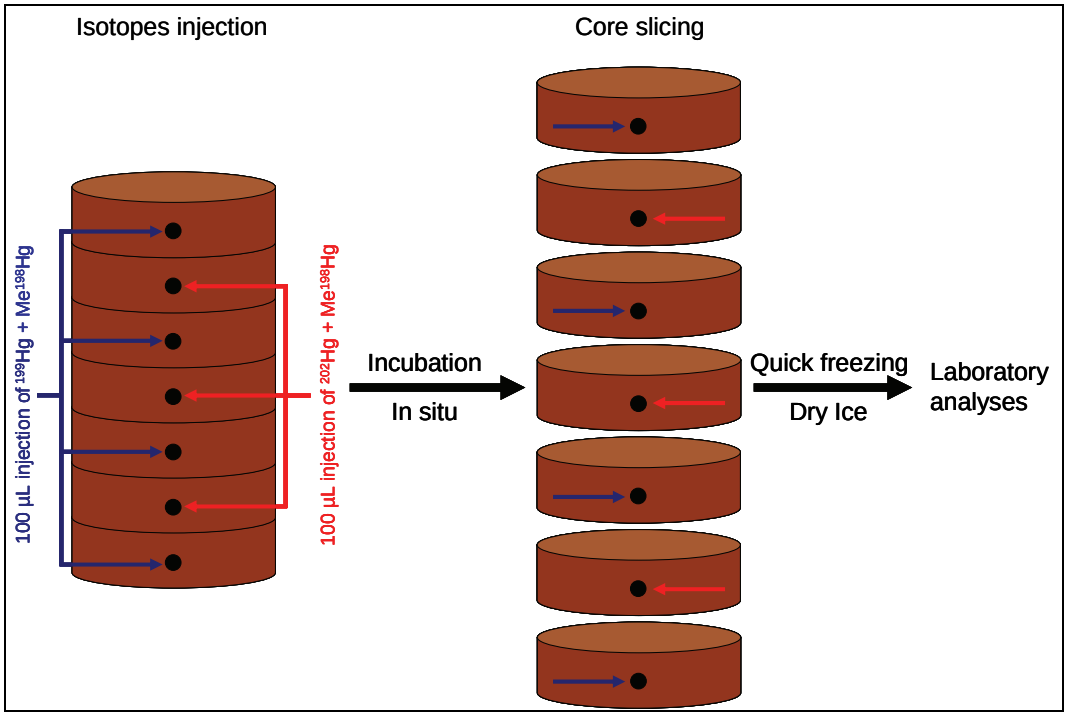

Figure 3-1. Methylation/demethylation rate protocol in sediment core.

Methylmercury determination

A method modified from Hintelmann and Evans (1997) was used. Approximately 0.2 g of sample was weighed into 30-mL Teflon vials. $CH_3{}^{201}HgCl$ (55 pg) was added as an internal standard. Then 200 µL of H_2SO_4 (9 M) and 500µL of KCl (20%) were added, and the vessel was placed into a heating block at 140 °C. MeHg was distilled from the sample under a supporting nitrogen stream (80 mL min^{-1}). Distillation time was approximately 60 to 90 min per sample. A reaction vessel was filled with 100 ml Milli-Q water, and the distillate was added for measurement of MeHg. Then 0.2 ml of acetate buffer (2 M) was added to adjust the pH to 4.9. Sodium tetraethylborate (100 µL, 1% w/v) was added and the solution was left sitting at room temperature for 20 min for the tetraethylborate to react. Tenax adsorber traps were connected to the reaction vessel and the generated MeHg was purged from the solution using nitrogen (200 mL min^{-1}) and collected on the Tenax trap. Finally, Hg species were thermally desorbed from the trap (250 °C), separated by gas chromatography, and quantified by ICP/MS (Micromass Platform). The following isotopes of Hg were measured: ^{199}Hg, ^{202}Hg (methylated Hg), ^{198}Hg (MeHg demethylation assay), ^{201}Hg (internal standard) and ^{200}Hg (to calculate ambient MeHg). Peak areas were used for quantification, and concentrations of

individual isotopes were calculated using an Excel spreadsheet, employing matrix algebra, as described in Hintelmann and Ogrinc (2003).

Hg analysis QA/QC

For each batch of samples, the following set of QA/QC samples was measured: three reagent blanks (THg) or bubbler blanks (MeHg) and a certified reference material (IAEA 356 marine sediment and MESS-3 marine estuary sediment for sediment analysis and NIST 1515 apple leaves for plant analysis). Individual distillation yields were determined using the added internal ^{201}Hg isotope standard.

Results and Discussion

Redox potential and pH

Reducing conditions were measured in the sediment cores from the three sites (Figure 3-2).

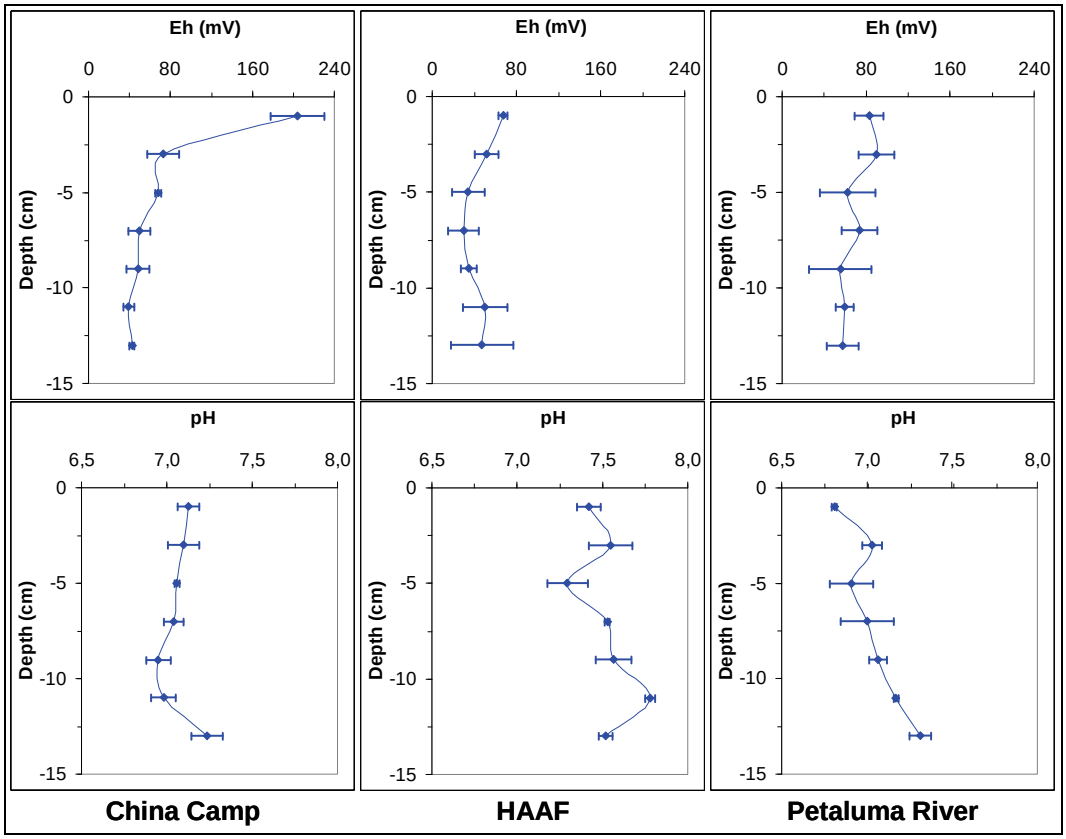

Figure 3-2. Redox potential (Eh) and pH measured in situ in sediment cores from China Camp, HAAF, and the Petaluma River (July 2006). Mean values ± standard deviations (N=2).

Most bacteria in marine sediments meet their energy needs by decomposing organic matter, a process that in turn drives many other sedimentary geochemical processes. To obtain energy in this way, bacteria chemically oxidize the organic matter yielding carbon dioxide, water, and the conversion of the oxidant to a reduced form (reductant). Depending on the oxidant available, decomposition yields different amounts of energy for microbial growth and metabolism. The sedimentary biogeochemistry of Hg is closely coupled to that of the redox-active elements iron, manganese, and sulphur, which in turn are all driven by carbon cycling. The microbial oxidation of organic compounds in sediments leads to the accumulation of chemically reduced iron (Fe), manganese (Mn), and sulfur (S) solutes and minerals and the appearance of reduced conditions. The redox potential measured in CC, HAAF, and PR sediments reflects the activity of the above biogeochemical processes.

The decomposition of organic matter also influences the sediment pH: microbial oxidations of iron oxide, manganese oxide, and sulfates lead to the liberation of H^+ (Berner 1980). Consequently, the pH measured in the various cores is slightly more acidic than in the overlying seawater, which is buffered by carbonates to a pH range of 7.5-8.4.

Measuring rates of methylation and demethylation

The Hg stable isotope tracer approach used in the current study provides a method for the simultaneous determination of in situ methylation and demethylation rates in the same sediment volume. These experiments were designed to provide rates of methylation and demethylation that are directly comparable to other environmental parameters, which can also, in turn, affect these rates. The use of the specially designed corer minimizes the physical disturbance of sediment core removal and replacement (Best et al. 2005). Tracer studies are based on the mixing of negligible levels (<1% of the standing pool size) of tagged molecules into a known environmental pool size and measuring the rate of conversion of the tagged chemical. Multiplication of the rate of conversion of the tagged molecule by the size of the pool at the time when the tagged molecules are added gives the rate of change for the entire pool. This is only a summary of the method employed to give a general understanding of the principles involved; however, the details of the method are outlined elsewhere (Hintelmann and Ogrinc 2003). Currently required assumptions introduce uncertainty into the derivation of the net methylation rates. It is assumed that the added isotopic Hg tracers will behave in the sediment the same as

the relevant Hg species (THg, reactive Hg, bioavailable Hg, and MeHg). However, it is not known what these relevant Hg species are and they have not been measured in the volumes of sediment tested in this study. In the current case, it is assumed that all measured THg is available for methylation and this value is used for the required multiplication. This may result in the overestimation of the natural methylation rate, and, therefore, these methylation rates may be considered as 'potential' rates, as discussed previously by Best et al. (2007).

In previous studies, sediment cores were quick-frozen and later on sliced (Best et al. 2005, 2007). During the freezing process, material freezes from the side to the center of the core resulting in an unavoidable expansion and uplifting of the interior sediment. Horizontal layers of the sediment core were consequently disturbed and the Hg-enriched isotopes (transformed or not) were physically transported vertically. It was therefore difficult to distinguish the vertical transport of the enriched isotope Hg species from this artifact from other transport modes (diffusion of the spike solutions, migration through vertical channel created by bioturbation, etc.). The sampling strategy changed in 2006, as compared to former years, to minimize any vertical perturbations: sediment cores were first sliced into 1-cm segments using a core tube constructed of pre-cut 1-cm-thick rings held together with silicone seal and duct tape and then these slices were flash frozen in order to stop the incubation. In this manner, the spiked Hg-enriched isotopes were confined to the 1-cm sample interval not significantly transported by sediment expansion during the freezing process.

Both odd and even enriched isotopes, originally spiked as $HgCl_2$, were found in all sediment core slices (Figure 3-3), revealing a vertical migration of the Hg spikes inside the sediment core. Dissolved Hg-enriched isotopes were most likely transported vertically by diffusion and/or through channels created by bioturbation and/or tidal flushing. Mobility of the dissolved phase in sediment is important and may contribute considerably to the export of Hg species from the sediment to the overlying water.

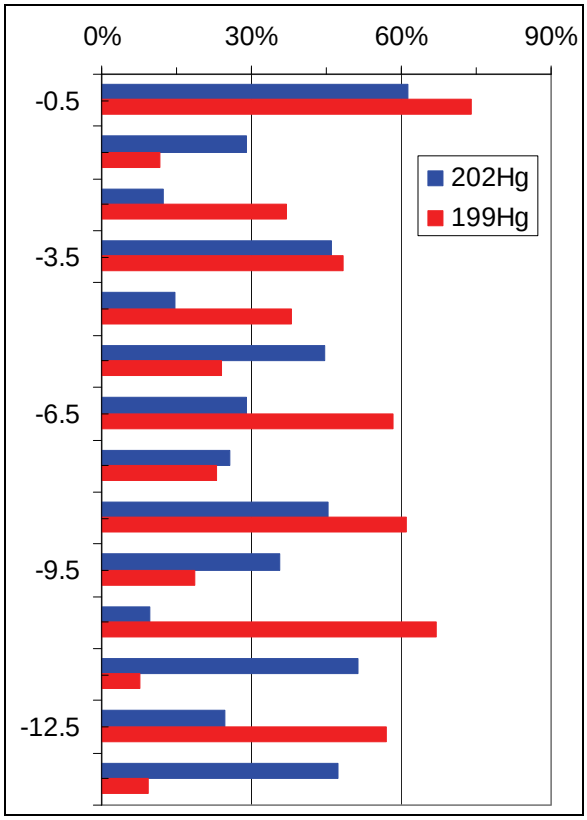

Figure 3-3. Hg-enriched isotopes recovery in the slices of a sediment core from HAAF (July 2006).

However, as both of the enriched Hg isotopes were found in all the sediment slices, it was possible to calculate the methylation rates from ^{199}Hg and ^{202}Hg. Assuming a first order kinetic process (Hintelmann et al. 2000), methylation rate constants (k_M) were simply the ratio of newly formed Me^{199}Hg and Me^{202}Hg divided by the total concentration of added ^{199}Hg(II) an ^{202}Hg(II), corrected for a 24-hr incubation period:

$$k_M(^{199}Hg) = \frac{[Me^{199}Hg]}{[^{199}Hg]} \times \frac{24\ hours}{incubation\ time}$$

$$k_M(^{202}Hg) = \frac{[Me^{202}Hg]}{[^{202}Hg]} \times \frac{24\ hours}{incubation\ time} \quad (3.5)$$

The rate constants $k_M(^{199}Hg)$ and $k_M(^{202}Hg)$ were not statistically different (Figure 3-4), because both inorganic Hg spikes were methylated at the same rate. Consequently, either Hg-enriched isotope could be used to calculate the methylation rate. Since the newly formed MeHg is eventually subject to the demethylation process, the gross rate constant of k_M is best obtained from measurements early in the assay, where demethylation has not yet significantly depleted the pool of MeHg. The concentration of newly methylated ambient Hg (M) is obtained by multiplying the measured rate constant by the concentration of total ambient Hg:

$$M = k_M \times [Hg]_{total}$$

This equation assumes that the total ambient Hg is equally available for methylation as is the added isotope-enriched spike, an assumption that is debatable. However, in the absence of more accurate predictors, this approach was used to calculate the 'potential' concentration of newly generated MeHg. Being a first-order process, the $Me^{198}Hg$ concentrations decrease exponentially over time. Hence, a demethylation rate constant, k_{Dm}, was calculated by linear regression of $\ln[Me^{198}Hg]$ versus time, with the slope of the regression being k_{Dm}. The % MeHg degradation per day, Dm, was then calculated as $Dm = 1\text{-}e^{-k_{Dm}} \times 100\%$.

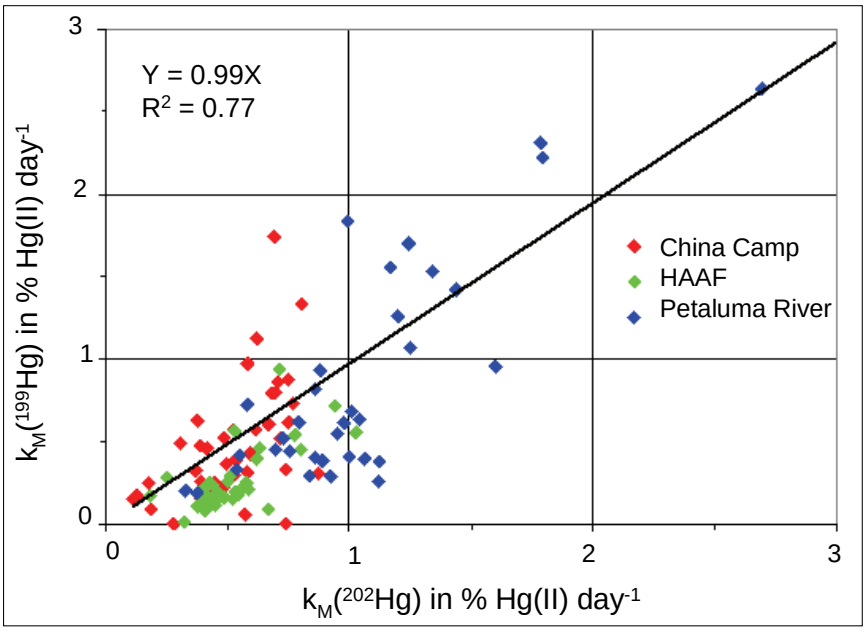

Figure 3-4. Methylation rate constants of sediment cores from China Camp, HAAF, and the Petaluma River.

The concentration of MeHg demethylated per day (D) was calculated by multiplying the % degradation (Dm) by the concentration of newly methylated MeHg (M): D = Dm x M = Dm x [THg] x k_M.

Eventually, combining both rates allows an estimate of the net concentration of MeHg that is newly generated from the pool of ambient inorganic THg:

$$net_{MeHg} = M\text{-}D = M\text{-}Dm \times M = (1\text{-}Dm) \times M = (1\text{-}Dm) \times [THg] \times k_M$$

Methylation, demethylation, and net methylation rates were calculated per 1-cm depth layer in the sediment cores from CC, HAAF, and PR. Depth profiles are presented in Figure 3-5. The sediments at CC and HAAF showed small variations in net methylation rates with depth. Average net methylation rates of 1.3 (±0.5) and 0.7 (±0.3) ng g^{-1} DW day^{-1} over a depth of 15 cm were found in CC and HAAF sediments, which did not differ significantly from those measured previously (Best et al. 2005, 2007). As expected, sediments from the PR, with a lower salinity and corresponding sulfate concentration, exhibited the greatest net methylation rates (3.3 ± 2.2 ng g^{-1} DW day^{-1}). At the latter site, MeHg production was greatest in the upper sediment layer, favoring MeHg export from the sediment to the overlying water. Such a steep gradient was not identified at both of the other sites.

DGT-based methylmercury concentrations in sediments

MeHg was measured in pore water using the DGT method. MeHg profiles with depth are presented in Figure 3-6. In CC, three DGT probes were deployed in the sediment within a 0.3-m radius to assess the reproducibility of the method. An average variation of 20% (± 10%) was found in the MeHg measurements from the three DGT probes. A similar variability has been reported previously (Mason et al. 1998) for MeHg in pore water extracted by centrifugation from three sediment cores collected within a 0.5-m radius. Thus, the observed differences for pore water are not likely to be due to analytical variability but rather to inhomogeneity in sediment pore water distributions. It is necessary to consider such sampling variability in order to interpret results and finally to understand the biogeochemistry of MeHg in sediments.

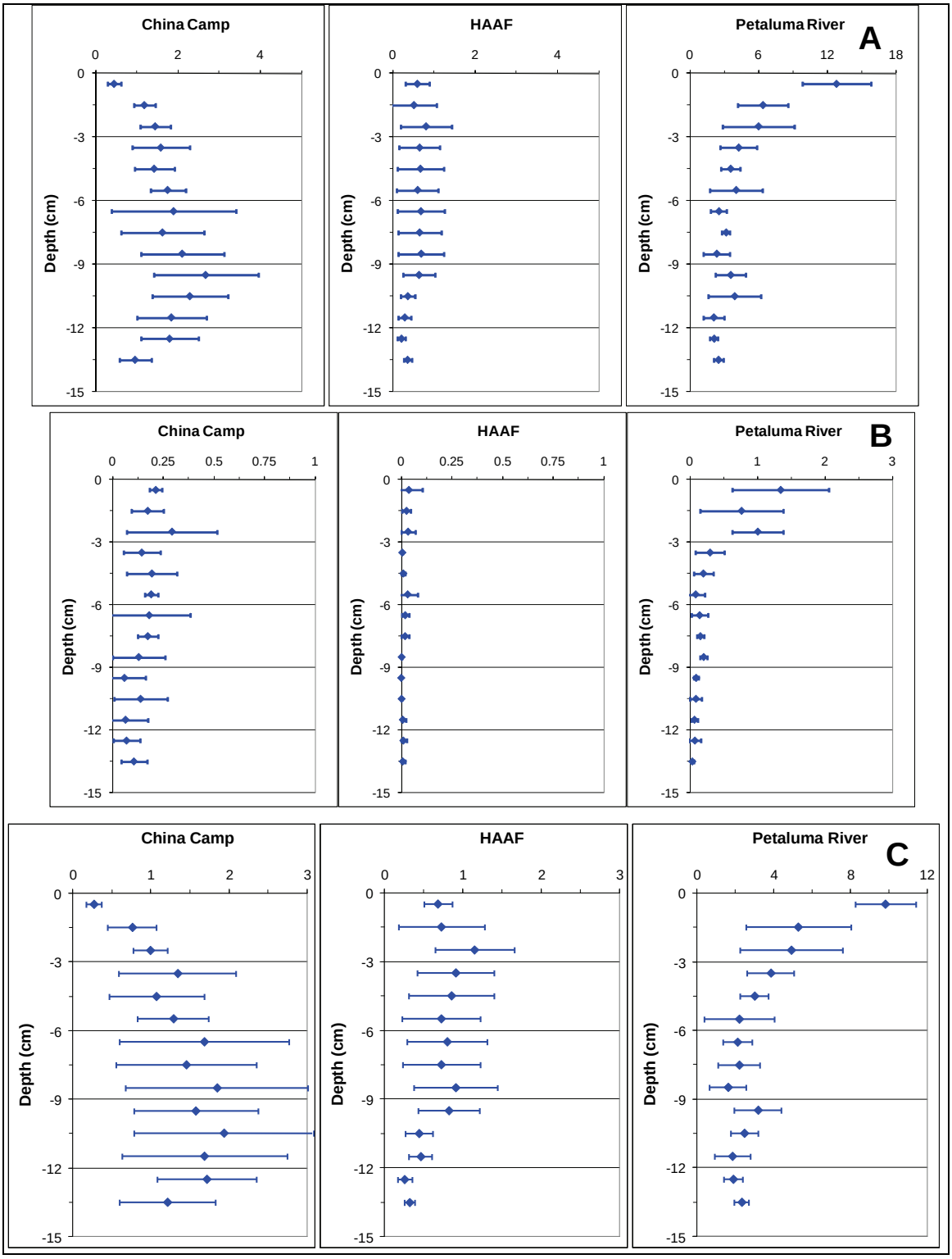

Figure 3-5. Methylation (A), demethylation (B), and net methylation rates (C; ng g^{-1} DW day^{-1}) determined in sediments from China Camp, HAAF, and the Petaluma River (July 2006). Mean values ± standard deviations of three incubated cores.

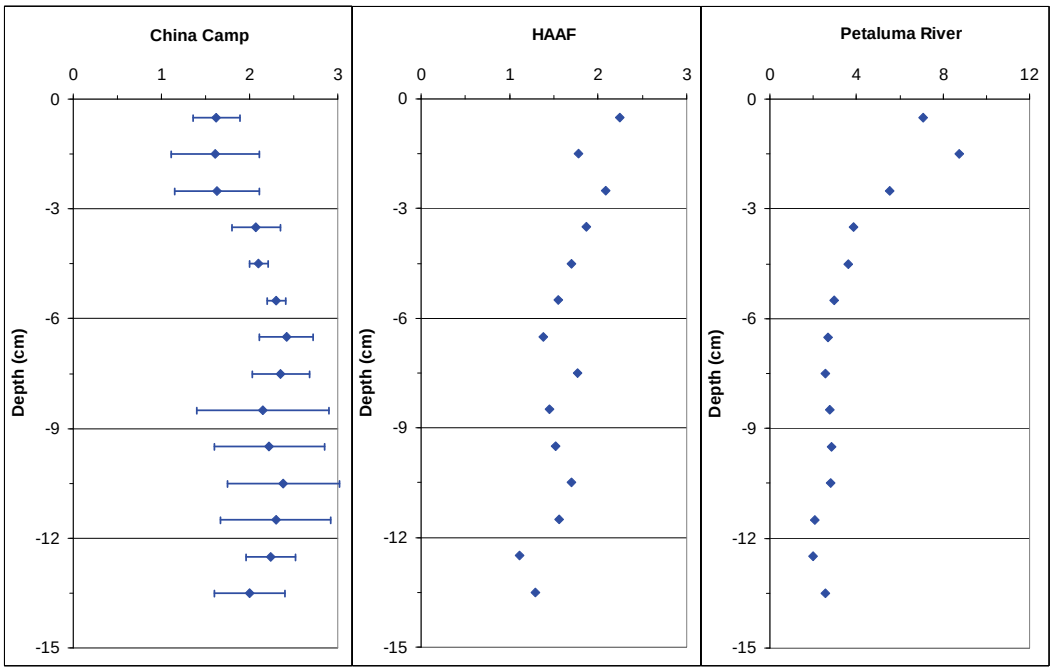

Figure 3-6. MeHg concentrations measured by DGT in sediment pore water (ng L^{-1}) from China Camp, HAAF, and the Petaluma River (July 2006). Mean values ± standard deviations of three DGT probes at China Camp, single values for both other sites.

Consistent with the July 2005 study (Best et al. 2007), the MeHg profile of the Petaluma River sediment showed a concentration gradient that peaks close to the sediment water interface, suggesting a release of MeHg into the river water by diffusive flux. Calculations using Fick's first law of diffusion (with a diffusive coefficient of MeHg in pore water of 5×10^{-6} cm^2 s^{-1}) resulted in a diffusive flux of 3.7 µg y^{-1} of MeHg per square meter of PR sediment. Therefore, the river sediments may be a considerable source of MeHg for the Bay. However, the diffusive MeHg flux determined in July 2005 was 4-5 times higher (Best et al. 2007), suggesting annual and/or spatial variability in the MeHg diffusive fluxes from pore water. The MeHg profiles of CC and HAAF sediment showed virtually no concentration gradient, indicating that the diffusive MeHg flux from these sediments is expected to be close to zero.

Relationship between DGT-based methylmercury concentrations and net methylation rates in sediments

The well-defined geometry of the DGT device enables quantitative interpretation of the mass accumulated, either in terms of dissolved concentrations, or re-mobilization fluxes from the sediment to pore water. In waters that are reasonably well mixed, the interpretation of DGT mea-

sured fluxes as labile metal concentrations in solution external to the DGT device is relatively straightforward (Zhang and Davison 1995). In sediments and saturated soils, calculations of metal fluxes are more complicated, due to the interaction of metal in solution and metal associated with the solid phase. Simplified calculations can provide estimates of a time averaged remobilization flux from solid phase to solution and estimates of pore water concentrations (Zhang et al. 1995). According to the DGT theory in sediment, the introduction of the DGT probe perturbs the pore water system in a well-characterized fashion (by introducing a local sink) while simultaneously recording a response. Metals diffuse from pore water to the DGT device where they are bound to the resin. The DGT device therefore induces a flux from the pore water to the resin, which may deplete the local pore water concentration. The magnitude of this local depletion in pore water concentrations depends on the re-supply rate of exchangeable metals to the pore water from the solid phase (due to changes in equilibrium between pore water and solid phase). The processes which remove exchangeable metals from pore water to solid phase are collectively referred to as 'sorption' and include adsorption, absorption, and surface precipitation; metals are remobilized by desorption, the reverse process. Based on the observed kinetics of metal remobilization in DGT studies, re-supply of metals to pore waters is controlled by these sorption/desorption processes (Harper et al. 1998).

Based on the relative flux of a given metal from pore water to the DGT and the rate of re-supply to pore water from the solid phase, local pore water concentrations may be affected in three manners (Zhang et al. 1998). The case where pore water is well-buffered and re-supply from the solid phase maintains constant pore water concentrations will be referred to as the 'sustained case' in the subsequent paragraph. The 'partially sustained case' refers to a situation where some re-supply occurs, but is insufficient to prevent a decrease in local pore water concentrations. The 'unsustained case' refers to a situation where no significant re-supply from the solid phase occurs and local pore water concentrations decrease with time during DGT deployment. For example, for a probe with a 0.8-mm thick diffusive gel, the average flux for 24-hr deployment is approximately 10% of the initially established flux and $C_{DGT} \approx 0.1\ C_{pore\ water}$ (Zhang et al. 1995; Harper et al. 1998). For the 'sustained case' the re-supply from the solid phase to pore water has a high rate and capacity. Pore water concentrations are, therefore, not depleted during DGT deployment.

For MeHg, the DGT theory is more complicated, as the governing biogeochemical processes include a local production of MeHg. This new MeHg source will affect the quantity of MeHg accumulated by DGT.

Net potential methylation rates were plotted versus MeHg concentrations calculated from DGT measurements in sediments at the three sites (Figure 3-7). A positive linear relationship between net methylation rate and MeHg concentration was found, which explained 79% of the variability in the data set. The latter illustrates that methylation, a biogeochemical process, strongly affected the quantity of MeHg accumulated by the DGT device in the sediment, and suggests that DGT measurements can be used to predict net potential methylation rates.

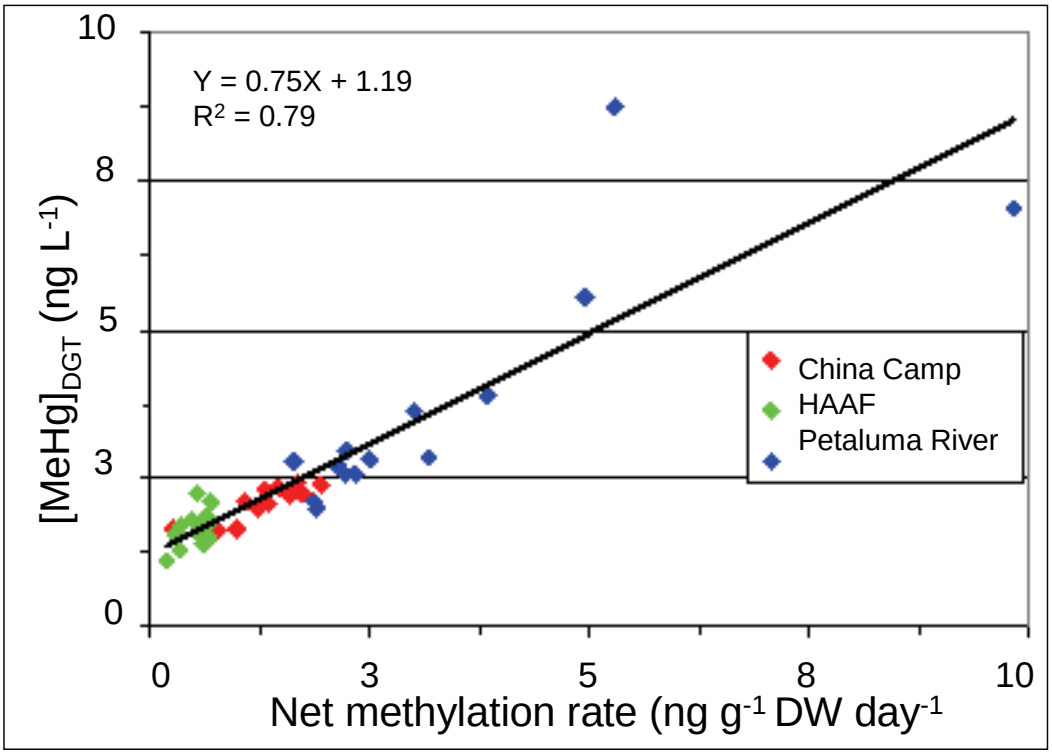

Figure 3-7. Net potential methylation rate (ng g^{-1} sediment dry wt day^{-1}) versus the concentration of $MeHg_{DGT}$ (ng L^{-1}) in China Camp, HAAF and Petaluma River sediments (July 2006).

In terms of quantity, MeHg accumulated by DGT devices represented <0.1 to 0.2% of the newly produced MeHg during the methylation process. Although most of this new MeHg is likely associated with the solid phase, a corresponding proportion will dissolve, assuming a distribution coefficient between the solid phase and pore water of 500-1000 for MeHg commonly reported in estuarine/marine sediment (Bloom et al. 1999;

Hammerschmidt et al. 2004). The local depletion of MeHg concentration in pore water adjacent to the DGT device is fully compensated by the natural in situ production of MeHg and its desorption from the solid phase. DGT measurements of MeHg in sediments correspond most likely to the 'sustained case' and a direct interpretation of the results in terms of pore water concentration is, therefore, possible.

DGT in contact with sediment mimics the main mechanism of metal uptake by organisms by lowering the concentration locally, which induces a diffusive supply and a release of metal from the solid phase. In the case of MeHg, DGT measurements also reflect the methylation process that generates new MeHg. Therefore, the DGT device is a promising tool for assessing exposure of organisms to MeHg in pore water of sediments, as it provides an integrated value of all reactions involved in Hg biogeochemical cycling.

Biogeochemistry of mercury cycle associated processes in coastal wetlands

The sediment biogeochemistry of mercury is closely coupled to that of the redox-active elements (i.e. iron, manganese, and sulfur), which, in turn, are driven by carbon cycling. The microbial oxidation of organic compounds in sediments leads to the accumulation of chemically reduced iron (Fe), manganese (Mn), and sulfur (S) solutes and minerals. Measurements of these chemicals in sediment pore water at a high spatial resolution can be used to establish a vertical segregation of biogeochemical processes within the San Pablo Bay sediments. This phase of the project is still in progress and will eventually establish correlations between MeHg production and major biogeochemical processes. An overview of the results of field and experimental mercury cycle studies associated with the Hamilton Wetland restoration project is provided in Chapter 6. Part of these results has been used to (re)calibrate the screening-level model QnD:HAAF. This model enables extrapolation and integration of selected processes and rates in time. Many data on environmental factors, collected as background information during field studies, have not yet been used. Recently published new insights greatly facilitate the selection and prioritization of processes and studies most important in MeHg production and export from coastal wetlands such as HAAF.

Conclusions

The following conclusions can be formulated based on field study results:

1. The present field study describes a new strategy to measure methylation and demethylation rates in sediment cores at a far higher resolution than in previous field studies using earlier developed and emerging technologies.
2. The newly generated values for net methylation rates in sediments of the three sites (CC, HAAF, and PR) of 1.3 (±0.5), 0.7 (±0.3), and 3.3 (± 2.2) ng g^{-1} DW d^{-1}, respectively, confirmed earlier published findings.
3. Sediment with a lower salinity than at CC and HAAF may form the source of considerable MeHg export to Bay water, while MeHg export from CC and HAAF by diffusive flux is expected to be close to zero.
4. DGT measurements can be used to predict net methylation rates in sediments, since DGT-generated values on MeHg concentrations were strongly correlated with measured net methylation rates at a high resolution scale.
5. The DGT device is a promising tool for the assessment of exposure of organisms to MeHg in porewater of sediments, as it provides an integrated value of all reactions involved in Hg biogeochemical cycling.

4 Comparison of Accumulation of Water- and Sediment-associated Mercury Species in Clams, Fish, and DGT: DGT as a Tool for Environmental Monitoring

Introduction

Mercury (Hg) in the environment is a problem of global concern. Increasing concentrations of atmospheric Hg from anthropogenic sources have led to increased Hg deposition, which is the principal source of Hg in surface waters. In the aquatic environment, bacteria transform inorganic Hg into monomethylmercury (MeHg), which is highly toxic and readily biomagnified in aquatic food webs. Seasonal variations of MeHg in the environment are largely unknown, but may vary to a large extent. Hence, spot sampling only provides a snapshot of the current MeHg exposure and biological monitoring programs are often put in place to gauge contaminant exposure. The uptake of trace metals by aquatic organisms is determined by the total concentration of labile species able to cross biological membranes. Diffusive Gradient in Thin Film (DGT) techniques depend on the diffusion of labile species across a gel membrane followed by accumulation on an ion-exchange resin. Therefore, the ability of the DGT technique to mimic the accumulation of MeHg by a bivalve mollusc (*Macoma balthica,* Baltic clam) and a fish (*Cyprinodon variegatus,* sheepshead minnow) was investigated. Both organisms have been proposed as Hg sentinels.

Objectives

The objectives of this study were to:

- Develop a novel and cost-effective approach to detect and measure the bioavailable fraction of MeHg within and near coastal wetlands using DGT devices.
- Evaluate DGT data as predictive of potential bioaccumulation in common estuarine organisms.

Materials and Methods

Clams

Monitoring coastal trace metal contamination using bivalve molluscs as quantitative bioindicators is widely performed in many international biomonitoring programs. As molluscs adjust quickly to changes in contamination, they may serve as useful indicators of temporal trends in environmental quality.

Mussels are commonly used to monitor Hg species in marine environments. Mussels from uncontaminated sites are generally transplanted to a contaminated site and used in monitoring the mobility and availability of Hg species from the contaminated site to marine organism (Odzak et al. 2000; Kljakovic-Gaspic et al. 2006). *M. balthica*, a deposit/filter feeding bivalve, has been used in several investigations of MeHg bioaccumulation (Riisgard et al. 1985; Boisson et al. 1998; Mouneyrac et al. 2000). Clams were field-collected from subtidal areas in Woods Hole, MA, and shipped overnight to the U.S. Army Engineer Research and Development Center (ERDC) in Vicksburg, MS. Clams were shipped in site water at 30 ‰. One half of the organisms were maintained at 30 ‰ while the other half were acclimated to 10 ‰ salinity by decreasing the salinity in the seawater by 5 ‰ each day.

Fish

The sheepshead minnow (*Cyprinodon variegatus*) and the fathead minnow (*Pimephales promelas*) are closely related, ecologically important, native, North American fish. The sheepshead minnow prefers estuarine waters, while the fathead minnow is a freshwater species. Both minnows are considered opportunistic feeders and are able to tolerate a wide range of environmental conditions including high temperatures, low oxygen levels and high turbidities. Sheepshead minnows are abundant in estuaries along the southeastern and eastern coasts of the United States and are widely used in routine toxicity testing of whole effluent and receiving waters (American Society for Testing and Materials (ASTM) 2008). They have been used as experimental organisms in numerous ecotoxicological investigations (e.g., Manning et al. 1999; Klerks and Moreau 2001; Lytle et al. 2003; Jonsson et al. 2004). Fathead minnows have been used extensively as indicator species in both laboratory and field studies to characterize the extent and mode of action of aquatic pollutants (Benoit et al.

1982; Devlin et al. 1982). MeHg has been shown to affect the gonadal development (Hammerschmidt et al. 2002), reproduction (Drevnick and Sandheinrich 2003) and feeding behavior (Grippo and Heath 2003) of adult fathead minnows.

For the present study in seawater, juvenile sheepshead minnows (*Cyprinodon variegatus*) were purchased from Aquatic BioSystems (Fort Collins, CO) and shipped overnight in reconstituted seawater at 20 ‰ to the ERDC, in Vicksburg, MS, approximately one week before experiment initiation. One half of the organisms were maintained at 20 ‰, while the other half were acclimated to 10 ‰ salinity by decreasing the salinity in the seawater by 5 ‰ each day. MeHg uptake and distribution kinetics in sheepshead minnows have been described (Leaner and Mason 2001; 2004). A large part of the Hg burden in fish is methylated and is thought to accumulate primarily from dietary sources (Hall et al. 1997), but direct, aqueous accumulation also can contribute (Post et al. 1996). In the fish experiment, both MeHg uptake routes were considered and explored.

DGT

DGT-based measurement methods have been developed by Davison and Zhang (1994). The DGT device is comprised of an ion-exchange resin immobilized in a gel (resin gel), which is separated from the test solution by an ion-permeable gel (diffusive gel). Concentration gradients develop across the diffusive gel and the contaminants are transported to the resin gel where they are fixed and accumulated during the deployment time.

After the DGT device is removed from the sampling site, the mass of metal in the resin layer is determined analytically. The well-defined geometry of the DGT device enables quantitative interpretation of the mass accumulated in terms of the average dissolved concentration. The mass of MeHg accumulated by the resin inside the DGT unit is controlled by the first Fick's law of diffusion and depends on its dissolved concentration, its diffusive coefficient (D) in polyacrylamide gel, and some physical properties of the diffusive gel layer itself such as thickness Δd, surface area A, and deployment time t of the DGT device.

$$M = D_{MeHg} \times \frac{A \times t}{\Delta d} \times \int_0^t [MeHg]\, dt \tag{4.1}$$

As MeHg accumulation is driven by diffusion of the labile MeHg species through the gel for DGT and through biological membranes for live organisms, the mass of MeHg accumulated by the DGT should be correlated to the amount of MeHg accumulated by the organisms.

Isotopic tracers

To mimic the chronic MeHg exposure in natural systems, bioaccumulation experiments were performed at realistic environmental concentrations. However, organisms available for research are already preloaded with natural MeHg. Hence, it can represent an analytical challenge to differentiate the MeHg bioaccumulated during the experiment from the natural MeHg background. Therefore, isotope-enriched MeHg was used as a tracer, $Me^{199}Hg$ (91.95%, Trace Sciences International Corp.) as the aqueous tracer, and $Me^{202}Hg$ (97.7%, Institute for Reference Material and Measurements) as the fish food tracer. The isotope-enriched material is not radioactive, has the same properties as the natural MeHg, and presents the advantage to be easily distinguished analytically from the ambient MeHg (i.e. MeHg background in the experimental organisms).

Food preparation

Contaminated diets were prepared by mixing fish food (Tetramin flakes) with reagent alcohol containing dissolved isotope-enriched MeHg chloride ($Me^{202}Hg$, 97.7%). Alcohol was evaporated overnight from the fish food in an acid glass pan in a fume hood. Diets were prepared once, homogenized and frozen until use. MeHg concentration and mobility were analyzed in food subsamples. Sheepshead minnows were fed $Me^{202}Hg$-contaminated food (5-10% of body mass per day) to generate $Me^{202}Hg$ burdens in fish.

Experimental design

Two sets of experiments were conducted in 2006. In February 2006, MeHg accumulation by DGT and clams (*Macoma balthica*) from the aqueous phase was investigated. Six tanks of 30 L were filled with reconstituted seawater and spiked with $Me^{199}Hg$ (100 ng L^{-1}). Two different salinities (10 and 30 ‰) were chosen to examine the impact of this parameter on MeHg accumulation by DGT and clams. The effect of MeHg speciation on its accumulation by DGT and clams was addressed by adding humic substance (Aldrich) to the tank. MeHg has a strong affinity to the thiol groups of the dissolved organic matter (DOM) and forms stable

complexes (Hintelmann et al. 1997). Transport of these macro-molecules through the diffusive gel layer of the DGT is delayed and the MeHg mass accumulated by the DGT is greatly affected (Best et al. 2007). After four days of equilibration, 15 DGTs and 20 clams were deployed in each tank. Exact tank conditions are summarized in Table 4-1.

Table 4-1. Experimental conditions and change in levels of dissolved MeHg concentration during the experiments conducted in February 2006.

Tank	Salinity (‰)	Humic substance	[$Me^{199}Hg$] (ng L^{-1})
1	10	no	9 - 0.03
2	10	yes	46 - 1.1
3	30	yes	38 - 0.6
4	30	no	5.5 - 0.05
5	30	no	0.3 - 0.001
6	30	no	1 - 0.02

After 1, 3, 7, 14, and 21 days, three DGTs and three clams were removed from each tank. DGTs were peeled and resin gels were extracted and kept refrigerated until analysis. Clam shells were opened; tissues were rinsed with seawater, weighed, and frozen until analysis. At each sampling time, 125 mL of seawater was filtered through 0.45-µm cellulose nitrate membranes (Whatman) and collected in 125-mL acid-cleaned glass bottles, double-bagged, preserved to 1% HCl and stored at 4 °C until analysis.

In December 2006, similar experiments were conducted including fish (sheepshead minnows, *Cyprinodon variegatus*). However, the experimental design was modified to counterbalance the depletion of MeHg in seawater over time observed in the previous experiment. Seawater was pumped continuously to the tank and spiked on line with $Me^{199}Hg$ to maintain a steady dissolved concentration of 0.1 ng L^{-1} in the tank. A circulating pump was used inside the tank to homogenize the water. The experiment design is presented in Figure 4-1.

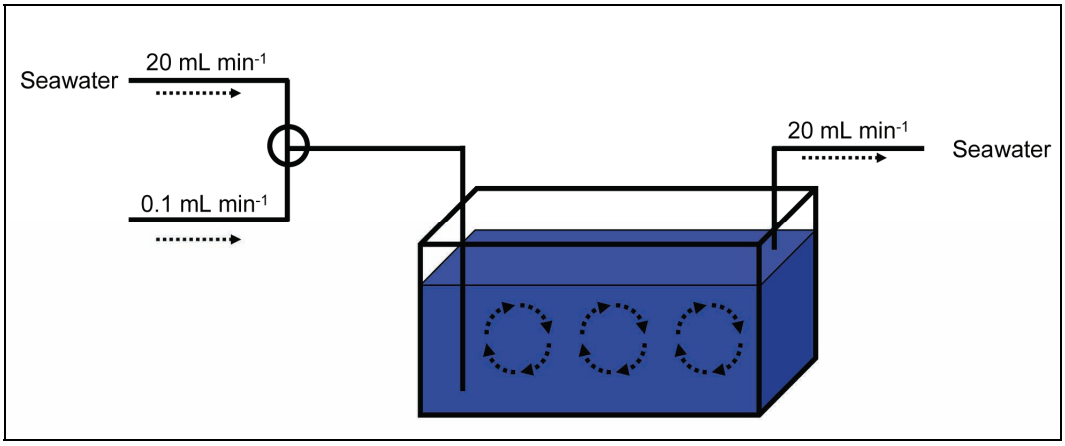

Figure 4-1. Experimental design to maintain a constant concentration of dissolved $Me^{199}Hg$.

Two tanks were filled with 30 L of seawater at a salinity of 10 and 30 ‰ and initially spiked at 0.1 ng L^{-1} $Me^{199}Hg$. After two days of equilibration, 15 DGTs, 18 fish, and 20 clams were deployed in each tank. After 3, 5, 7, 10, and 14 days, three DGTs, three fish, and three clams were removed from each tank. DGTs were peeled and resin gel was extracted and kept refrigerated until analysis. Clam shells were opened; clam tissues and fish were rinsed with seawater, weighed, and frozen until analysis. At each sampling time, 125 mL seawater were filtered through 0.45-µm cellulose nitrate membranes (Whatman) and collected in 125-mL acid-cleaned glass bottles, double-bagged, preserved to 1% HCl, and stored at 4 °C until analysis.

Methylmercury determination

Resin gels from the DGTs were eluted by soaking in 2 mL of 1.3-mM thiourea in 0.1-M HCl for 24 hr. Prior to the elution, an internal standard $Me^{201}Hg$ (25 pg) was spiked on the resin. MeHg was measured in an aliquot of the elution solution, after aqueous-phase ethylation using $NaBEt_4$, by GC-ICP-MS.

Fish and clam samples were digested using an alkaline digestion to isolate MeHg from biological matrices (Hintelmann and Nguyen 2005). The whole sample (0-0.2 g wet weight) was dissolved in 8 mL of 20% KOH in methanol at 47 °C for 24 hr. Prior to the alkaline digestion, an internal standard $Me^{201}Hg$ (500 pg) was spiked on the biological tissue. A 50-µL aliquot of the alkaline digest was processed for aqueous ethylation and MeHg was determined by GC-ICP-MS.

Seawater samples were distilled in the laboratory. An approximately 50-mL sample was transferred into a 50-mL glass vial. An internal standard $Me^{201}Hg$ (25 pg), 200 µL of H_2SO_4 (9M), and 500 µL of KCl (20%) were added. The distillation vials were placed in a heating block at 140 °C. MeHg was distilled from the sample under a supporting nitrogen stream (80 mL min^{-1}). Distillation time was approximately 3-4 hr per sample.

MeHg was measured after aqueous-phase ethylation using a method modified from Hintelmann and Evans (1997). Distillates (water samples), aliquots of thiourea eluant solution (DGT), or alkaline digestion solutions (fish and clams) were added to a reaction vessel filled with 100 ml Milli-Q water. In addition, 0.2 ml of acetate buffer (2 M) was added to adjust the pH to 4.9. Sodium tetraethylborate (100 µL, 1% w/v) was added and the solution was left sitting at room temperature for 20 min for the tetraethylborate to react. Tenax adsorber traps were connected to the reaction vessel and the generated MeHg was purged from the solution using nitrogen (200 mL min^{-1}) and collected on the Tenax trap. Finally, Hg species were thermally desorbed from the trap (250 °C), separated by gas chromatography, and quantified by ICP/MS (Micromass Platform). The following isotopes of Hg were measured: ^{199}Hg (aqueous tracer), ^{202}Hg (food tracer), ^{201}Hg (internal standard) and ^{200}Hg (to calculate ambient MeHg). Peak areas were used for quantification, and concentrations of individual isotopes were calculated using an Excel spreadsheet as described in Hintelmann and Ogrinc (2003).

The analytical procedure is summarized in Figure 4-2.

Mercury analysis and quality control

QA/QC was performed on a regular basis by analyzing MeHg in bubbler blanks, thiourea blanks (DGT), KOH-methanol blanks (fish and clams) and distillation blanks (seawater). MeHg was also analyzed in certified reference materials after alkaline digestion: dogfish muscle tissue (DORM-2; NRCC, Ottawa, ON, Canada), lobster hepatopancreas (TORT-2; NRCC, Ottawa, ON, Canada), and oyster tissue (NIST 1566b; NIST, Gaithersburg, MD, USA). Individual elution or digestion yields were determined using the added internal ^{201}Hg isotope standard.

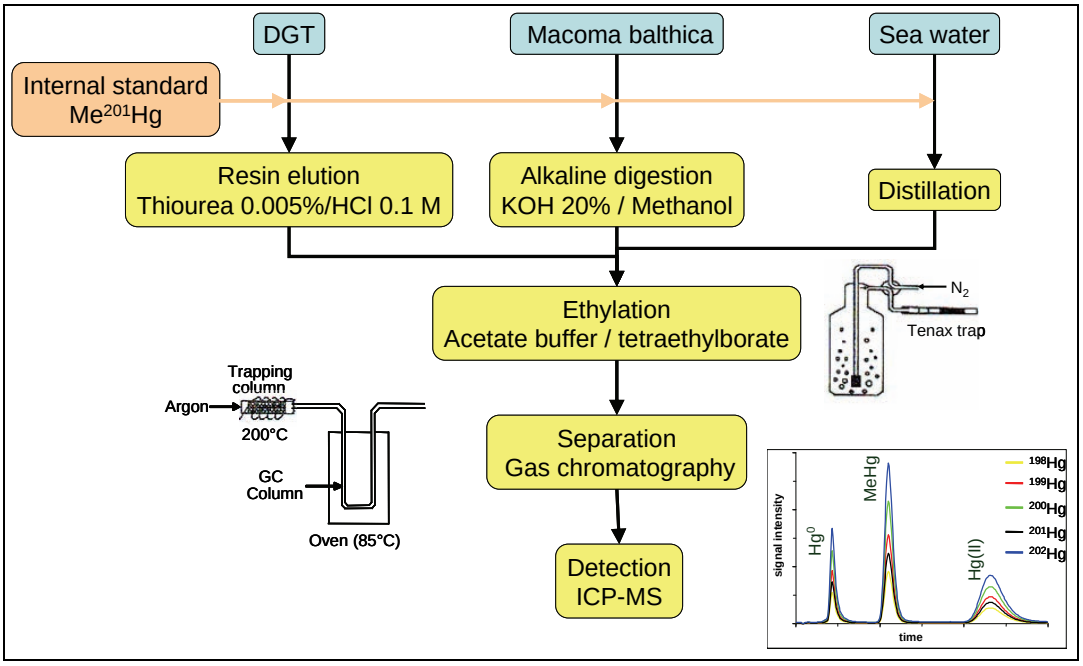

Figure 4-2. Analytical procedure for the determination of MeHg in seawater, fish, clams, and DGT.

Results and Discussion

Stability of $Me^{199}Hg$ concentration in seawater using a single addition of $Me^{199}Hg$

Dissolved [$Me^{199}Hg$] continuously decreased with time in all tanks. During the initial first four equilibration days (in the absence of biota), the initial 100 ng L^{-1} $Me^{199}Hg$ spike was depleted by 55% in the tanks with humic substances and by more than 90% in the seawater only tank (Table 4-1). After addition of clams and DGTs to the tanks, [$Me^{199}Hg$] continued to decline, albeit at a slower rate (Figure 4-3). The $Me^{199}Hg$ loss can be explained by wall adsorption, demethylation processes, or evaporation and may have affected the magnitude of $Me^{199}Hg$ accumulation by DGT and clams.

However, it was still possible to express the mass of MeHg accumulated by DGT as a time-averaged concentration (Equation 4.1). Time-averaged $Me^{199}Hg$ concentrations between two measurements were obtained by subtracting the mass of MeHg accumulated at t_1 from the mass of MeHg accumulated at t_2 (Equation 4.2).

$$\int_{T_1}^{T_2} [MeHg]\, dt = \frac{(M_2 - M_1) \times \Delta d}{D_{MeHg} \times A \times t} \quad (4.2)$$

Using this approach, the DGT estimated [$Me^{199}Hg$] depletion coincided with directly measured concentrations (Figure 4-3). In other words, the $Me^{199}Hg$ mass accumulated by the DGTs was directly related to its dissolved concentration.

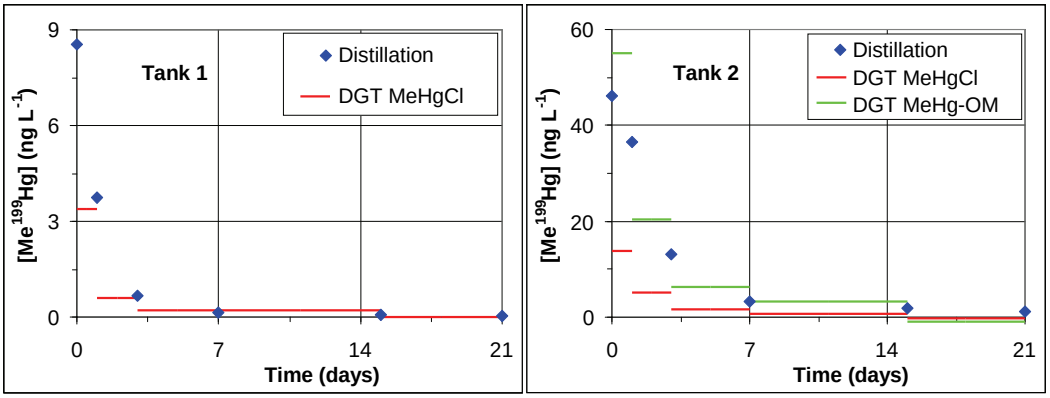

Figure 4-3. MeHg concentration in tank 1 (seawater only; ng L^{-1}) and tank 2 (seawater plus humic substances) over time, measured directly in seawater and monitored by DGT.

However, the $Me^{199}Hg$ concentrations calculated from the DGTs were lower than the directly measured concentrations in the tanks spiked with humic substance. This was attributed to complete MeHg complexation by the excess humic substance, resulting in larger MeHg-"molecules" diffusing into the gel. Thus, the presence of DOM affected the DGT technique by slowing down the diffusion of MeHg through the diffusive gel and reducing its accumulation by the resin. Using a diffusive coefficient of 1.25×10^{-6} cm^2 s^{-1} for the MeHg-DOM complex (Best et al. 2007) for the calculation, a better agreement between the $Me^{199}Hg$ concentrations in DGTs and those measured directly was found (Figure 4-3). MeHg accumulated by DGTs was greatly affected by its speciation in the dissolved phase.

$Me^{199}Hg$ accumulated by clams and DGT while $Me^{199}Hg$ exposure concentration is declining

Because MeHg is evenly distributed in soft tissue, gills, and digestive glands, all mussel tissues can be used as a bioindicator of MeHg pollution in the environment (Kljakovic-Gaspic et al. 2006). Therefore, an MeHg concentration measured in soft tissue is representative of exposure of the organism to MeHg. *Macoma balthica* exhibits a very slow elimination rate of Hg (Riisgard et al. 1985), and, therefore, the $Me^{199}Hg$ in this clam reflected most likely the total $Me^{199}Hg$ amount accumulated during the exposure period.

The $Me^{199}Hg$ accumulated by clams increased with time in tank 1 (Figure 4-4a), despite its larger uncertainty. The trend in $Me^{199}Hg$ accumulation by clams over time was similar to that by DGT. $Me^{199}Hg$ accumulation by clams was correlated with $Me^{199}Hg$ accumulation by DGT (Figure 4-4b), as expected since the $Me^{199}Hg$ in clams and DGT both originated from water. MeHg accumulation is regulated in clams by the filtration of water and in DGTs by the diffusion of dissolved MeHg through a membrane. In the other tanks, $Me^{199}Hg$ accumulation in clams also increased over time and was correlated with $Me^{199}Hg$ accumulation by DGT (Figure 4-5). Changes in salinity and in MeHg speciation appeared to affect MeHg accumulation by clams and DGT equally. Both sentinels can, therefore, be used to estimate MeHg exposure from the aqueous phase. Since MeHg uptake is associated with biological processes (e.g., clam filtration activity), larger variations in MeHg bioaccumulation by clams were expected. A similar uncertainty has previously been reported for MeHg accumulation by mussels transplanted to a contaminated site (Kljakovic-Gaspic et al. 2006). The overall uncertainty associated with $Me^{199}Hg$ accumulation by clams and DGT was calculated as the average precision of the measurement reproducibility for each sampling time in all tanks. Precisions of 38% (N=90) and 7% (N=90) have been estimated for MeHg accumulated by clams and DGT, respectively. Having DGTs showed a better reproducibility, and the DGT technique appears to be a promising tool to estimate exposure to MeHg in the aqueous phase. Moreover, in contrast to clams, DGTs do not have a MeHg background. The MeHg in the DGT corresponds without ambiguity to MeHg accumulated during the exposure period.

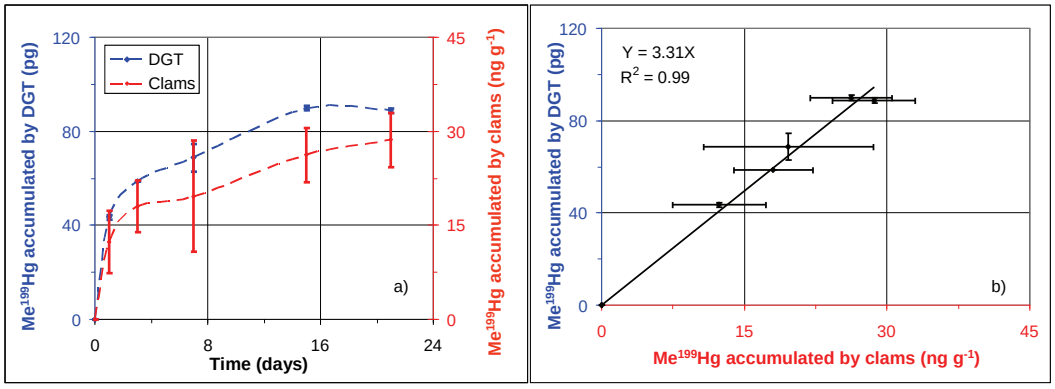

Figure 4-4. $Me^{199}Hg$ accumulation in tank 1; a) $Me^{199}Hg$ accumulated by clams and DGT over time in tank 1. b) $Me^{199}Hg$ accumulated by clams versus $Me^{199}Hg$ accumulated by DGT in tank 1. Mean values ± standard deviations (N=3).

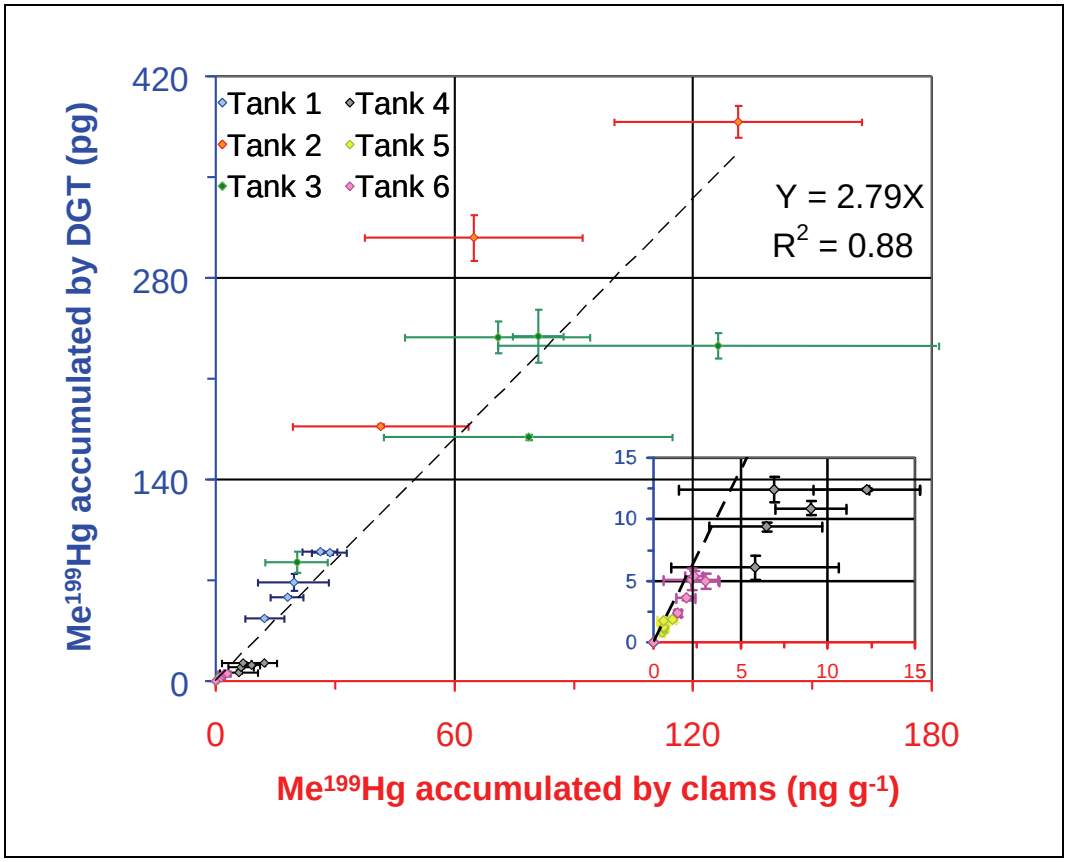

Figure 4-5. $Me^{199}Hg$ accumulated by clams versus $Me^{199}Hg$ accumulated by DGT in all tanks. Mean values and standard deviations (N=3).

Stability of MeHg concentration in seawater under continuous flow conditions

To counterbalance the depletion of MeHg in seawater over time, Me199Hg spiked seawater was pumped continuously through the tank to maintain a constant concentration. During the experiment, the seawater was regularly sampled to monitor MeHg concentration in the dissolved phase (Table 4-2).

Table 4-2. MeHg concentrations monitored in the dissolved phase of the December 2006 experiments. Mean values ± standard deviations (N=6).

Tank	Salinity (‰)	[$Me^{199}Hg$] (pg L^{-1})	[$Me^{202}Hg$] (pg L^{-1})
1	10	58 ± 28	50 ± 42
2	30	33 ± 19	31 ± 22

Measured $Me^{199}Hg$ concentrations were two to three times lower than the predicted, nominal concentrations. While the new experimental design did not completely eliminate the loss of $Me^{199}Hg$ (adsorption, demethylation, evaporation processes), the $Me^{199}Hg$ concentration was more constant. Somewhat unexpected, a relatively large fraction of $Me^{202}Hg$, initially spiked onto the fish food, was also measured in the dissolved phase. Two diet subsamples were analyzed and 49.2 ± 2.5 ng $Me^{202}Hg$ g^{-1} dry weight was found in the fish food. Mobility of $Me^{202}Hg$ from the food was investigated by leaching contaminated diets in MilliQ and in seawater for 24 hr at 47 °C, but very little MeHg dissociated from the diet into the water. Only 1 to 2% of the $Me^{202}Hg$ spike was leached from food into MilliQ and seawater.

Assuming a 2% $Me^{202}Hg$ dissociation from the food material as the source of the $Me^{202}Hg$ in water, and further considering the daily amount of food added to the tanks, the $Me^{202}Hg$ concentration in the dissolved phase can be predicted (Figure 4-6). Additional assumptions were: (i) instantaneous dissociation of $Me^{202}Hg$ from the food, (ii) a constant inflow of fresh seawater to the tanks, and (iii) all dissociated $Me^{202}Hg$ was stable and remained in the dissolved phase. Predicted concentrations were 5-10 times

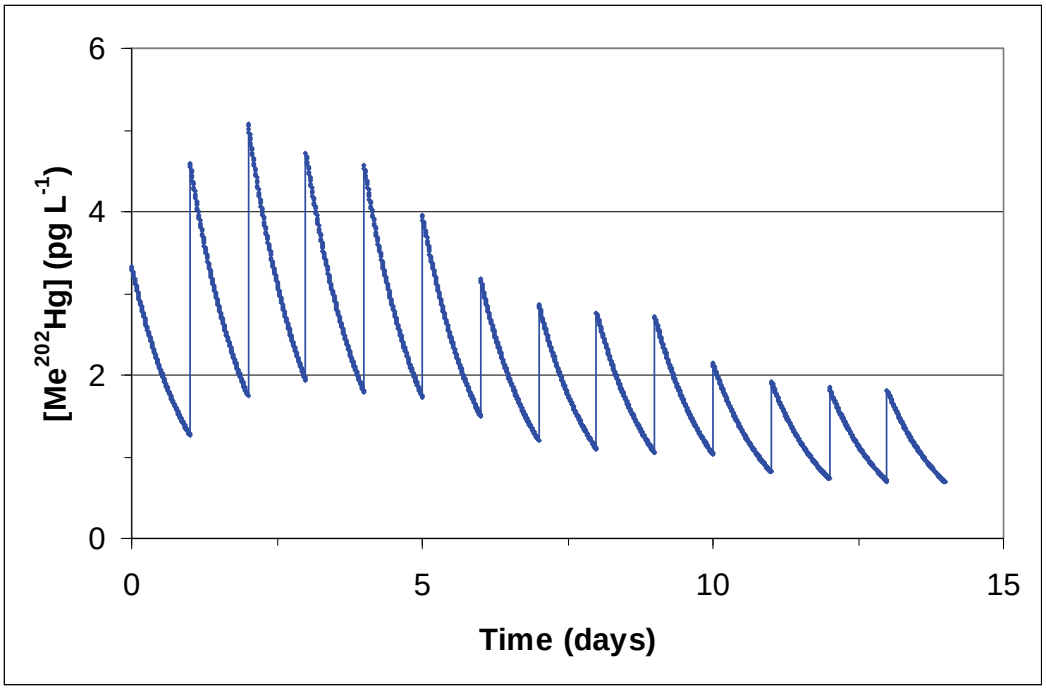

Figure 4-6. Prediction of variation in $Me^{202}Hg$ concentration over time in the dissolved phase assuming the daily amount of food introduced into the tank, a 2% instantaneous $Me^{202}Hg$ dissociation from food, a constant inflow of fresh seawater, and a conservative behavior of $Me^{202}Hg$.

less than measured. It was therefore concluded that $Me^{202}Hg$ leaching from the fish food flakes was not the main source of the $Me^{202}Hg$ in the dissolved phase. Nevertheless, regardless of the source of $Me^{202}Hg$ in the seawater, its dissolved concentrations will have an impact on its uptake by different organisms.

Methylmercury accumulated by DGT

Both MeHg tracers in the dissolved phase were accumulated by the DGTs (Figure 4-7). Accumulation of $Me^{199}Hg$ and $Me^{202}Hg$ appeared to be linear over time, suggesting stable levels of dissolved MeHg during the experiment in the two tanks. Therefore, time-averaged concentrations for both MeHg isotopes were calculated according to Fick's equation (Table 4-3).

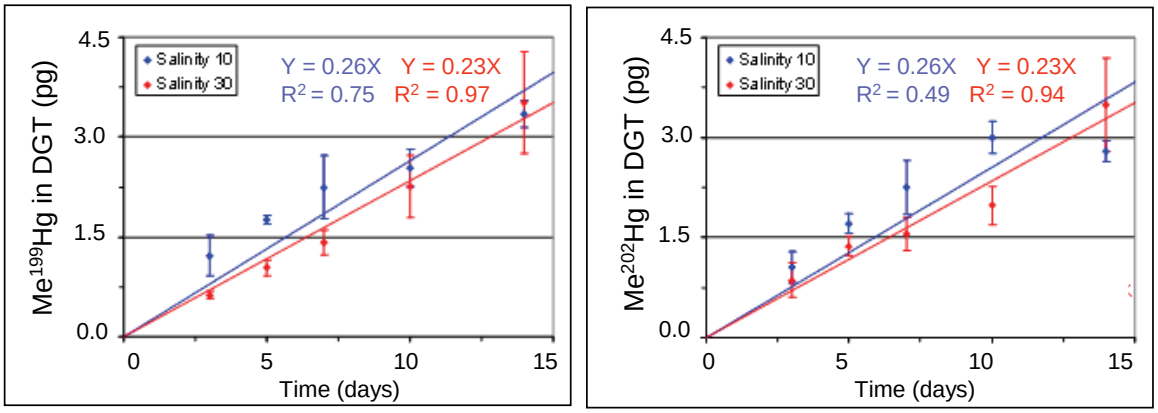

Figure 4-7. $Me^{199}Hg$ and $Me^{202}Hg$ accumulated by DGT over time. Mean values ± standard deviations (N=3).

Table 4-3. Average MeHg concentrations monitored by DGT in the dissolved phase for the experiments conducted in December 2006. Mean values± standard deviations (N=15).

Tank	Salinity (‰)	[$Me^{199}Hg$] (pg L^{-1})	[$Me^{202}Hg$] (pg L^{-1})
1	10	23.0 ± 5.1	22.2 ± 4.5
2	30	16.0 ± 1.5	18.0 ± 2.5

The MeHg concentrations calculated from the DGT contents were less than those measured directly in the tanks. Based on the diffusive coefficient for MeHgCl in polyacrylamide, the DGT concentrations corresponded to only 43 ± 9% and 49 ± 9% of $Me^{199}Hg$ and to 44 ± 22% and 46 ± 23% of $Me^{202}Hg$ in the two tanks (salinity 10 and 30 ‰, respectively). Using a lower diffusive coefficient in the DGT calculations (i.e. assuming the presence of other MeHg complexes), total MeHg concentrations

matched better. In the two seawater tanks, MeHg speciation in the dissolved phase was, therefore, not only dominated by chloride. Furthermore, in each tank, the discrimination by DGT was similar for both MeHg isotopes and $Me^{199}Hg$ and $Me^{202}Hg$ complexation was comparable.

The overall uncertainty associated with MeHg accumulated by DGTs was calculated as the average precision of the measurement reproducibility for each sampling time in the two tanks. Precisions of 14% and 15% were estimated, respectively, for $Me^{199}Hg$ and $Me^{202}Hg$ accumulated by DGT (N=30). Because of the extremely low MeHg levels in these experiments, it is not surprising that the overall uncertainty associated with MeHg accumulation was higher than found in the previous set of experiments.

Methylmercury accumulated by clams

As both MeHg tracers were present in the dissolved phase, both accumulated in the clams (Figure 4-8). Because the MeHg concentrations in seawater were stable, a linear relationship between MeHg uptake by clams and time was established. However, despite the fact that the monitored levels of the MeHg isotopes were the same in the water of each tank, $Me^{199}Hg$ appeared to be preferentially assimilated by the clams. The larger uncertainty in the $Me^{202}Hg$ concentration over time observed in seawater was probably related to the different times at which the MeHg isotopes appeared in the water. While $Me^{199}Hg$ was added directly to the water and immediately available for uptake, $Me^{202}Hg$ was spiked to the food and presumably took longer to leach into the water, causing a delayed uptake of $Me^{202}Hg$.

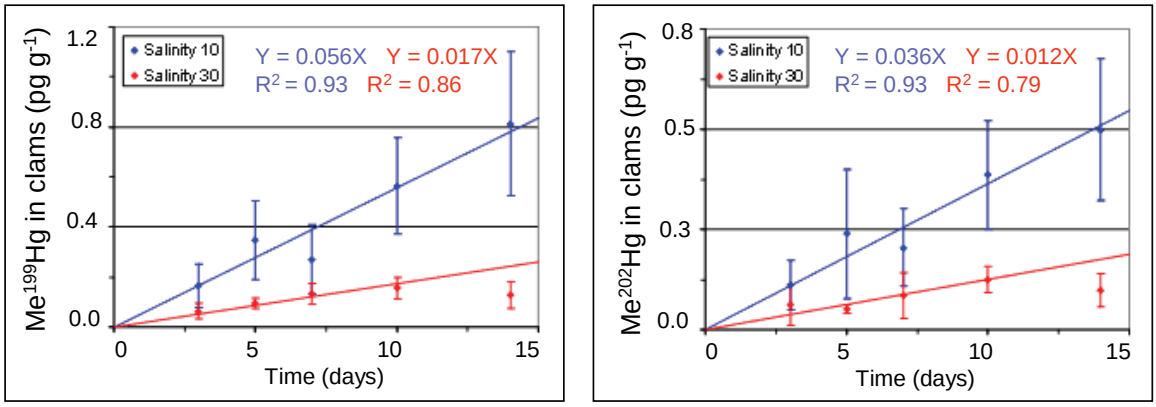

Figure 4-8. $Me^{199}Hg$ and $Me^{202}Hg$ accumulated by clams over time. Mean values ± standard deviations (N=3).

Yet, MeHg uptake by clams was similar for both isotopes suggesting that the aqueous phase served as sole source of MeHg in the tank. In other words, in this experiment, MeHg was not assimilated by the clams from food. Furthermore, MeHg accumulation in clams appeared to be higher for both isotopic tracers at lower rather than at higher salinity (a factor of 1.8 to 2.2). Lee et al. (1998) observed an inverse relationship between salinity and uptake of selected metals (Cd and Cr) in clams (*Potamocorbula amurensis* and *Macoma balthica*) whereas uptake of other metals (Zn for example) was not significantly affected. Both geochemical and physiological mechanisms may be involved in the response of metal influx to salinity change (Wright 1995). The most common geochemical explanation for increased metal uptake at low salinities is a change in metal speciation and the related increase of the free metal ion activity (Campbell 1995). Filtration rate, a physiological process, is also influenced by salinity: as the amount of water processed by the gills may vary with salinity, metal uptake by the organism will be affected. Moreover, the reduction of Ca^{2+} concentration at lower salinity can also promote metal uptake by reducing the competition between Ca and metal for the same transport site on the gill epithelium assuming a diffusion process (Bjerregaard and Depledge 1994). According to the DGT results in this experiment, MeHg speciation in the dissolved phase was similar in both tanks. Differences in MeHg uptake should, therefore, be attributed to a physiological response to change in salinity. Further research is needed to identify this physiological response and its influence on MeHg uptake.

The overall uncertainty associated with MeHg accumulated by clams was calculated as the average precision of the measurement reproducibility for each sampling time in the two tanks. Precisions of 39% and 51% have been estimated, respectively, for $Me^{199}Hg$ and $Me^{202}Hg$ accumulated by clams (N=30). Due to the extremely low MeHg levels in these experiments, the overall uncertainty associated with accumulated MeHg was slightly higher than found in the previous set of experiments.

In the previous experiment, where only a single dose of MeHg was added to the seawater, a strong correlation was found between MeHg accumulated by DGT and clams. Results obtained under continuous flow conditions showed a weaker correlation between DGT and clam contents for both MeHg isotopes (Figure 4-9). The large uncertainty associated with the MeHg accumulated by clams contributed greatly to this weakened correlation. However, combining the two data sets did not affect the overall correlation between MeHg accumulated by DGT and clams.

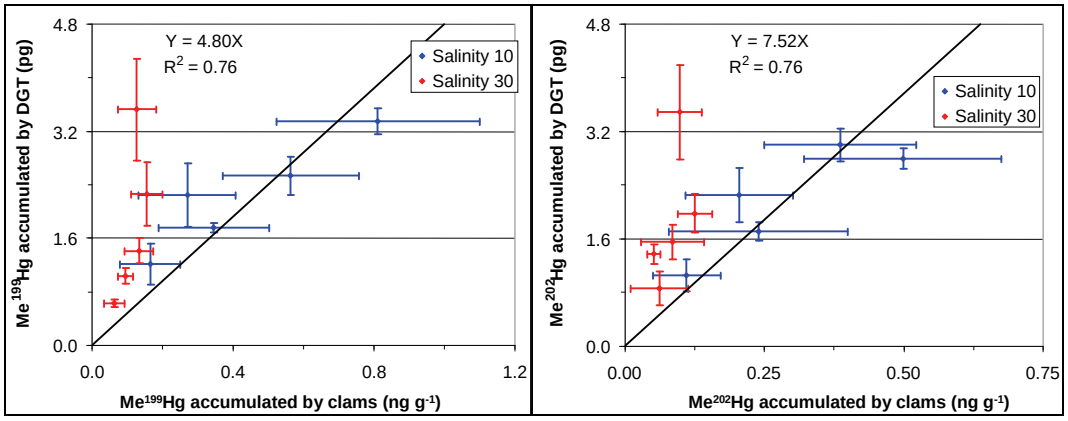

Figure 4-9. $Me^{199}Hg$ and $Me^{202}Hg$ accumulated by DGT versus $Me^{199}Hg$ and $Me^{202}Hg$ accumulated by clams (December 2006). Mean values ± standard deviations (N=3).

Figure 4-10 summarizes the overall correlation observed in the two experiments on MeHg accumulated by DGT and clams ($MeHg_{DGT}$=2.79 x $[MeHg]_{clam}$, R^2=0.89). Despite the changes in environmental factors (salinity, MeHg speciation, and temperature), DGTs reasonably predict MeHg accumulated by clams from the aqueous phase.

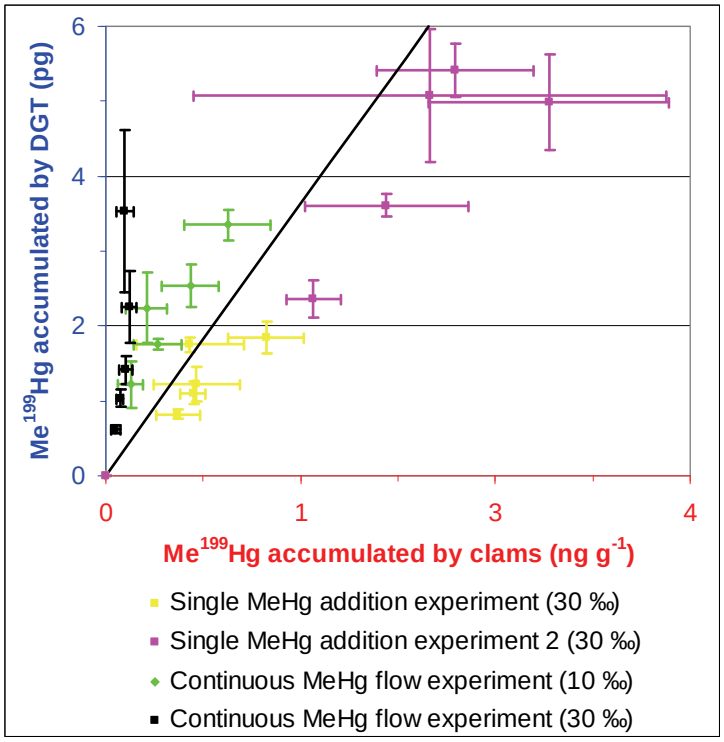

Figure 4-10. $Me^{199}Hg$ accumulated by DGT versus $Me^{199}Hg$ accumulated by clams in all tanks (February and December 2006). Mean values and standard deviations (N=3).

Methylmercury accumulated by fish

Both MeHg tracers were accumulated by fish (Figure 4-11). Accumulation of $Me^{202}Hg$ exceeded that of $Me^{199}Hg$, supporting the importance of food source over aqueous phase in MeHg bioaccumulation. Due to the significant fish mortality in the two tanks, only two fish were sampled in tank 1 (salinity 10 ‰) at 7 days and at 7, 10, and 14 days in tank 2 (salinity 30 ‰). The overall uncertainty associated with MeHg uptake by fish was calculated as the average precision of measurement reproducibility for each sampling time in the two tanks. Precisions of 47% and 26% were estimated, respectively, for $Me^{199}Hg$ and $Me^{202}Hg$ uptake by fish (N=26). Because of this large uncertainty and the low number of fish harvested, a linear relationship for MeHg bioaccumulation in fish with time was considered. Fish assimilated $Me^{199}Hg$, the water tracer, at a rate similar to that in clams. The gill, which serves as a passage for gases and other dissolved constituents from the external to the internal environment, is, therefore, a key organ for MeHg uptake from the aqueous phase. As a relatively small fraction of $Me^{202}Hg$ was in the dissolved phase, its concentration in fish resulted from both water and food exposure. The contributions of these two contrasting routes in MeHg bioaccumulation were calculated, and indicated that over 97% of the $Me^{202}Hg$ in fish originated from food in both tanks and only 3% from water. As the present experiments were conducted at environmentally relevant concentrations, the results likely reflect field conditions.

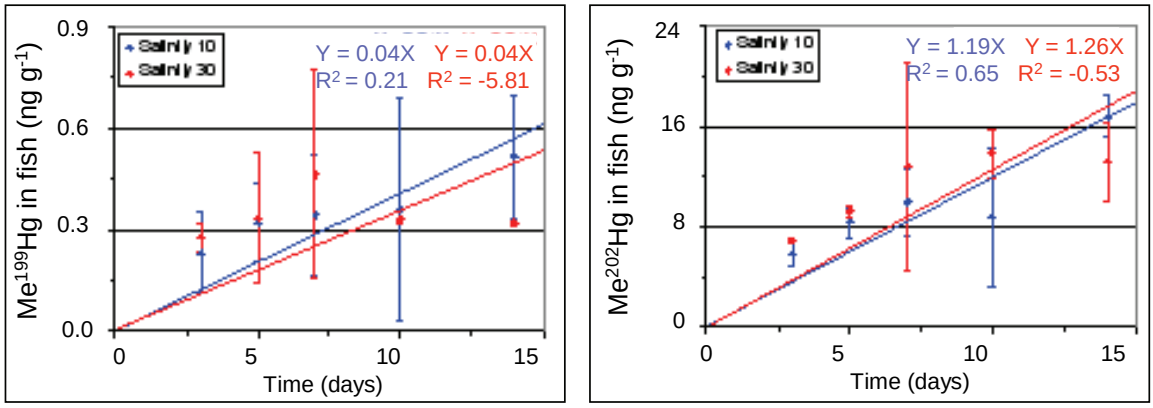

Figure 4-11. $Me^{199}Hg$ and $Me^{202}Hg$ accumulated by fish over time. Mean values ± standard deviations (N=3; except for salinity 10 ‰ 7 days and salinity 30 ‰ 7, 10, 14 days, where N=2).

Accumulation of MeHg in fish was correlated with MeHg in DGT (Figure 4-12), similar to accumulation in clams. The DGT results reflected the MeHg concentrations in fish for both isotopic tracers.

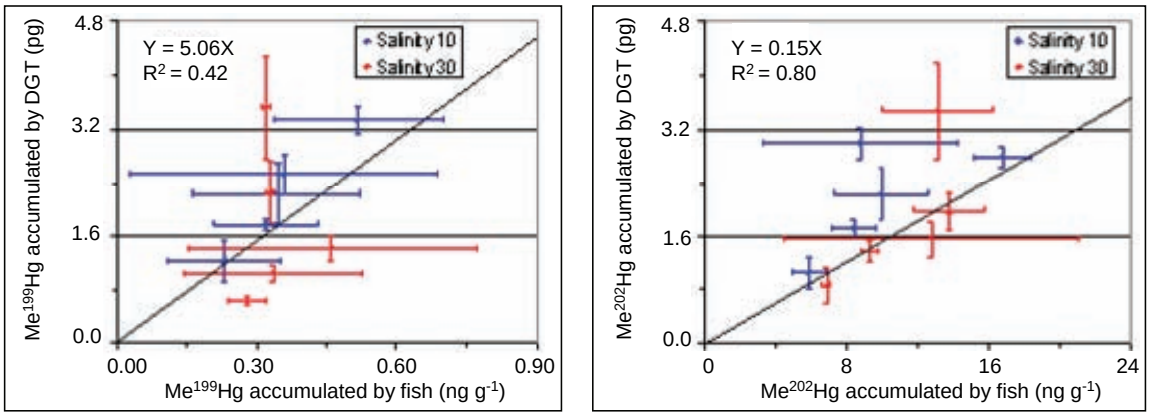

Figure 4-12. $Me^{199}Hg$ and $Me^{202}Hg$ accumulated by fish versus accumulated by DGT (December 2006). Mean values ± standard deviations (N=3).

Fish and DGT have different MeHg accumulation pathways, with fish accumulating $Me^{202}Hg$ largely directly from food and DGT from water. However, in the present experiment the level of $Me^{202}Hg$ in the dissolved phase was directly related to the amount of fish food delivered to the tank, and, therefore, the MeHg accumulated by fish was correlated with MeHg accumulated by DGT. Thus, DGTs can mimic direct MeHg uptake from the water by fish. However, in the field the MeHg available in food depends on the local food web, and, therefore, the relative contributions of MeHg from food and from the water may vary considerably with site.

Conclusions

The following conclusions can be drawn based on experiment results:

1. Laboratory experiments indicated a strong correlation between MeHg accumulation in clams and DGTs. Changes in salinity and in MeHg speciation in the dissolved phase equally affected MeHg accumulation by clams and DGTs. Both sentinels can, therefore, be used to estimate MeHg exposure from water. Thus, DGT appears to be a promising tool to describe the first step of MeHg biomagnification.

2. A large part of the Hg burden accumulated by fish is methylated and thought to accumulate primarily from dietary sources, but direct accumulation from water may also contribute. In the present study, both MeHg uptake routes were considered and investigated using two different MeHg isotopic tracers. Over 97% of the MeHg accumulated in fish was attributed to food and only 3% to water. Because the experiments were conducted at environmentally relevant concentrations and salinities, the results will

likely reflect in situ environmental conditions. As a coincidence of the MeHg release from food to water, a strong correlation between MeHg accumulated in fish and DGT was found for both MeHg isotopic tracers. Based on having a similar diffusion process, DGT devices may mimic MeHg uptake by fish from water. Under field conditions the MeHg availability in food depends on the local food web; therefore, the relative contributions of MeHg from food and from water may vary considerably.

3. Compared to organisms used for monitoring, MeHg values generated by DGTs are more reproducible and DGTs are easier to handle. Moreover, DGTs do not have a variable MeHg background as organisms have. MeHg in the DGT device corresponded without ambiguity to MeHg accumulated from water during the exposure period. Only a few DGT units would be required to assess the bioavailability of MeHg. As a larger number of fish and/or clams would have to be deployed and analyzed to reach the same goal, DGT sentinels may form a promising and relatively inexpensive means to estimate aqueous bioavailable MeHg in the environment. However, 1 pg MeHg accumulated by DGT would correspond to a relatively large range of MeHg accumulated by clams and a different range accumulated by fish. The latter ranges may change with changes in salinity and DOM, and knowledge of the links between MeHg body burdens and toxicity is still extremely limited.

5 Exploring Food Web Sources, Pathways, and Mercury Bioaccumulation in a San Pablo Bay Salt Marsh Using Multi-source Mixing Models

Introduction

Understanding the complex flow of organic matter through food webs is a fundamental pursuit of theoretical, basic, and applied ecology. Quantitative knowledge about food web structure has practical applications in measuring the effects of anthropogenic inputs, such as pollutant bioaccumulation in higher order predators (Cabana and Rasmussen 1994), in assessing the impacts of introduced species, and comparison of food webs geographically or temporally, such as may be needed to assess restoration and conservation efforts or to test the effect of climate change.

Many marsh restoration and enhancement projects are currently planned or underway in the San Francisco Bay area (Goals Project 1999). The re-establishment of wetlands in the San Francisco Bay/delta system, for which dredged sediment is used, has the potential for mobilizing mercury present in the sediments. The origin of this contamination in the Bay system is largely from the historic mining of mercury in the nearby coastal mountains. The total Hg (THg) levels in San Francisco Bay sediment range from 400 -1,080 ng g^{-1} dry weight (DW). This has resulted in total sedimentary THg levels at or greater than those in sediments relative to other aquatic ecosystems perceived to present a Hg environmental toxicity risk (e.g., the Everglades). The introduction of inorganic mercury to any wetland environment raises concerns related to the production of monomethylmercury (MeHg). MeHg is the most toxic Hg species and cause of the greatest concern. MeHg is a potent toxin that efficiently biomagnifies in food webs.

Although the importance of marshes as sources of MeHg has been realized, studies of the internal cycling of mercury (Hg) or production of MeHg within wetlands were only initiated during the last decade. It is to be expected that marsh restoration projects will create not only new habitats with their associated food webs, but also impact food webs and

total mean daily loads (TMDLs) of Hg in San Francisco Bay. To date studies on food webs associated with San Francisco Bay marshes are scarce and no clear understanding of Hg bioaccumulation pathways exists.

Consumer diets, organic matter sources, and trophic levels can be estimated using empirically determined tracer levels in mixing models. Consumer stable isotope ratios reflect their foods (Peterson and Fry 1987; Sackett 1989) and trophic position in the food web, with fractionation rates of less than 1 ‰ per trophic level for $\delta^{13}C$ (Peterson and Fry 1987; Post 2002), 3 -3.6‰ per trophic level for $\delta^{15}N$ (Peterson and Fry 1987; Fry 1988; Post 2002; or more, according to McCutchan et al. 2003) and no significant change in $\delta^{34}S$ (Peterson et al. 1986; Peterson and Howarth 1987; Fry 1988, 1991; Michener and Schell 1994). Particularly for estuarine work the sulfur-carbon combination is the most powerful because of the favorable signal-to-noise ratio, where signal represents the difference originating from various food sources and noise represents the difference originating from various samples of the same food source (Peterson et al. 1986). The combination of carbon, nitrogen, and sulfur is powerful, because ambiguous carbon isotope values can be resolved by reference to sulfur isotope values, while nitrogen isotopes add information on trophic level but may vary with annual plant growth and senescence cycles (Cloern et al. 2002). The resolution of organic matter sources is more powerful when multiple isotopes are used simultaneously, but the mathematics can be difficult to implement. The scope of many multiple food source mixing models is limited by the sources and tracers (1-2 sources, 1-2 tracers), or the models focus on trophic structure rather than flow reconstruction, although some models do allow for a more complex set of potential sources. In many cases this modeling is an overly simplistic way of partitioning food resources, particularly in estuarine systems, which can have multiple source inputs (Peterson and Howarth 1987; Cifuentes et al. 1988; Fry 1988). A set of two complementary mixing models has been identified, i.e. SOURCE and STEP, that use linear programming techniques with multiple tracers, to estimate the dominant primary producer sources of consumers, and their diets and trophic levels, regardless of the number of sources and trophic steps (Lubetkin and Simenstad 2004).

Results of a recent study on food webs associated with the China Camp tidal salt marsh adjacent San Pablo Bay area suggested that inputs from bay macroalgae, C_4-grasses, marsh-diatoms, marsh-cyanobacteria, and

marsh-pool filamentous algae provide the organic matter that forms the base of the food web, supporting invertebrates, fish, mammals and birds. These organisms together occupy four habitat types, i.e., the bay, the low-, mid- and high-salt marsh. MeHg accumulation among these organisms decreased in the order of song birds> fish> mammals, and did not follow ranking into their approximate trophic levels based on their $\delta^{15}N$-values.

Objectives

The objectives of the current study were to use the companion multiple source mixing models SOURCE and STEP to quantify food web sources and trophic structure using multiple stable isotopes, and, thus, contribute to elucidating the trophic relationships leading to MeHg bioaccumulation.

Methods

The SOURCE and STEP models were developed by Lubetkin and Simenstad (2004), and tested on a data set from a study tracing organic matter flows in a saltmarsh estuary. For clarity, both models are summarized below. Both models follow a mathematically simple, first-order approach.

Systematic mathematical assumptions

For SOURCE and STEP to work, the tracers and sampling procedure must conform to some basic assumptions, which require the following.

1. All equations must be linearly independent.
2. Consumer uptake of the tracer must be linear with respect to tracer concentration in the food source, and the assimilation rate of the tracer must be known. This implies that a threshold level of the tracer is not required before uptake occurs, nor is there a saturation level after which no more of the tracer is incorporated into its tissue. Even if certain tracers do not strictly meet this assumption, if uptake is approximately linear over the range of values of interest, the tracer may still be used in these models.
3. Each source must have a distinct tracer signature. SOURCE and STEP are based solely on the tracer signatures in the system; therefore, the models predict that any organisms having similar tracer signatures will function similarly, regardless of how different their biological roles in the ecosystem may be. To be considered distinct, the source tracer signatures must exceed a certain difference measure (see Nearest Neighbor Distance).

4. Tracer signatures of all major organic matter sources contributing to the food web must be known. That is, if a food source is important enough to be a significant contributor to many consumers, directly or indirectly, a sample of the source has been obtained and its tracer signature analyzed.
5. At the level of the individual organisms, variation in tissue level fractionation has been accounted for in the sampling protocol, and the tracer levels are representative of the whole organisms or that part eaten by consumers.
6. In SOURCE it is also assumed that all organisms have the same fractionation rates for each tracer. In reality, there will be some variability about the magnitude of trophic level shifts and in the average tracer values for each organism.

In these models, the working definition of an organism's trophic level is the number of times an average unit of primary production was metabolically processed to become the tissue of the organism of interest; autotrophs are defined as trophic level zero. Trophic levels are not restricted to integers. Thus, a strict herbivore would have trophic level 1, but a consumer that eats both plants and other animals would have a trophic level greater than 1, proportionally reflecting the mixture (Equation 5.9).

SOURCE: Primary producer inputs and trophic level

SOURCE estimates the mixture of autotrophic sources that have been assimilated, directly or indirectly, into a consumer's tissues and the consumer's trophic level. By mass balance, consumer tracer signatures will reflect the mixture of food or prey in the diets, and through them the mixture of autotrophic sources at the base of each trophic pathway. In addition, the tracer signatures reflect the biofractionation that occurred at each trophic transfer.

Mathematically, n autotrophic sources contribute fractions s_1 to s_n to a consumer's diet. Each source i contributes its own characteristic tracer values, t_i, u_i, and v_i, to the consumer. If the average trophic level shifts for tracers t, u, and v are α, β, and γ, respectively, the consumer's overall tracer levels C_t, C_u, and C_v, are a reflection of its diet and trophic level, L, such that

$$s_1 + s_2 + s_3 + ... + s_n = 1 \quad (5.1)$$

$$s_1 t_1 + s_2 t_2 + s_3 t_3 + ... + s_n t_n + \alpha L = C_t \quad (5.2)$$

$$s_1 u_1 + s_2 u_2 + s_3 u_3 + ... + s_n u_n + \beta L = C_u \quad (5.3)$$

$$s_1 v_1 + s_2 v_2 + s_3 v_3 + ... + s_n v_n + \gamma L = C_v \quad (5.4)$$

where $0 \leq s_i \leq 1$.

As there are more sources than tracers, it is mathematically impossible to find an exact solution to this mixing model. All of the variables cannot be solved simultaneously, so sets of linear equations for subsets of sources are solved iteratively in sequence. For example, with three tracers there are four equations, so any combinations of four variables can be considered to simultaneously find a unique solution for that combination. In practice, the subset of unknowns solved for in SOURCE always includes the organism's trophic level because excluding the trophic level would disregard the effects of biofractionation. SOURCE solves for L and all possible mixtures of as many sources as there are tracers to find valid corner point solutions (i.e., s_1, s_2, s_3 and L, then s_1, s_2, s_4 and L, and so on through all combinations of three sources). For each combination of three sources and L there is exactly one mixture that will have C_t, C_u, and C_v, which is found using Gaussian elimination (Hillier and Liebermann 1990). Each resultant mixture is a corner point of the solution space (Hillier and Liebermann 1990). There will be mathematical solutions for all the combinations of sources, but some are not physically or biologically possible because not all the fractions fall between 0 and 1. In the example only two corner points are acceptable that outline the solution space. With larger numbers of sources, there are more corner points to consider, and more than two may fall within the allowed solution space.

STEP: Direct calculation of consumer diet pathways

The tracer data can be used to determine the direct links between consumers and their diets, composed by autotrophic as well as heterotrophic sources, with STEP. Here each consumer's signature is modeled as a composite of the foods it ate modified by one metabolic fractionation.

Mathematically, STEP is represented as:

$$f_1 + f_2 + f_3 + \ldots + f_m = 1 \tag{5.5}$$

$$f_1 t_1 + f_2 t_2 + f_3 t_3 + \ldots + f_m t_m = C_t - \alpha \tag{5.6}$$

$$f_1 u_1 + f_2 u_2 + f_3 u_3 + \ldots + f_m u_m = C_u - \beta \tag{5.7}$$

$$f_1 v_1 + f_2 v_2 + f_3 v_3 + \ldots + f_m v_m = C_v - \gamma \tag{5.8}$$

where f_1 to f_m are the fractions that each of the m potential foods contribute to the consumer's diet. Whereas the s_is in SOURCE are measures of the autotrophic sources the consumer assimilates directly and indirectly, the f_is in STEP quantify direct incorporation of foods. Again, each fraction must fall between 0 and 1. The pool of potential foods may, in theory, include all organisms in the system for which there are tracer measurements. Thus, 'cannibalism' is allowed, where cannibalism refers to consumption of food organisms that have the same general trophic level and feeding practices, and hence similar tracer signatures. In cases where biological knowledge of the system would give sufficient reason to exclude one or more organisms as potential foods, the number of unknowns to examine for that organism can be reduced.

STEP simultaneously solves for combinations of as many foods as there are equations (i.e., with three tracers there are four equations, and sets of four foods can be examined at a time) and calculates the center of mass of the acceptable corner points where all the fractions fall between 0 and 1, generating estimates of each consumer's diet. STEP is applied to each consumer in the system (and each could potentially have a unique list of possible foods to consider). Once all the direct diets have been estimated, trophic levels are calculated for each consumer. Each consumer's trophic level is a weighted average of the trophic levels of its food plus one:

$$f_1 L_1 + f_2 L_2 + f_3 L_3 + \ldots + f_m L_m + 1 = L \tag{5.9}$$

Where the f_is are the fractions of each food that contribute to the consumer's diet, L_is is the trophic levels of those foods, and L is the trophic level of the organism of interest. Once the diet of the consumer is known, that information can be used with the information about its diet items' diets, and so on, iteratively through the food web, to estimate the

consumer tissue's primary producer's origins. These results can then be compared with SOURCE model estimates.

Nearest neighbor distance

Both models use only the tracer signatures to distinguish between source inputs, so those values must be distinct if the organic matter sources are to be considered separately (Sackett 1989; Michener and Schell 1994). To determine how much the difference between any two signatures affects the accuracy of the calculated estimates, a 'nearest neighbor' criterium was developed that related source separation to the discrimination power of the models (Lubetkin and Simenstad 2004; Lubetkin 1997). Lubetkin and Simenstad (2004) defined the squared normalized distance between the source signatures in r-space, where r is the number of tracers measured. Each of the r tracers may have a distinct range of values that it can take, and the ranges differ from tracer to tracer. The relationship of the squared nearest neighbor distance (NND^2) between points in r-space to $|\varepsilon_i|$ can be used to determine the minimum value of separation for two sources to be considered distinguishable using their tracer levels. Note that two sources may have statistically different tracer values, using a two-sample t-test or some other measure (Rosing et al. 1998), without being far enough apart in tracer space to be distinguishable by the models.

Model performance

Both models have been evaluated by the developers using two methods. The first assumed perfect data (i.e., there was no error in measured tracer signatures or variability between samples of the same species) for the tracer signatures of all the organisms in the system and precisely known trophic level shifts. These simulations made it possible to analyze how the models perform under ideal conditions and focused on the mathematical validity of the center of mass estimates. The second method introduced variability into the tracer signatures and trophic level shifts, such as would be expected in real data from multiple samples (Post 2002; Olive et al. 2003), to examine how natural variability in the data would affect the model's performances. The strategy behind these simulations was to create flows through four different-sized 'food webs,' use those flows to calculate the resultant tracer signatures in primary and secondary consumers, and then evaluate how well SOURCE and STEP performed in recreating the flows using only the tracer signatures. Each of the simulated data sets consisted of randomly assigned trophic links from producers to primary

consumers and secondary consumers. Those links were used to calculate signature amounts of three tracers in each consumer based on the tracer signatures of the producers. The tracer signatures also had a trophic level component, with trophic level shifts analogous to $\delta^{15}N$, $\delta^{13}C$, and $\delta^{34}S$ (strong, weak, and none). Flows were created based on four to seven sources in each set of simulations. All simulations and analyses were conducted using the programming language S-PLUS. The models' performances were evaluated by calculating the differences between the model-estimated diet fractions, primary producer sources and trophic levels, and the true values of those quantities. For true values of the contributing organic matter sources s_1 to s_n, the error of each estimate is $\varepsilon_i = s'_i - s_i$ for i in 1 to n, where s_i' is the center of mass estimate of the contribution from the ith organic matter source. For example, if a consumer was estimated to have 60% of its diet derived from primary producer A and the true value was 55%, the resulting ε_i was $0.60 - 0.55 = 0.05$.

SOURCE has a tendency to overestimate those sources that contribute relatively small amounts to the consumer's tracer signature and underestimate the importance of those that are more dominant. When all three tracers were used, 75-95% of the estimates had $|\varepsilon_i| < 0.10$. Of those estimates more than half were within 0.05 of the true values. As expected, using a greater number of tracers improved estimate accuracy. The overall accuracy of STEP was higher than that of SOURCE. The estimates of proportional contributions of primary producers to consumer diets using STEP (average $|\varepsilon_i|$ ranging from 0.03 to 0.05) were closer to the true values than the SOURCE estimates, as were the indirectly calculated trophic levels. In the simulations with variability in the data, SOURCE estimates had an average standard deviation of 0.20 when all three tracers were used, and 0.28 when the two strongly fractionating tracers were used, while STEP had lower average standard deviations of 0.14 and 0.16, respectively. Generally, the standard deviations from the center of mass estimates from both models were greater than the true error of the estimates. Therefore, the standard deviation could be used as a measure for the model's precision. More than 86% of the trophic level estimates generated by STEP were within 0.3 trophic levels of the true values and more than a third were within 0.1 (Note that these are not fractions, so a difference of 0.3 does not represent 30% error).

Case study China Camp salt marsh

SOURCE and STEP were applied to $\delta^{13}C$, $\delta^{15}N$, and $\delta^{34}S$ data of food web organisms associated with a tidal salt marsh at China Camp on San Pablo Bay, California (Best et al. 2007, Chapter 7). The isotopic signatures of 13 primary producer sources and 18 consumers were included in the simulations. The primary producer sources included the marsh macrophytes *Spartina foliosa* and its litter, *Salicornia virginica* and its litter, *Distichlis spicata*, *Atriplex triangularis*, particulate organic matter from the marsh pond and bay, phytoplankton from the marsh pond and bay, epipelic marsh diatoms and cyanobacteria, marsh filamentous algae, and the bay macroalgae *Ulva* and *Fucus* species. The consumers included invertebrates, fish, mammals, and birds, and fell into a variety of overlapping feeding categories. As $\delta^{34}S$ is less commonly measured than $\delta^{14}C$ and $\delta^{15}N$, the results of SOURCE and STEP using just $\delta^{14}C$ and $\delta^{15}N$ were examined and then results with all three isotopes were studied to illustrate how the inclusion of more information affected the estimates.

Results and Discussion

Simulation results

After calculating their isotopic nearest neighbor distances, the producers were categorized into nine groups and the consumers into eight groups. Among the producers, six groups were composed by a single species, considering 'POM' and 'phytoplankton' as one species, and three groups by two to three species (Table 5-1). Among the consumers, five groups were composed by a single species and four groups by four to five species with within-group differing habitats (Table 5-2). With SOURCE, the average standard deviation was 0.25 when all three isotopes were used, and 0.30 when only $\delta^{14}C$ and $\delta^{15}N$ were used with the China Camp data. With STEP the average standard deviation was 0.14 when all three isotopes were used, and 0.17 with only $\delta^{14}C$ and $\delta^{15}N$. All four values were lower than the corresponding values from the simulations.

Table 5-1. Primary producer sources and stable isotope ratios of samples collected from the China Camp marsh and adjacent San Pablo Bay area. Data are sample size (N) and mean values (SD). Group distinction based on the criterium of squared nearest neighbor distance between groups being >0.10. POM = particulate organic material.

Primary producer source	Marsh/bay	N	$\delta^{13}C$ (‰)	$\delta^{15}N$ (‰)	$\delta^{34}S$ (‰)
Group 1					
POM	Bay	2	-24.2 (0.2)	5.9 (0.8)	16.5 (0.9)
Group 2					
POM	Marsh	2	-21.7 (0.8)	3.4 (1.3)	13.4 (0.8)
Group 3					
Spartina foliosa (C_4)[a] (Pacific cordgrass)	Marsh	6	-14.8 (0.5)	8.8 (3.0)	7.8 (4.2)
Spartina foliosa-litter	Marsh	3	-15.6 (0.6)	7.7 (0.9)	8.7 (1.6)
Group 4					
Salicornia virginica (C_3)[a] (common pickleweed)	Marsh	5	-27.7 (0.9)	6.4 (1.5)	12.9 (1.2)
Salicornia virginica-litter	Marsh	3	-26.1 (0.4)	9.1 (0.6)	14.6 (0.9)
Group 5					
Phytoplankton	Bay	2	-29.5 (3.9)	12.2 (0.6)	11.9 (0.1)
Group 6					
Phytoplankton	Marsh	3	-23.0 (0.1)	4.9 (0.3)	3.6 (2.1)
Diatoms	Marsh	3	-20.2 (0.2)	4.4 (1.1)	5.6 (0.4)
Cyanobacteria	Marsh	3	-20.9 (1.3)	4.4 (0.4)	7.6 (1.4)
Group 7					
Filamentous algae	Marsh	3	-16.9 (0.9)	2.0 (1.3)	13.7 (4.7)
Distichlis spicata (C_4) (saltgrass)	Marsh	3	-14.8 (0.3)	5.1 (0.2)	14.5 (0.2)
Group 8					
Ulva sp.	Bay	3	-15.6 (0.4)	13.5 (0.2)	18.2 (0.7)
Fucus sp.	Bay	3	-16.7 (0.7)	14.4 (1.3)	17.6 (0.4)
Group 9					
Atriplex triangularis (C_3) (fathen)	Marsh	3	-27.4 (0.4)	2.7 (1.1)	16.6 (0.3)

Note: [a] Three of the five samples were collected at the HAAF marsh. These samples did not differ significantly in stable isotope composition and Hg species from other samples of the same plant species.

Table 5-2. Consumers and stable isotope ratios of samples collected from the China Camp marsh and adjacent San Pablo Bay area. Data are sample size (N) and mean values (SD). Group distinction based on the criterium of squared nearest neighbor distance between groups being >0.10.

Consumer	Marsh/bay	N	$\delta^{13}C$ (‰)	$\delta^{15}N$ (‰)	$\delta^{34}S$ (‰)
Group 1					
Microtus californicus (California vole)	Marsh	1	-23.2 (-)	10.7 (-)	14.7 (-)
Reithrodontomys raviventris (Salt marsh harvest mouse)[a]	Marsh	1	-23.1 (-)	12.7 (-)	14.9 (-)
Laterallus jamaicensis coturniculus (California black rail)[b]	Marsh	1	-24.8 (-)	13.5 (-)	15.8 (-)
Geukinsia demissa (Ribbed mussel)	Bay	9	-23.1 (1.1)	11.1 (1.2)	15.5 (1.3)
Group 2					
Snail sp.	Marsh	1	-25.5 (-)	4.1 (-)	10.2 (-)
Group 3					
Melospiza melodia samuelis (Song sparrow)[c]	Marsh	3	-20.6 (0.8)	12.7 (0.0)	15.0 (0.2)
Potamocorbula amurensis (Asian clam)	Bay	1	-20.9 (-)	11.6 (-)	13.3 (-)
Shrimp sp.	Bay	6	-19.6 (0.4)	15.4 (1.6)	14.7 (1.4)
Carcinus maenas (European green crab)	Bay	8	-19.0 (3.5)	14.1 (1.4)	15.4 (0.7)
Group 4					
Macoma balthica (Baltic clam)	Bay	3	-18.0 (2.6)	13.1 (0.8)	11.9 (1.0)
Nereis vexillosa (Pile worm)	Bay	2	-15.8 (0.5)	14.2 (0.0)	11.4 (2.0)
Worm sp.	Bay	2	-17.1 (0.2)	14.9 (0.5)	10.4 (3.1)
Leptocottus armatus (Pacific staghorn sculpin)	Bay	9	-17.6 (2.6)	16.3 (1.2)	13.5 (0.7)
Platichthys stellatus (Starry flounder)	Bay	8	-18.3 (3.8)	15.3 (1.5)	11.8 (1.6)
Group 5					
Orchestia traskiana (Amphipod)	Marsh	6	-22.5 (1.2)	8.0 (1.3)	17.2 (0.5)
Group 6					
Hemigrapsus oregonensis (Yellow shore crab)	Marsh	2	-16.0 (1.0)	13.5 (0.9)	15.7 (0.7)
Group 7					
Clevelandia ios (Arrow goby)	Bay	3	-14.8 (1.6)	15.6 (1.2)	12.7 (0.6)
Group 8					
Cicindela sp. (Tiger beetle)	Marsh	1	-22.3 (-)	2.2 (-)	6.7 (-)

Notes: Specimen found dead: [a] in HAAF marsh (December 2004); [b] in China Camp marsh (April 2002); [c] in China Camp marsh (March and June 2000, May 2002).

Based on trends in the collective isotopic distributions without a modeling approach, Best et al. (2007, Chapter 7) have suggested that inputs from bay macroalgae, C_4 grasses, marsh diatoms, -cyanobacteria, and -filamentous algae provide the organic matter that forms the base of the food web associated with the China Camp salt marsh, supporting invertebrates, fish, mammals, and birds. Since no specific or quantitative information could be derived from these trends, multiple source mixing modeling was explored to deliver this type of information.

SOURCE estimates of autotrophic sources in consumer diets were made using all three isotopes. Estimates>5% are described below. Major producer contributors are listed with their diets in order of decreasing fraction, to the diet of

- Consumer group 1 (CG1; vole, harvest mouse, black rail, mussel) were producer group 9 (PG9) with 38%> PG1> PG4> PG2> PG8.
- CG3 (song sparrow, Asian clam, shrimp, green crab) were PG8 with 19%> PG1> PG7> PG4.
- CG4 (Baltic clam, worms, sculpin, flounder) were PG3 with 27%> PG6> PG8> PG7> PG2> PG1.
- CG6 (shore crab) were PG8 with 60%> PG7> PG3.
- CG7 (goby) were PG7 with 46%> PG3> PG8> PG6.

The SOURCE predictions of the diets of CG2 (snail spec.), CG5 (amphipod), and CG8 (Tiger beetle) generated negative values indicating that not enough relevant information was available to predict their diets. Three stable isotope-based predictions were less variable than the predictions based on the two isotopes $\delta^{13}C$ and $\delta^{15}N$ (smaller standard deviations) (Figure 5-1).

STEP estimates of direct food-based interactions between the evaluated producers and consumers were also made using all three isotopes. STEP estimates of diet composition characterized higher order consumers as directly consuming a smaller percentage of primary producers than lower order consumers (Figure 5-2). Because of the increased number of potential food sources, STEP examined many more combinations of food sources than SOURCE did. According to Lubetkin and Simenstad (2004), the smaller fractions estimated using STEP ($f_1 \leq 10\%$) probably reflect a few mathematically possible but biologically unlikely combinations of food sources that yielded the appropriate consumer isotopic signatures.

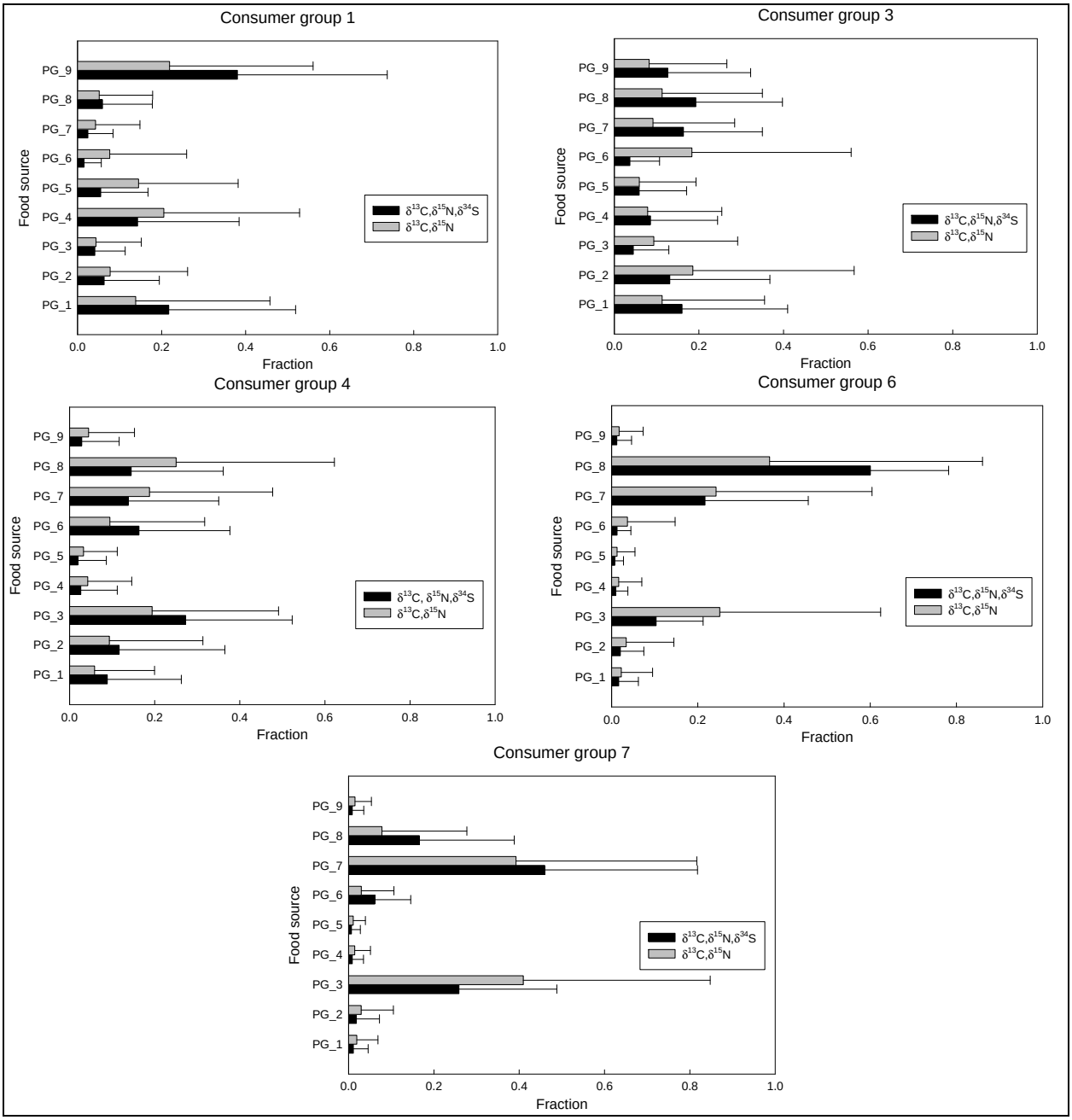

Figure 5-1. SOURCE estimates of the fractions derived from each food source for selected consumer groups. Black bars show estimates based on all three isotopes and grey bars based on $\delta^{13}C$ and $\delta^{15}N$. Mean values and standard deviations. Abbreviations: PG = producer group.

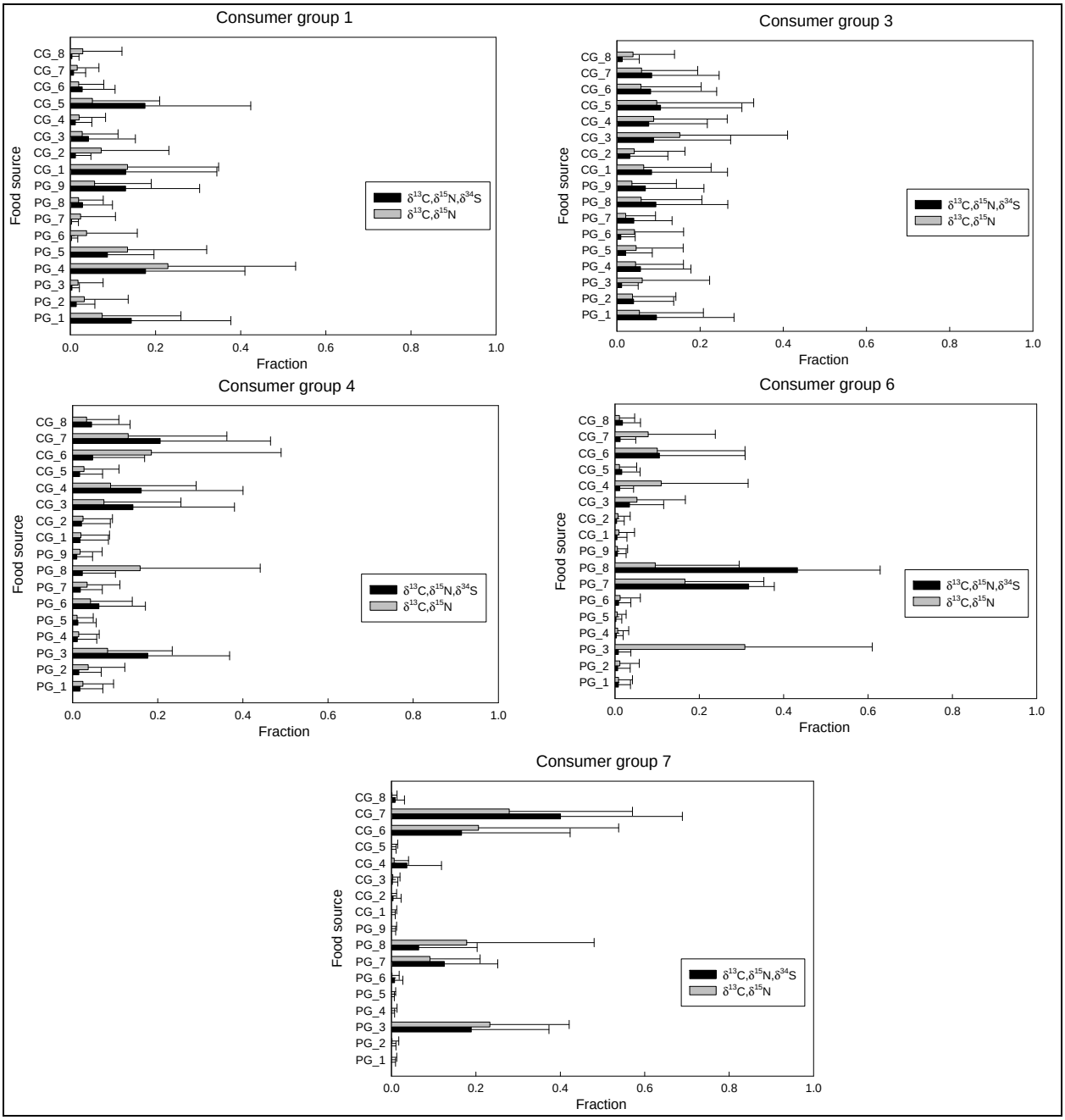

Figure 5-2. STEP estimates of the fractions derived from each food source for selected consumer groups. Black bars show estimates based on all three isotopes, and grey bars based on $\delta^{13}C$ and $\delta^{15}N$. Mean values and standard deviations. Abbreviations: CG = consumer group; PG = producer group.

Since these small sources do not significantly contribute to the diet (Lubetkin 1997), they are not further discussed here. The major foods for each diet were as follows:

- CG1 (vole, harvest mouse, black rail, ribbed mussel) were PG1 of 14%, PG4 of 18%, PG9 of 13%, CG1 of 13%, CG5 of 18%.
- CG3 (song sparrow, Asian clam, shrimp, green crab) were PG1 of 10% and CG5 of 10%.
- CG4 (Baltic clam, worms, sculpin, flounder) were PG3 of 18%, CG3 of 14%, CG4 of 16%, and CG7 of 21%.
- CG6 (shore crab) were PG7 of 32%, PG8 of 43%, and CG6 of 11%.
- CG7 (goby) were PG3 of 19%, PG7 of 13%, CG6 of 17%, and CG7 of 40%.

Estimated trophic levels

The trophic levels calculated using SOURCE and STEP using all three isotopes covered a range of values reflecting the diet overlap between (groups of) organisms.

SOURCE trophic level estimates increased in the order of CG5 (amphipods) at 0.13< CG6 (shore crab)< CG1 (vole, harvest mouse, black rail, ribbed mussel)< CG3 (song sparrow, Asian clam, shrimp, green crab)< CG4 (Baltic clam, worms, sculpin, flounder), CG7 (goby) at 2.48 (Table 5-3). Two SOURCE estimates fell between 0 and 1, i.e., for CG5 (amphipods) and CG6 (shore crab), indicating that at least for those organisms too large a trophic level shift was used (of 3‰; Macko et al. 1982; Post 2002). Two other SOURCE trophic level estimates were negative, i.e., for CG2 (snails) and for CG8 (*Cicindela* spec.), indicating that insufficient information on the food sources for these organisms was available for the calculations.

STEP trophic level estimates increased in the same order as SOURCE estimates. Levels were of CG6 (shore crab) at 1.21, of CG1 (vole, harvest mouse, black rail, ribbed mussel) at 1.40, of CG3 (song sparrow, Asian clam, shrimp, green crab) at 1.77, of CG4 (Baltic clam, worms, sculpin, flounder) at 2.19, and of CG7 (goby) at 2.22 (Table 5-3). STEP levels could not be calculated for CG2, CG5, and CG8 for reasons stated above. STEP levels were slightly higher for CG6 but less than SOURCE levels for CG1, CG3, and CG7, reflecting the method by which they were calculated.

Three stable isotope (C, N, S) based estimates differed from the predictions based on the two C and N isotopes.

Construction of a food web associated with the China Camp salt marsh based on stable isotope data

Using the STEP estimated trophic levels as a basis for the overall structure and natural history information to relate organisms to marsh habitat, feeding mode, food items, predators, and continent of origin (endemic or exotic; Table 5-4), a food web diagram was constructed for the China Camp salt marsh and adjacent San Pablo Bay area (Figure 5-3). In this diagram the SOURCE value was used for CG5 to enable placing amphipods as a food source in the web. In this diagram only major food web relationships explaining $\geq$10% of the diet are outlined and discussed, because this level has been described as the probable cut-off level for resolution (Lubetkin and Simenstad 2004).

Following this diagram, the China Camp salt marsh and adjacent San Pablo Bay area encompassed three habitats based on elevation: high marsh, low marsh, and nearshore bay.

On the high marsh, main sources of photosynthetically derived energy (producers) were the higher plants *S. virginica*, *D. spicata*, *A. triangularis*, and marsh-filamentous algae in the marsh ponds. Of the higher plants, *S. virginica* was a considerable food source of the herbivorous consumers, vole and harvest mouse. *D. spicata* was also a considerable food source of the harvest mouse as well as a minor food source of the carnivorous goby in the nearshore bay, probably indirectly through its detritus concentrated in worms (Figure 5-2). *A. triangularis* served as a minor food source of the harvest mouse. The filamentous algae of the marsh ponds were the major food source of the herbivorous/ omnivorous shore crab, a mobile inhabitant of the low marsh. The food sources of the omnivorous black rail, with an isotopic composition similar to those of the vole and harvest mouse, were in decreasing order of importance amphipods on the low marsh, and ribbed mussel and POM in the nearshore bay. The greatest trophic level was represented by the song sparrow that fed to a limited extent on amphipods on the low marsh.

Table 5-3. Estimated trophic levels of consumers collected from the China Camp marsh and adjacent San Pablo Bay area, calculated using SOURCE and STEP with $\delta^{13}C$, $\delta^{15}N$, and $\delta^{34}S$. NA = Not applicable.

Consumer	Marsh/bay	SOURCE		STEP	
		C, N, S	C, N	C, N, S	C, N
Group 1		1.77	1.49	1.40	1.39
Microtus californicus	Marsh				
Reithrodontomys raviventris	Marsh				
Laterallus jamaicensis coturniculus	Marsh				
Geukinsia demissa	Bay				
Group 2		-1.07	-0.71	NA	NA
Snail sp.	Marsh				
Group 3		1.83	1.98	1.77	1.84
Melospiza melodia samuelis	Marsh				
Potamocorbula amurensis	Bay				
Shrimp sp.	Bay				
Carcinus maenas	Bay				
Group 4		2.18	1.97	2.19	1.93
Macoma balthica	Bay				
Nereis vexillosa	Bay				
Worm sp.	Bay				
Leptocottus armatus	Bay				
Platichthys stellatus	Bay				
Group 5		0.13	0.43	NA	NA
Orchestia traskiana	Marsh				
Group 6		0.86	1.31	1.21	1.67
Hemigrapsus oregonensis	Marsh				
Group 7		2.48	2.53	2.22	2.00
Clevelandia ios	Bay				
Group 8		-0.73	-1.16	NA	NA
Cicindela sp.	Marsh				

Table 5-4. Natural history information relating to marsh habitat, feeding mode, food items, predators, and continent of origin (endemic or exotic) of consumers, grouped by STEP based on their $\delta^{13}C$, $\delta^{15}N$, and $\delta^{34}S$ isotopic signatures, which were collected from the China Camp marsh and adjacent San Pablo Bay area.

Consumer	Marsh/bay	Feeding mode	Food items	Predators	EN/EX	Source
			Group 1			
Microtus californicus	High marsh	Herbivorous	*Salicornia*, other marsh vegetation	Many mammalian and avian	EN	1
Reithrodontomys raviventris	High marsh	Herbivorous	In summer *Salicornia and Distichlis* leaves, seeds, stems, *Atriplex* seeds; in winter grass, leaves	Snowy egret, Great egret, Great blue heron	EN	2, 3, 4, 5
Laterallus jam. coturniculus	High marsh	Omnivorous	Terrestrial insects (spiders), aquatic invertebrates (amphipods); possibly seeds	Harrier, great egret, great blue heron; possibly rats, feral cats, red foxes	EN	6
Geukinsia demissa	Nearshore bay	Suspension feeder; herbivorous	*Spartina* detritus; phytoplankton	Shore birds	EN	7
			Group 2			
Snail sp.	High marsh	Herbivorous	Higher plants; algal mats	?	?	
			Group 3			
Melospiza m. samuelis	High marsh	Predator; insectivore; seed eater	Insects feeding (in)directly on *Salicornia*; seeds; amphipods	Cats, hawks, owls	EN	4, 8, 9
Potamocorbula amurensis	Nearshore bay	Suspension feeder; omnivorous	Phytoplankton, zooplankton, bacteria, larvae, detritus	Diving ducks (scaup); starry flounder	EX	10, 11, 12, 13
Crangon franciscorum[a]	Nearshore bay	Predator; detritivorous	Mysids, amphipods, detritus	Benthivorous fish (staghorn sculpin, starry flounder)	EN	14, 15, 16, 17, 18

Consumer	Marsh/bay	Feeding mode	Food items	Predators	EN/EX	Source
			Group 3			
Palaemon macrodactylus[a]	Nearshore bay	Predator; detritivorous	Mysids, detritus	Benthivore fish (staghorn sculpin, starry flounder)	EX	15, 16, 17, 18
Carcinus maenas	Nearshore bay	Predator; omnivorous	Largely native benthic bivalves, shore crabs, sculpin, gobies, appendages; also worms, green algae	Larger crabs (*Cancer* and *Hemigrapsus* species)	EX	19, 20, 21, 22, 23
			Group 4			
Macoma balthica	Nearshore bay	Deposit/suspension feeder; herbivorous	Detritus, phytoplankton	Ducks, shore birds, gulls; siphon-eating fish (sculpin), crabs, shrimp	EX	13, 24, 25
Nereis vexillosa	Nearshore bay	Deposit feeder; omnivore; detritivorous	Detritus of *Spartina*, *Salicornia*, seagrass, macroalgae	Shore birds	EN	26, 27, 28
Worm sp.	Nearshore bay	Deposit feeder; detritivorous?	Detritus of *Spartina*, *Salicornia*, seagrass, macroalgae	?	?	
Leptocottus armatus	Nearshore bay	Predator; benthivorous	Shrimp, gobies, shore crab, amphipods, bivalve siphon tips	Diving ducks, great blue heron, western grebe, caspian tern, loons, cormorants, gulls, marine mammals	EN	29, 30
Platichthys stellatus	Nearshore bay	Predator; benthivorous	Amphipods, shrimp, bivalves	Marine birds and fish	EN	10, 31, 32

Consumer	Marsh/bay	Feeding mode	Food items	Predators	EN/EX	Source
			Group 5			
Orchestia traskiana	Low marsh	Deposit feeder; detritivorous	Senescent plant materials (*Spartina* and other plant species), microbes	Shore birds, song sparrows, shrimp, benthivore fish	EN	7, 33, 34
			Group 6			
Hemigrapsus oregonensis	Low marsh	Herbivore; omnivorous	Ulva, diatoms, green algae, small invertebrates, appendages; scavenges, may filterfeed	Shore birds, *Carcinus maenas*, otters	EX	35
			Group 7			
Clevelandia ios	Nearshore bay	Predator; benthivorous	Small invertebrates (copepods, amphipods, nematodes, worms); siphon tips; potential egg clutch and filial cannibalism	Staghorn sculpin	EN	21, 36, 37, 38
			Group 8			
Cicindela sp.	High marsh	Predator; insectivorous	Brine flies from marsh ponds; Carabid and Tenebrionid beetles around San Francisco Bay	Shore birds	EN	39

Notes: [a] Most likely shrimp species.

1. Lidicker 2000. 2. Fisler 1965. 3. Shellhammer 1998. 4. Maffei 2000a. 5. Shellhammer 2000. 6. Trulio and Evens 2000. 7. Peterson et al. 1986. 8. Smith et al. 1984. 9. Greenberg 1990. 10. Peterson 1997. 11. National Introduced Marine Pest Information System (NIMPIS) 2002. 12. Poulton et al. 2002. 13. Richman and Lovvorn 2004. 14. Carlton 1979. 15. Sitts and Knight 1979. 16. Grenier et al. 2002. 17. Takekawa et al. 2002. 18. Hieb 2006. 19. Cohen et al. 1995. 20. Williams 2004. 21. Maginnis 2006. 22. Jensen et al. 2007. 23. Washington Department of Fish and Wildlife (WDFW) 2009. 24. Black 1980. 25. Olafsson 1986. 26. Roe 1975. 27. Cohen and Carlton 1995. 28. Olivier et al. 1996. 29. Tasto 2000. 30. Meyer 2003. 31. Simstead et al. 1979. 32. Kline 2000. 33. Lopez et al. 1977. 34. Best unpublished 2009: derived from food items in present table. 35. Kozloff and Price 1996. 36. Svensson et al. 1998. 37. Hieb 2000. 38. Svensson and Karnemo 2007. 39. Maffei 2000b.

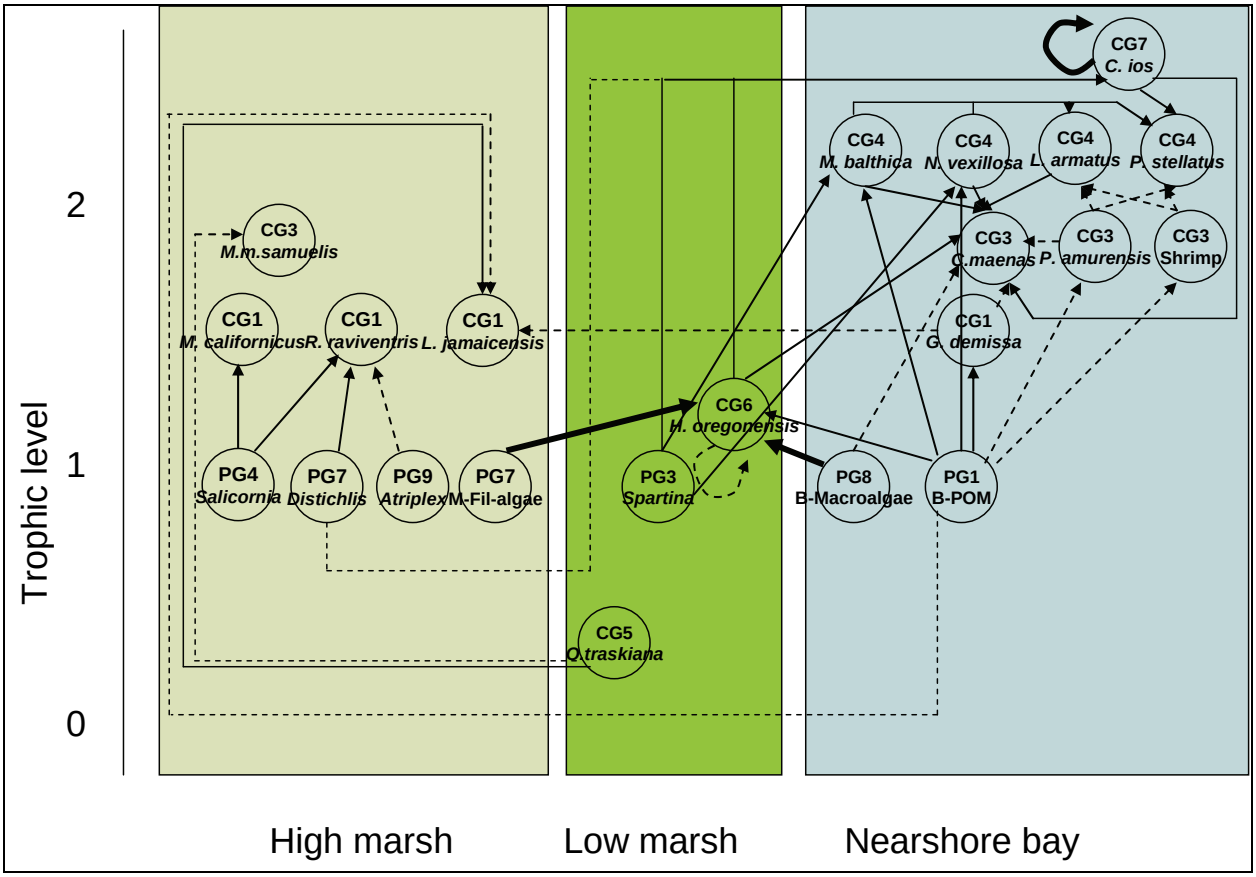

Figure 5-3. A food web associated with the China Camp salt marsh and adjacent San Pablo Bay area based on $\delta^{13}C$, $\delta^{15}N$, and $\delta^{34}S$ data evaluated by STEP[a] and natural history information provided in Table 5-5. Arrows go from the source/prey to the consumer/predator. The interrupted lines represent interactions accounting for 10-14% of an organism's diet. Lines represent food items contributing between 15% and 24% to an organism's diet. Heavy lines indicate that more than 25% of an organism's diet is estimated to come from a particular source/prey item. For clarity, estimated trophic interactions representing less than 10% of a consumer's diet are not shown. Abbreviations: CG = consumer group; PG = producer group. [a] For consumer group 5, SOURCE evaluation data are used, since data availability was insufficient.

On the low marsh, the main producer was *S. foliosa*. This plant species was a considerable food source for the deposit/suspension-feeding Baltic clam, deposit-feeding pile worm, and benthivorous goby in the nearshore bay largely via its senescent plant fragments and detritus. No specific large food source was identified for the deposit-feeding detritivorous amphipods, and therefore none was included in the diagram. However, most likely food sources for amphipods are detritus from higher marsh plants, of which not all were included in the present data set, and adherent microbes (Table 5-4). The major food sources for the herbivorous/omnivorous shore crab were filamentous algae in the marsh ponds and *Ulva* in the nearshore bay, followed by appendages of its own species.

In the nearshore bay, the main producers were bay-POM and macroalgae (*Ulva* and *Fucus* species). Bay-POM was an important food source of the suspension-feeding ribbed mussel, deposit/suspension-feeding Baltic clam, and deposit-feeding pile worm. It was a minor food source of the suspension-feeding Asian clam and shrimp in the nearshore bay, but also served as important food source of the herbivorous/omnivorous shore crab from the low marsh and a minor food source of the omnivorous black rail from the high marsh. The macroalgae served as a minor food source of the omnivorous green crab in the nearshore bay and were the main food source for the herbivorous/omnivorous shore crab of the low marsh. The ribbed mussel itself was a minor food source of the omnivorous green crab. Among the consumers at the next trophic level, CG3, the suspension-feeding, omnivorous Asian clam and shrimp used bay-POM as a minor food source. Additional major potential food sources of the latter animals, identified from literature but not included in the analyzed samples, were zooplankton, bacteria, and larvae for the Asian clam and mysids for the shrimp (Table 5-4). The omnivorous green crab predated mainly on animals of higher trophic levels (CG4 and CG5), Baltic clam (siphon tips), pile worm, sculpin, and goby, and the shore crab from a lower trophic level (CG6). In addition, the green crab used bay-macroalgae and Asian clams (siphon tips) as minor food sources.

Among the consumers of the next trophic level, CG4, the deposit/ suspension-feeding Baltic clam and deposit-feeding pile worm fed largely on *S. foliosa* litter and bay-POM. Sculpin and flounder both predated on the same and on lower trophic levels, but their isotopic signature pointed to different diets. Both fed largely on Baltic clam, pile worm, to less extent on Asian clam, and shrimp, but flounder fed also on goby. The consumer of the greatest trophic level identified, CG7, goby, had the largest variation in diet. Goby had its own species as main food source, which may be explained by egg clutch and filial cannibalism as described for other goby species (Svensson et al. 1998; Svensson and Karnemo 2007). Goby fed to a considerable extent on shore crab and *S. foliosa* detritus, and to a limited extent on *D. spicata* detritus. Since goby is not likely to consume detritus directly, the detritus may enter this fish with food items that feed largely on detritus, such as amphipods and worms.

Based on this diagram and information from literature relating to San Francisco Bay, three main points are apparent:

- Macrophytic primary producers of the salt marsh form important food sources of consumers. Live plants provide leaves and stems to graze, seeds to consume to vole and harvest mouse, and plant saps to insects which are consumed by song sparrows on the high marsh. Dead plants provide plant fragments and detritus, which contribute to the DOM pools in the nearshore bay. *S. virginica* and *D. spicata* are most important on the high marsh, while *S. foliosa* is most important on the low marsh and particularly in the nearshore bay (present study).

- Phytoplankton production in the nearshore bay is low because the turbidity of the water and elevated ammonium levels limit phytoplankton growth, while high filter-feeding activity of the exotic Asian clam removes phytoplankton (Cloern 1987; Cole and Cloern 1987; Kimmerer and Orsi 1996; this study). Thus, the bay-POM pool is dominated by detritus originating from marsh macrophytes. This result emphasizes the relatively minor role of bay phytoplankton for the China Camp marsh-associated food web, in contrast to results of several other salt marsh food web studies where *S. foliosa* detrital inputs to the food web are dominant in supporting consumers in Atlantic coastal salt marshes but phytoplankton or benthic algae may be equally important in gulf systems (as discussed by Kwak and Zedler 1997).

- Consumers in the nearshore bay are largely benthivorous, because of the low phytoplankton production. Consumers of all trophic levels feed partly on higher plant fragments and/or bay-POM, of which the relative contributions decrease with increasing trophic level. Higher order consumers are relatively more carnivorous than lower order consumers. The goby shows a considerable tendency to consume its own species. Two exotic species may strongly impact the food web: the Asian clam by removing phytoplankton and zooplankton (Nichols et al. 1990; Carlton et al. 1990; Kimmerer and Orsi 1996; this study), and the green crab by predation on largely native higher and lower order consumers (this study).

Pathways leading to MeHg bioaccumulation

In a recent study on food web(s) associated with the China Camp salt marsh by Best et al. 2007 (Chapter 7), the THg and MeHg concentrations

in the biota were also determined (Tables 5-4 and 5-5). Results indicated that the MeHg levels in birds were significantly greater than in the other consumer groups, and generally decreased in the order of birds> fish> invertebrates>mammals, but no clear relationship between trophic level based on $\delta^{15}N$ isotopic ranking and MeHg levels could be identified.

MeHg bioaccumulation in consumers with the greatest MeHg levels was evaluated, following the pathways identified by the current food web analysis and taking other information on the natural history of these organisms into consideration.

On the high marsh, the California black rail showed considerable MeHg bioaccumulation (1,130 ng g^{-1} DW; Table 5-5). Significant food sources of this bird are amphipods and bay-POM, among which amphipods may contribute 18% to the diet with a MeHg concentration of 103 ng g^{-1} (DW) and bay-POM 14% with a MeHg concentration of 1ng g^{-1}, pointing to amphipods as the main MeHg source. The song sparrow exhibited the greatest MeHg bioaccumulation of all organisms analyzed (of 1,343 ng g^{-1}; Table 5-5). The minor food source identified for this bird was amphipods, which may contribute 10% to the diet with a MeHg concentration of 103 ng g^{-1}, in this case also pointing to amphipods as an important MeHg source for this bird. A large part of the diet of song sparrows may consist of insects feeding directly or indirectly on *S. virginica* and seeds of the same plant species (Table 5-4). Although the vegetative plant material of *S. virginica* has a low level of MeHg (Table 5-4), the insects feeding on this plant may contain elevated levels of MeHg, as demonstrated by *Cicindela* spec. (Table 5-6), and seeds may have elevated MeHg levels as well, potentially leading to great MeHg levels in song sparrows.

On the low marsh, the shore crab showed moderate MeHg bioaccumulation (90 ng g^{-1}; Table 5-6). Most MeHg in this species may originate from the consumption of appendages of its own species, since the majority of this animals' diet is largely composed of plant materials with low MeHg concentrations (Table 5-5; Figure 5-3).

Table 5-5. Total-Hg, MeHg, and MeHg:THg ratios in primary producer sources of samples collected from the China Camp marsh and adjacent San Pablo Bay area. Data are sample size (N) and mean values (SD). Group distinction based on the criterium of squared nearest neighbor distance between groups characterized by three stable isotope ratios being >0.10. POM = particulate organic material. ND = not determined.

Primary producer source	Marsh/bay	N	THg (ng g^{-1} DW)	MeHg (ng g^{-1} DW)	MeHg : THg (x 100)
			Group 1		
POM	Bay	2	144 (-)	1.05 (-)	0.73 (-)
			Group 2		
POM	Marsh	2	ND	ND	ND
			Group 3		
Spartina foliosa (C_4)	Marsh	6	19 (7)	0.76 (0.31)	4.02 (0.73)
Spartina foliosa-litter	Marsh	3	61 (8)	0.97 (0.02)	1.67 (0.33)
			Group 4		
Salicornia virginica (C_3)	Marsh	5	21 (10)	1.02 (0.42)	5.29 (2.69)
Salicornia virginica-litter	Marsh	3	36 (7)	0.96 (0.02)	2.88 (0.61)
			Group 5		
Phytoplankton	Bay	2	578 (45)	41.0 (7.32)	7.16 (1.82)
			Group 6		
Phytoplankton	Marsh	3	654 (36)	16.9 (15.00)	2.29 (1.10)
Diatoms	Marsh	3	273 (4)	8.87 (1.08)	3.25 (0.42)
Cyanobacteria	Marsh	3	276 (10)	7.45 (2.57)	2.68 (0.86)
			Group 7		
Filamentous algae	Marsh	3	38 (11)	2.98 (0.58)	8.13 (1.75)
Distichlis spicata (C_4)	Marsh	3	23 (2)	0.61 (0.07)	2.73 (0.35)
			Group 8		
Ulva sp.	Bay	3	40 (13)	1.48 (0.19)	3.97 (1.42)
Fucus sp.	Bay	3	26 (3)	0.85 (0.08)	3.32 (0.17)
			Group 9		
Atriplex triangularis (C_3)	Marsh	3	9 (2)	0.30 (0.02)	3.36 (0.73)

Table 5-6. Total-Hg, MeHg, and MeHg:THg ratios in consumers collected from the China Camp marsh and adjacent San Pablo Bay area. Data are sample size (N) and mean values (SD). Group distinction based on the criterium of squared nearest neighbor distance between groups is characterized by three stable isotope ratios being >0.10.

Consumer	Marsh/bay	N	THg (ng g^{-1} DW)	MeHg (ng g^{-1}DW)	MeHg :THg (x100)
Group 1					
Microtus californicus	Marsh	1	50 (-)	44.9 (-)	90.1 (-)
Reithrodontomys raviventris	Marsh	1	25 (-)	17.5 (-)	69.7 (-)
Laterallus jamaicensis coturniculus	Marsh	1	1,652 (-)	1,130 (-)	68.5 (-)
Geukinsia demissa	Bay	9	171 (55)	74.6 (29.17)	43.1 (3.94)
Group 2					
Snail sp.	Marsh	1	131 (-)	36.0 (-)	27.5 (-)
Group 3					
Melospiza melodia samuelis	Marsh	3	1,678 (588)	1,343 (448)	80.5 (1.57)
Potamocorbula amurensis	Bay	1	127 (-)	60.5 (-)	47.5 (-)
Shrimp sp.	Bay	6	119 (34)	90.7 (28.10)	76.0 (5.39)
Carcinus maenas	Bay	8	263 (137)	216 (118.28)	80.3 (10.31)
Group 4					
Macoma balthica	Bay	3	310 (198)	76.7 (53.13)	18.3 (4.69)
Nereis vexillosa	Bay	2	174 (31)	26.2 (17.61)	16.2 (13.04)
Worm sp.	Bay	2	1,815 (626)	6.50 (2.10)	0.40 (0.26)
Leptocottus armatus	Bay	9	205 (83)	220 (98.60)	106 (6.31)
Platichthys stellatus	Bay	8	181 (37)	186 (39.47)	103 (4.24)
Group 5					
Orchestia traskiana	Marsh	6	126 (26)	103 (13.70)	83.1 (7.55)
Group 6					
Hemigrapsus oregonensis	Marsh	2	152 (20)	90.4 (23.87)	61.1 (23.78)
Group 7					
Clevelandia ios	Bay	3	258 (201)	276 (195.86)	111 (7.63)
Group 8					
Cicindela sp.	Marsh	1	173 (-)	161 (-)	93.4 (-)

In the nearshore bay, sculpin, flounder and goby showed considerable MeHg bioaccumulation (of 220, 186 and 276 ng g^{-1}; Table 5-6). Based on the present food web analysis, the diet of sculpin may consist of 14% Asian clam+shrimp with MeHg concentrations of 61 and 90 ng g^{-1}, 16% Baltic clam+pile worm with MeHg concentrations of 77 and 26, pointing to Asian clam, Baltic clam and shrimp as important MeHg sources. Following the same reasoning, the diet of flounder may consist of 14% Asian clam+shrimp with MeHg concentrations of 61 and 90 ng g^{-1}, 16% Baltic clam+pile worm with MeHg concentrations of 77 and 26, and 21% goby with a MeHg concentration of 276 ng g^{-1}, pointing to goby, Asian clam, Baltic clam, and shrimp as important MeHg sources. Finally, the diet of goby may consist of 19% *S. foliosa* detritus and 13% *D. spicata* detritus, both with MeHg concentrations $\leq$1 ng g^{-1}, 17% shore crab with a MeHg concentration of 90 ng g^{-1}, and 40% goby with MeHg concentration of 276 ng g^{-1}, pointing to goby and shore crab as important MeHg sources.

Conclusions

The following conclusions result from the studies described in this chapter:

1. Two companion multiple source mixing models were used with site-specific isotopic tracer values of primary producers and consumers relating to the China Camp salt marsh associated food web(s), to estimate fractional ranges for contributing food sources.

2. Both models follow a mathematically simple first order approach. SOURCE estimates the mixture of autotrophic sources that have been assimilated, directly or indirectly, into a consumer's tissues and the consumer's trophic level. STEP estimates the mixture of autotrophic and heterotrophic sources that have been assimilated into a consumer's tissues and the consumer's trophic level.

3. Based on their isotopic nearest neighbor distances, the producers were categorized in nine groups and the consumers in eight groups.

4. SOURCE estimates using all three isotopes indicated contributions to consumer diets > 5% of the producer groups 1 (bay-POM), 2 (marsh-POM), 3 (*S. foliosa*+litter), 4 (*S. virginica*+litter), 6 (marsh-microalgae), 7 (marsh filamentous algae+*D. spicata*), and 8 (bay macroalgae).

5. STEP estimates characterized higher order consumers as directly consuming a smaller percentage of primary producers than lower order consumers, and included an increased number of potential food sources. STEP was used to estimate food source contributions to the consumers using all three isotopes, and to calculate the trophic levels. Using the STEP-estimated trophic levels as a basis for the overall structure as well as natural history information, a food web diagram was constructed for the China Camp salt marsh and adjacent San Pablo Bay area.

6. Three main points became apparent. First, macrophytic primary producers of the salt marsh formed important food sources of consumers: live plants were most important on the high marsh and dead plants contributed to the DOM pools in the nearshore bay. Secondly, the bay-POM pool was likely dominated by detritus originating from marsh macrophytes, because bay phytoplankton production is low. Thirdly, consumers in the nearshore bay were largely benthivorous and fed partly on higher plant fragments and/or bay-POM, of which the relative contributions decreased with increasing trophic level. Higher order consumers are relatively more carnivorous than lower order consumers. The goby showed a considerable tendency to consume its own species.

7. An evaluation of MeHg accumulation in the consumers with the greatest MeHg levels following the pathways identified by the current food web analysis suggested that consumption of amphipods, seeds from higher plants such as *S. virginica*, selected higher trophic level organisms (shore crab, Baltic clam, Asian clam, shrimp, goby) may contribute the most, while the central role of detritus-associated MeHg must be further explored.

6 Recalibration of a Screening-level Model Integrating Physical, Chemical, and Biological Processes that Drive Mercury Cycling in San Pablo Bay Salt Marshes

Introduction

Stakeholders involved in wetland restoration activities on the former Hamilton Army Air Field (HAAF) aim at restoring San Pablo Bay wetland habitat, while minimizing conditions for monomethylmercury (MeHg) production and its subsequent trophic transfer to San Francisco Bay fisheries. Sufficiently detailed information on environmental mercury levels at HAAF was lacking in 2002 when field and experimental mercury cycle studies associated with the Hamilton Wetland restoration project started. That is, a mechanistic understanding was lacking of the factors that control these levels and the means to use this information in ecosystem models supporting environmental management decisions was lacking also. These field and experimental studies generated information on various aspects of environmental chemistry of mercury (Hg) and MeHg, and their fate and effects on ecological receptors. Therefore, a screening-level modeling approach was followed to integrate the information from these HAAF-related MeHg studies (Best et al. 2005, 2007) into a tool that directly links the environmental information in such a way that practical management decisions related to design, construction, and maintenance of coastal wetland areas can be based on the simulation results. This screening-level model contains greatly simplified descriptions of relationships between Hg and MeHg chemicals in sediment, water, and marsh organisms for which measured data became available from HAAF-related studies. As more knowledge becomes available, more accurate descriptions of relationships, and descriptions of other processes and interactions may be incorporated in the model, since the model design is simple and straightforward.

The *Questions and Decisions* ™ (QnD) screening model system was created as a tool to incorporate ecosystem and management issues into a user-friendly framework to evaluate consequences of alterations in any of its components (Kiker et al. 2006). The system has been implemented as

an object-oriented JAVA program and can be deployed as a stand-alone program or as a web-based (browser-accessed) applet. QnD links the spatial components within geographic information system (GIS) files to the climatic, abiotic, and biotic interactions in an ecosystem. The program integrates the equations once per hour, and computes daily values by adding 24-hr results.

QnD can be constructed using any combination of measured data or estimated interactions of the ecological, management, social, and/or economic forces influencing an ecosystem. It facilitates use of the developing data set as a basis for screening-level predictions relating to coastal wetland sites and to scale up for landscape-scale simulations. QnD:HAAF Version 1 (QnD:HAAF V1) was developed as a framework for the evaluation of consequences of wetland restoration for MeHg emissions at the former HAAF from 2005 onwards (Best et al. 2005, Chapter 7). QnD:HAAF is being applied in an iterative, interactive manner to identify critical abiotic and biotic drivers of salt marsh Hg and MeHg cycling and guide subsequent work on HAAF and San Francisco Bay salt marshes. Scientific, economic, and social issues may also be incorporated and linked in a manner that enables the evaluation of their relative impacts through scenario projections. As further learning occurs, those drivers shown to be important can be explored and subsequently expanded; those judged unimportant can be discarded. Whereas these major structural changes would require substantial code rewriting of other models (e.g., Mercury Cycling Model; Hudson et al. 1994), these changes are rapidly made in QnD. QnD achieves modeling nimbleness by keeping compartments, processes, and interactions conceptually simple. Thus, the QnD:HAAF system can serve as a capstone to integrate research and monitoring results into a more management-focused model.

QnD:HAAF Version 2 (QnD:HAAF V2) was developed in 2006-2007, using QnD :HAAF V1 as a basis. Similar to V1, V2 is focused on addressing consensus technical questions formulated at the CALFED Stakeholders' Workshop on Mercury in San Francisco Bay held 8-9 October 2002 at Moss Landing Marine Laboratories.

These questions included:

- What are the present levels of MeHg in San Francisco Bay wetlands with respect to biota, sub-habitats, and location within the Bay?

- What are the rates of MeHg production?
- What factors control MeHg production? Can these be managed?
- Are some wetlands larger mercury exporters than others?
- Can the effects of wetland restoration on MeHg production and export be modeled/predicted?

V2 differs from V1 by inclusion of:

1. HAAF base map containing 100- x 100-m grid-cells and digital elevation information.
2. Verified, realistic elevation assignments to the spatial areas and tidal movements pertaining to 2005.
3. Revised formulation of net methylmercury production matching field data collected after 2003.
4. MeHg diffusion from sediments.
5. Module for Hg deposition and volatilization from wetlands.

Additional revisions and expansions planned and formulated for the present QnD:HAAF modeling project, but not yet funded, were:

1. Expansion with descriptions of mercury species conversions and relationships with salinity.
2. Expansion with a management options module.
3. Addressing issues identified by gap analysis, including more realistic descriptions of biota-environment relationships.

The next section describes the QnD model components in more detail for the HAAF wetland ecosystem.

QnD:HAAF V2 model description

QnD:HAAF V2 is organized in three object categories (Chemicals, Organisms and Drivers; Figure 6-1), which exist within a 'virtual' landscape of spatial areas and habitats (Figure 6-2). The Chemical and Organism objects participate in specific processes that cause changes in the ecosystem. For example: within a High Marsh (spatial area object), a crab (organism object) may take MeHg up from the sediment (chemical object). A more complete description of the spatial areas, habitats, chemicals and organism objects and their associated processes is provided below.

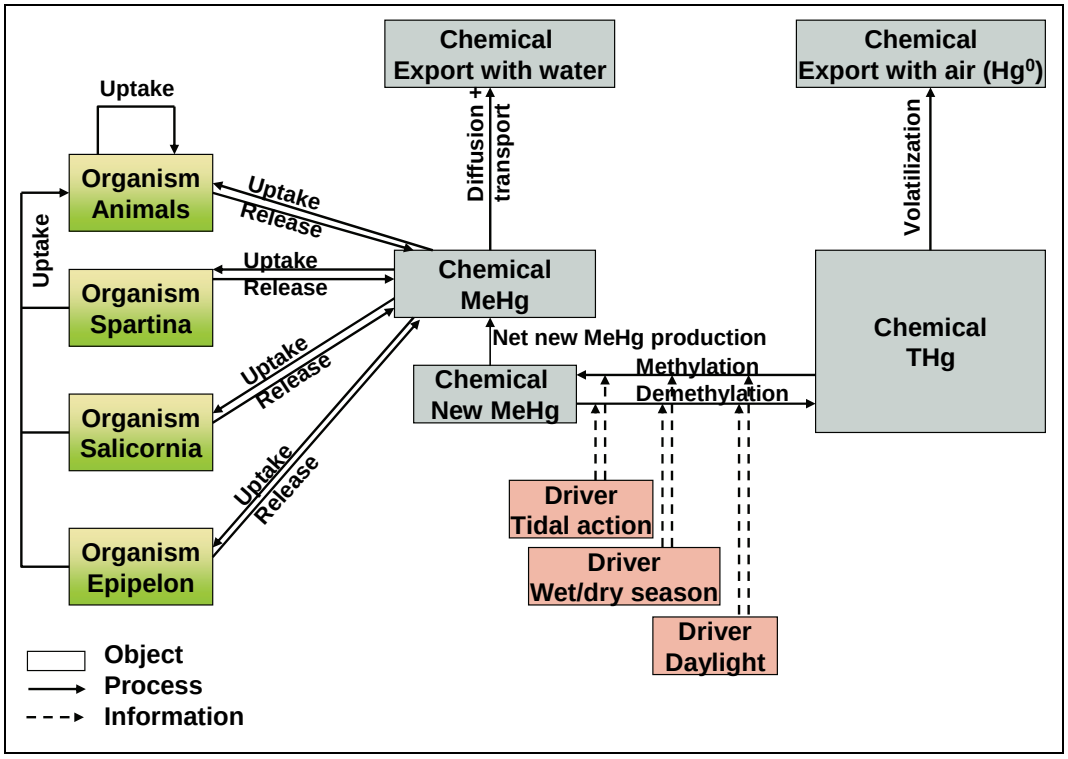

Figure 6-1. Diagram of QnD:HAAF V2 object categories, composed of chemicals, organisms, and drivers.

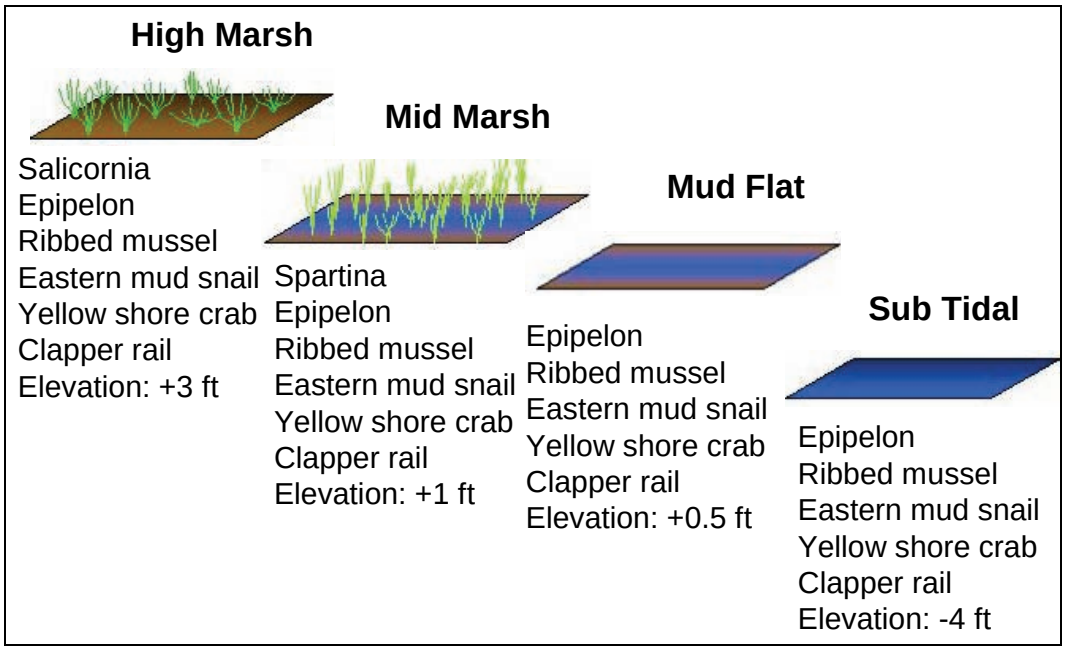

Figure 6-2. Spatial areas with associated biota within QnD:HAAF V2.

Spatial areas

QnD:HAAF V2 utilizes four stylized wetland areas for rapid model explorations in time (Figure 6-2). This spatial simplification allows the use of data from initial feasibility studies with simplified modeling concepts, instead of attempting to fit a complex model to an ecosystem in which no data have been collected. In QnD:HAAF, the selected scale of each spatial area is 10 x 10 m (100 m^2), all mass data are on a dry weight basis, and all simulated data are on a square meter basis. The High Marsh area represents *Salicornia virginica* (pickleweed)-dominated marshes at an elevation of +3 ft (1 m) above Mean High Water (MHW), which are rarely flooded. The Mid Marsh area represents *Spartina foliosa* (cordgrass)-dominated marshes at an elevation of +1 ft (0.333 m), which are partially flooded as part of the daily tidal cycle. The third spatial area represents the Mud Flat zone at an elevation of +0.5 ft (0.167 m) that is partially submerged. The fourth spatial area represents the Sub Tidal zone at -4 ft (-1.333 m), which is completely submerged. The elevation of each spatial area is kept constant. Resident biota for each spatial area are listed in Figure 6-2.

The model can also simulate ecosystem components and processes for an entire map, composed of 100- x 100-m grid cells to which any of the known spatial areas has been assigned based on its geo-referenced digital elevation information (U.S. Geological Survey (USGS) 2006). The QnD:HAAF V2 base map is provided in Figure 6-3. Simulations for an entire map require far more computation time than for each spatial area, and usually lead to oversimplifications of the original question to keep the computation time manageable. However, they provide spatial information and may indicate where hotspots of net MeHg production occur, thus facilitating the development of an effective management approach to prevent emission.

Habitats

Habitats may exist within, and occupy a fraction of, each spatial area. The habitats are assumed to be homogeneous and harbor different combinations of biota and chemicals. In the current QnD:HAAF V2, no specialized habitats within the spatial areas are distinguished, i.e., one default habitat occupies 100% of the spatial area. In later model versions, a plant- and a non-plant influenced habitat within each spatial area may be introduced. This modification would allow QnD to simulate the effects of

depositing dredged material on a vegetated area. This management action may convert a portion of a vegetated wetland temporarily into a mud flat with altered mercury dynamics.

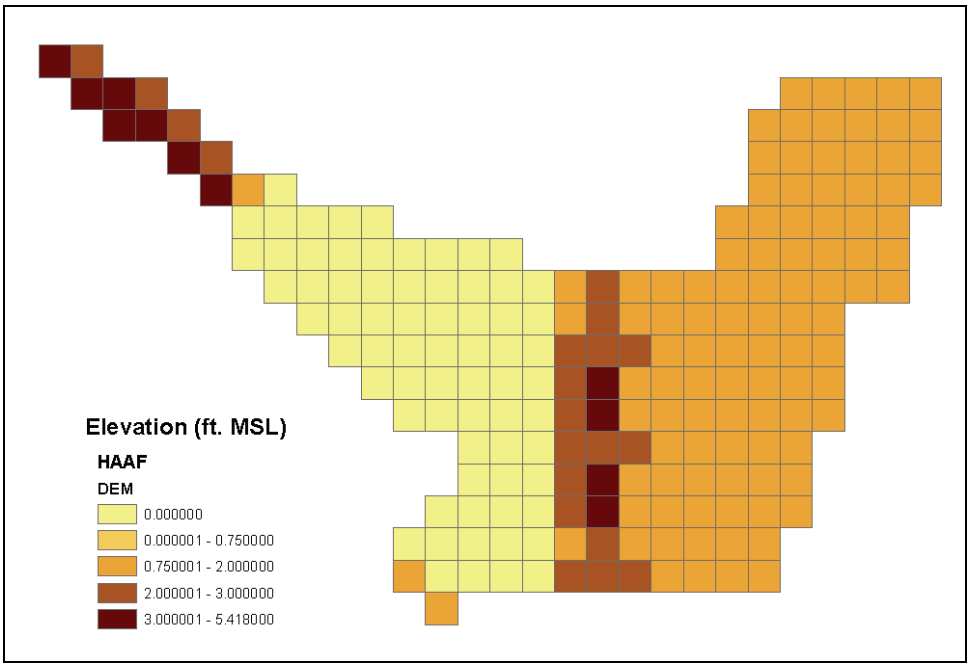

Figure 6-3. QnD:HAAF V2 base map.

Environmental drivers and time scales

Three environmental drivers were selected to link processes at time scales varying from current to seasonal.

- Tidal action and its effect on redox potential, because maximum methylation rates typically follow the redox cline, which varies tidally and seasonally, and frequently interacts with the sediment water interface (Ulrich et al. 2001).
- Wet and dry season, with wet season lasting from 1 November to 30 April, and dry season from 1 May to 30 October in San Francisco Bay, because high temperatures as occur in summer generally favor methylation of metals, and low temperatures as occur in winter favor demethylation processes.
- Daylight, because daylight stimulates photosynthesis in wetland vegetation. This increases DOC release in the rhizosphere (upper sediment layer) that may complex Hg^{2+}, decreasing its availability for microbes on one hand, increasing microbial biomass on the other hand, as well as increasing radial oxygen loss, thereby elevating redox potential and decreasing methylation (Gribsholt and Kristensen 2003).

Validated tidal water level predictions for Richmond on San Francisco Bay pertaining to 2005 were used as the basis from which periods of interest were selected (National Oceanic and Atmospheric Administration (NOAA) 2006). Richmond was considered as a site with tidal characteristics similar to those at HAAF. No long-term tidal information for HAAF was available. In general, SI units are used, except for elevation and water depth where data are provided in feet (1 foot = 0.3048 m)for easy import of water level data from the on-line tide simulator.

For initial QnD:HAAF V2 testing, two hourly time series were constructed, i.e., one representing a wet season (1–14 February 2005) and one representing a dry season (1–14 June 2005), respectively.

Water depth at each spatial area was calculated by subtracting its local elevation derived from the base map hourly from the tidal water level following (Equation 6A.1). Equations are provided at the end of this chapter, variables and constants are listed in Table 6-1. The spatial area is considered submerged and susceptible to decreasing oxygen diffusion when the calculated local water depth (WaterDepth) has a positive sign. The spatial area is considered extending above the water level and susceptible to oxygen diffusion from the ambient air when the calculated local water depth has a negative sign. WaterDepth is subsequently used to calculate the number of hours when the spatial area is under or above the water level, which, in turn, governs changes in redox potential. The simplified relationship between water depth and period under/above water is presented in Figure 6-4. The cumulative numbers of hours under and above the water level, respectively, are used to calculate the hourly change in redox potential (mV; Figure 6-5). The maximum and minimum values of hourly change in redox potential do not change as they represent the stable redox potential values of areas that are, respectively, above and below water for longer periods (e.g., the High Marsh or Sub Tidal spatial areas). The hourly change in redox potential is then added to the cumulative redox potential for each spatial area. The fluctuations in redox potential in all spatial areas were delimited by an assigned upper boundary of 300 mV and a lower boundary of –300 mV. These initial redox relationships were estimated from redox dynamics reported in Bartlett and Craig (1981a, 1981b) and were further validated with on-site measurements (Chapter 3, this report).

Table 6-1. Variables and constants, grouped according to model components and processes.

Var/constant	*c/v*[a]	Value	Unit	Description	Source
Environmental drivers					
Tidal and redox processes					
WaterDepth	*v*		ft MSL	Local water depth of the spatial area	C (U-d)
TidalDepth	*v(tab)*		ft MSL	Tide predictions Richmond, CA, 2005 (validated)	1
$Elev_{base}$	*v(tab)*		ft MSL	Digital elevation map surficial sediment layer, 1999 (DEM, georeferenced)	2
Mercury dynamics in sediment					
Mercury species pools					
Load (Hg2+, Sal-marsh	*v*	8446750	ng m^{-2}	Total mass of Hg^{2+}	3
Conc (Hg2+, Sal-marsh	*v*	299	ng g^{-1}DW	Hg^{2+} concentration	3
Load (Hg2+, Spar-marsh	*v*	10113500	ng m^{-2}	Total mass of Hg^{2+}	3
Conc (Hg2+, Spar-marsh	*v*	358	ng g^{-1}DW	Hg^{2+} concentration	3
Load (Hg2+, Mud Flat	*v*	9972250	ng m^{-2}	Total mass of Hg^{2+}	3
Conc (Hg2+, Mud Flat	*v*	353	ng g^{-1}DW	Hg^{2+} concentration	3
Load (Hg2+, Sub Tidal	*v*	9972250	ng m^{-2}	Total mass of Hg^{2+}	3
Conc (Hg2+, Sub Tidal	*v*	353	ng g^{-1}DW	Hg^{2+} concentration	3
Load (MeHg, Sal-marsh	*v*	88987.5	ng m^{-2}	Total mass of MeHg	3
Conc (MeHg, Sal-marsh	*v*	3.15	ng g^{-1}DW	MeHg concentration	3
Load (MeHg, Spar-marsh	*v*	81642.5	ng m^{-2}	Total mass of MeHg	3
Conc (MeHg, Spar-marsh	*v*	2.89	ng g^{-1}DW	MeHg concentration	3

Var/constant	*c/v*[a]	Value	Unit	Description	Source
Load (MeHg, Mud Flat	*v*	67235	ng m^{-2}	Total mass of MeHg	3
Conc (MeHg, Mud Flat	*v*	2.38	ng g^{-1}DW	MeHg concentration	3
Load (MeHg, Sub Tidal	*v*	67235	ng m^{-2}	Total mass of MeHg	3
Conc (MeHg, Sub Tidal	*v*	2.38	ng g^{-1}DW	MeHg concentration	
Depth	*c*	5	cm	Sediment depth included in model	C (U-d)
Methylation of mercury in sediments					
BD	*c*	0.565	g DW cm^{-3}	Sediment bulk density	4
$MeHg_n$	*v*		ng DW	Total mass of Hg methylated /h /area	
Methylation of mercury in sediments					
TotalHg	*v*	[b]	ng DW	Total mass of Hg^{2+}	
$BaseRate_{meth}$ (Sal-marsh)	*v(tab)*	2.271 x 10-4	ng new MeHg $ng^{-1}Hg^{2+}$ h^{-1}	THg methylation into NewMeHg	3
$BaseRate_{meth}$ (Spar-marsh)	*v(tab)*	2.313x 10-4	ng new MeHg $ng^{-1}Hg^{2+}$ h^{-1}	THg methylation into NewMeHg	3
$BaseRate_{meth}$ (Mud Flat)	*v(tab)*	6.354x 10-4	ng new MeHg $ng^{-1}Hg^{2+}$ h^{-1}	THg methylation into NewMeHg	3
$BaseRate_{meth}$ (Sub Tidal)	*v(tab)*	6.354x 10-4	ng new MeHg $ng^{-1}Hg^{2+}$ h^{-1}	THg methylation into NewMeHg	3
$BaseRate_{demeth}$ (Sal-marsh)	*v(tab)*	0.035833	ng new MeHg $ng^{-1}Hg^{2+}$ h^{-1}	NewMeHg demethylation into THg	3
$BaseRate_{demeth}$ (Spar-marsh)	*v(tab)*	0.028125	ng new MeHg $ng^{-1}Hg^{2+}$ h^{-1}	NewMeHg demethylation into THg	3
$BaseRate_{demeth}$ (Mud Flat)	*v(tab)*	0.030625	ng new MeHg $ng^{-1}Hg^{2+}$ h^{-1}	NewMeHg demethylation into THg	3
$BaseRate_{demeth}$ (Sub Tidal)	*v(tab)*	0.030625	ng new MeHg $ng^{-1}Hg^{2+}$ h^{-1}	NewMeHg demethylation into THg	3
NewMeHg	*v*	[b]	ng DW	Total mass of methylated pool at hour i resulting from methylation	

Var/constant	*c/v*[a]	Value	Unit	Description	Source
Season(month)Sal-marshW	*v(tab)*	1.8	-	Seasonal month-characteristic effect on methylation rate	3
Season(month)Spar-marshW	*v(tab)*	2.5	-	Seasonal month-characteristic effect on methylation rate	3
Methylation of mercury in sediments					
Season(month)Mud FlatW	*v(tab)*	2.5	-	Seasonal month-characteristic effect on methylation rate	3
Season(month)Sub TidalW	*v(tab)*	2.5	-	Seasonal month-characteristic effect on methylation rate	3
Season(month)Sal-marshD	*v(tab)*	1.0	-	Seasonal month-characteristic effect on methylation rate	3
Season(month)Spar-marshD	*v(tab)*	1.0	-	Seasonal month-characteristic effect on methylation rate	3
Season(month)Mud FlatD	*v(tab)*	1.0	-	Seasonal month-characteristic effect on methylation rate	3
Methylation of mercury in sediments					
Season(month)Sub TidalD	*v(tab)*	1.0	-	Seasonal month-characteristic effect on methylation rate	3
$Redox_m$(hours)	*v(tab)*	0-1	-	Potential redox effect on methylation rate versus cumulative h above or under water	5
$Light_m$(daylight)	*v(tab)*	1.0	-	Daylight effect on methylation rate versus time of day	3
Demethylation of methylmercury in sediments					
$DemethHg_t$	*v*		ng DW		

Var/constant	*c/v*[a]	Value	Unit	Description	Source
$NewMeHg_t$	*v*		ng DW	Total daily mass of methylated pool at hour i resulting from demethylation of the newly methylated amount	
Season(month)Sal-marshW	*v(tab)*	1.1	-	Seasonal month-characteristic effect on demethylation rate	3
Season(month)Spar-marshW	*v(tab)*	1.3	-	Seasonal month-characteristic effect on demethylation rate	3
Season(month)Mud FlatW	*v(tab)*	1.3	-	Seasonal month-characteristic effect on demethylation rate	3
Season(month)Sub TidalW	*v(tab)*	1.3	-	Seasonal month-characteristic effect on demethylation rate	3
Season(month)Sal-marshD	*v(tab)*	1.0	-	Seasonal month-characteristic effect on demethylation rate	3
Season(month)Spar-marshD	*v(tab)*	1.0	-	Seasonal month-characteristic effect on demethylation rate	3
Season(month)Mud FlatD	*v(tab)*	1.0	-	Seasonal month-characteristic effect on demethylation rate	3
Season(month)Mud FlatD	*v(tab)*	1.0	-	Seasonal month-characteristic effect on demethylation rate	3
Export and diffusion of methylmercury from sediments					
MeHgWatExportAmount	*c*	0.0333	Percent h^{-1}	Fraction of total MeHg pool exported	6
MeHgWatDiffusionAmount Sal-marsh	*v(tab)*	0.000205327	ng MeHg g^{-1} h^{-1}	Fraction of total MeHg pool diffused from sediment into water column	7
MeHgWatDiffusionAmount Spar-marsh	*v(tab)*	0.000205327	ng MeHg g^{-1} h^{-1}	Fraction of total MeHg pool diffused from sediment into water column	7

Var/constant	*c/v*[a]	Value	Unit	Description	Source
MeHgWatDiffusionAmount Mud Flat	*v(tab)*	0.000205327	ng MeHg g^{-1} h^{-1}	Fraction of total MeHg pool diffused from sediment into water column	7
MeHgWatDiffusionAmount Sub Tidal	*v(tab)*	0.00005892	ng MeHg g^{-1} h^{-1}	Fraction of total MeHg pool diffused from sediment into water column	7
Volatilization of mercury from wetlands					
THgAirVol	*v*		ng Hg	Total mass of Hg volatilized	
$VolRate_{Marshtype}$ Sal-marsh	*v*	24	ng Hg g^{-1} h^{-1}	Total Hg volatilization by spatial area	8
$VolRate_{Marshtype}$ Spar-marsh	*v*	24	ng Hg g^{-1} h^{-1}		
$VolRate_{Marshtype}$ Mud Flat	*v*	1	ng Hg g^{-1} h^{-1}		
$VolRate_{Marshtype}$ Sub Tidal	*v*	1	ng Hg g^{-1} h^{-1}		
Biota					
Food web relationships[c]					
$MeHg_{Load}$	*v*	[c]	g DW	Total initial MeHg load organism by spatial area	
Org_{Biom}	*v(tab)*	[c]	g DW	Organism biomass	
$Conc_{MeHg}$	*v(tab)*	[c]	ng g^{-1} DW	Organism MeHg concentration	
$Intake_{Pred}$	*v*		g DW	Prey biomass consumed by a particular 'predator'	
$Biom_{Pred}$	*v(tab)*	[c]	g DW	'Predator' biomass	
$DemandRate_{Prey}$	*v(tab)*	[c]	g prey-DW per g predator-DW	Prey biomass required per unit predator weight	
$MeHgIntake_{Prey}$	*v*		ng MeHg	MeHg intake by 'predator' with prey	
PreyConsumed	*v(tab)*	[c]	g prey-DW	Prey biomass consumed	

Var/constant	*c/v*[a]	Value	Unit	Description	Source
			Food web relationships[c]		
MeHgPrey	*v(tab)*	[c]	ng g^{-1} prey-DW	MeHg concentration prey	
			Intake of methylmercury by biota from sediments		
$MeHgIntake_{Sed}$	*v*		ng MeHg	Intake of MeHg from sediment	
$Transfer_{Sed}$	*c*	0.14042	ng MeHg g^{-1} org-DW	Potential MeHg transfer rate from sediment into organisms	9
$Sat(MeHg_{Conc})$	*v(tab)*	0-1	-	Factor to reduce meHg uptake to 0 when the species-characteristic initial (equilibrium) MeHg concentration is reached	C (U-d)
			Loss of methylmercury from biota		
LossRatePlants	*c*	5.7078 x 10-3	Percent h^{-1}	MeHg loss rate with biomass /h, derived form salt marsh plant biomass data	10
LossRateAnimals	*c*	0.4167	Percent h^{-1}	MeHg loss rate with biomass /h, derived form *Daphnia magna* biomass data	11

1: NOAA 2006; 2: USGS 2006; 3. Best et al. 2007-Table 3-3; 4. Best et al. 2005-Table 3-5; 5. Bartlett and Craig 1981a, b; 6: Best et al. 2005-chapter 3; 7. Best et al.2007-chapter 4; 8. Lindberg et al. 2002; 9: Best et al. 2005-chapter 6; 10: Best et al. 2005-Table 3-11; 11: Tsui and Wang 2004.

Note: [a] A *c* indicates that the parameter is a constant. A *v* indicates a variable and tab indicates that the parameter is implemented in the model as a table; [b] Initial value equal to load characteristic for spatial area (see 'Mercury dynamics in sediment', this Table). [c] The food web relationships in QnD:HAAF V2 are the same as in V1, with species-characteristic data on biomass, MeHg concentration, and load read from Table 6-2, and data on prey demand and predator mass loss rates read from Table 6-3.

Abbreviations: tab = read from data table; C (U-d) = calibration (user-defined)

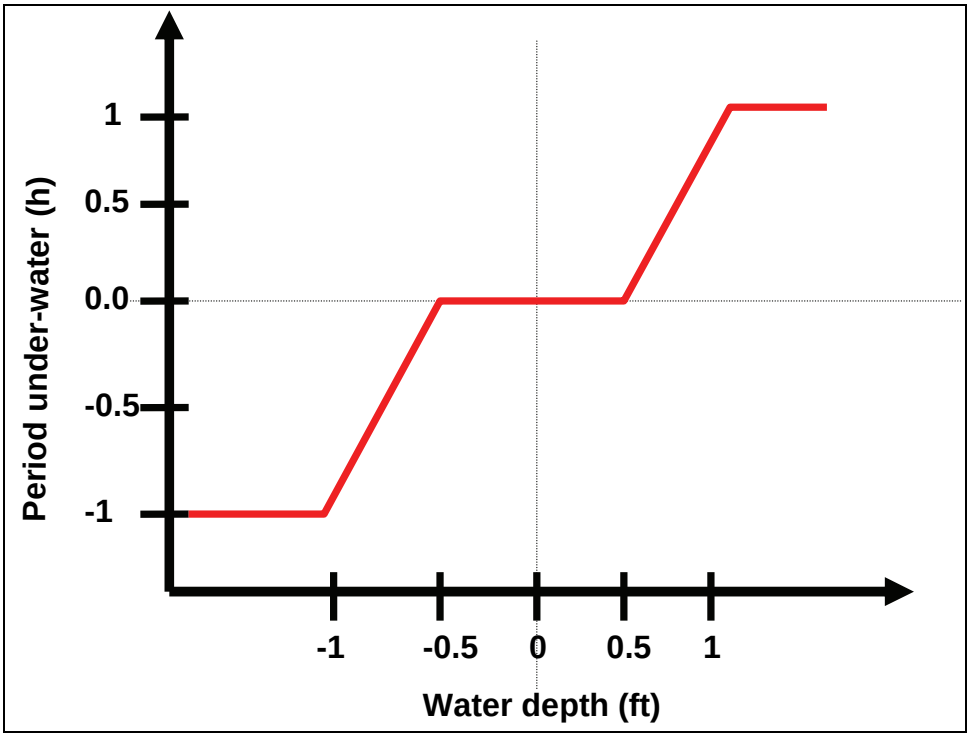

Figure 6-4. Simplified relationship between local water depth and period under water.

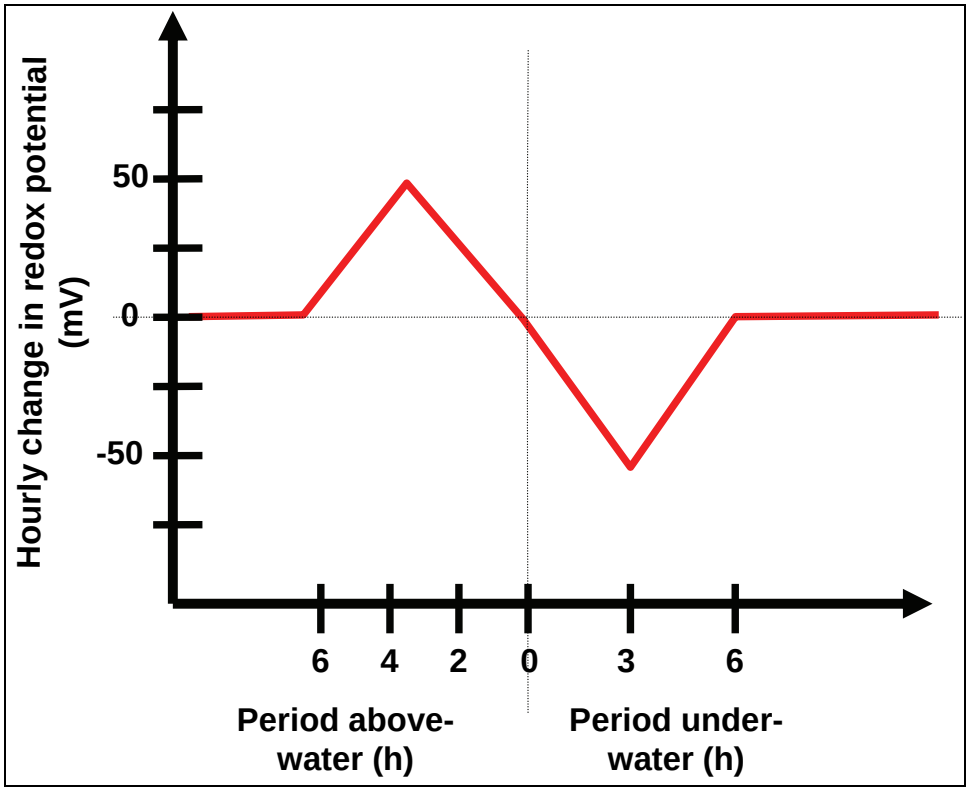

Figure 6-5. Relationship between period above and under water, and the hourly change in redox potential.

Relationships between redox potential, wet/dry season, daylight and mercury cycle related processes are summarized in the section 'mercury dynamics in sediments.'

Mercury dynamics in sediments

Mercury species pools

Two chemical Hg pools are distinguished and assumed to be available for transformation: THg and MeHg (Figure 6-1). Both pools are assumed to reside in the surficial 5-cm sediment layer and its associated pore water. The pools change in mass per unit area (ng m^{-2}), but have an associated, calculated concentration (ng g^{-1}). THg is transformed into new MeHg as a function of time of year (dry or wet season), redox potential (dependent on tidal movements), and time of day (light or dark conditions). The values assigned to the pools of mercury are defined by the analytical procedures used to measure THg and MeHg. A portion of the new MeHg pool is demethylated to THg. This amount is always less than, or equal to, the total new MeHg pool. The net remaining new MeHg is then subjected to chemical export. The entire THg and MeHg pools are assumed to be mobile, which may be an overestimate since only a fraction may be reactive and/or bioavailable to microbes. However, it is currently not known what and how large the reactive and bioavailable fractions are.

The initial inputs of the THg and MeHg pools originate from the TotalLoad pools (objects) that contain the chemical mass values (ng m^{-2}) and are calculated following Equation 6A.2. The initial concentrations and calculated loads of THg and MeHg are presented in Table 6-1. Initial concentrations have been derived from data collected at HAAF in 2003-4 (from Best et al. 2007, Table 3-3). All mercury-related calculations are carried out in nanograms (ng) on a dry weight basis, and subsequently ng is converted into concentration.

Methylation of mercury in sediments

In QnD:HAAF V2, mercury is methylated, and the amount of hourly methylated Hg in each spatial area ($MeHg_n$) is calculated as a percentage of the total available inorganic Hg^{2+} pool (*TotalHg*) following Equation 6A.3. Mercury then enters the new MeHg pool. The methylation process is affected by tidal movements, redox potential, season, and light/dark conditions (Figure 6-1). The base THg methylation rates represent the

means of the rates measured in the field in 2003-2004 in wet and dry season conditions (Table 6-1; from Best et al. 2007, Table 3-3). Methylation rates varied from 0.02271 percent of the Hg^{2+} pool converted per hour in the High Marsh to 0.06354 percent per hour in the Sub Tidal area (Table 6-1). The latter field data indicated that methylation rates were higher in bare than in vegetated sediments, in contrast to previous observations where the reverse was found. The base methylation rates used in QnD:HAAF V2 for vegetated sediments are in the same range, but in the bare sediments they are a factor of 3 higher than those used in V1.

The relative effect of redox potential on the methylation of Hg follows a stylized Gauss curve with a maximum of 1 at a redox potential between -100 and +100 mV, and minima of 0.1 at values more negative than -300 mV and more positive than 300 mV (Figure 6-6). This curve has been fitted to data of Bartlett and Craig (1981a, 1981b), and modified based on data of McFarland and Lee (2002). Methylation proceeds at the greatest rate between –100 and +100 mV potential.

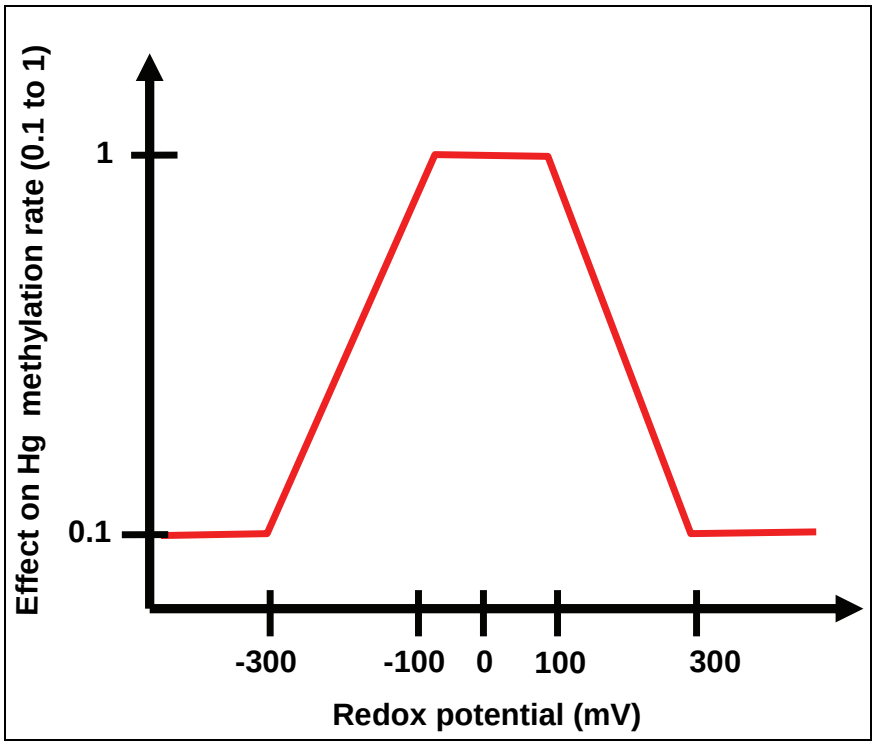

Figure 6-6. Effect of redox potential on mercury methylation rate (relative).

MeHg concentrations in HAAF sediments were far greater in the wet than in the dry season (McFarland et al. 2003). From their data it was not clear if these differences were caused by higher methylation or lower demethylation rates, or both. However, in situ determinations of methylation and demethylation rates at the China Camp marsh conducted in 2004 indicated that, indeed, both methylation and demethylation rates are greater in the wet than dry season (Best et al. 2007, Table 3-3). To enable the calculation of methylation rates accounting for effects of dry and wet season, multiplication factors relating dry to wet season activity were derived from the latter in situ determinations as ratios (Table 6-1). Since base methylation rates were measured in the dry season of 2003, the multiplication factors for the effects of dry season are 1.0. The multiplication factors accounting for the effects of wet season range from 1.8 in the High Marsh to 2.5 in the three other spatial areas. These factors are far lower than those used in QnD:HAAF V1, based on data from McFarland et al. (2003), which ranged from 1.6 to 8.8. The dry season in the model lasts from April through October and the wet season from November through March.

Methylation rates were generally 40 to 50% greater in light than in darkness in 2003, but the data set showed a high variability (Best et al. 2005, Chapter 3). Daytime in the model lasts from 6 am to 6 pm. No further field data are available that would enable distinction between methylation in light relative to methylation in darkness, and, therefore, in QnD:HAAF V2 factors accounting for the decreasing effect of darkness on methylation have been included but are currently inactive (=set to 1; Table 6-1).

Demethylation of methylmercury in sediments

In QnD:HAAF V2, the pool of new MeHg is demethylated, the amount of hourly demethylated MeHg in each spatial area ($DemethHg_t$) is calculated as a percentage of the new MeHg pool following Equation 6A.4, and returns as Hg to the active Hg^{2+} pool following a first-order rate equation (Delta Tributaries Mercury Council (DTMC)/Sacramento River Watershed Program (SRWP) 2002). Each day the surplus of the new MeHg pool is added to the MeHg pool. This approach matches the recently collected field data (Best et al. 2007-Chapter 3). The demethylation process is also affected by redox potential, tidal water movements, season, and light/dark conditions. The base MeHg demethylation rates have been derived from the rates measured in the field in 2003-2004, in wet and dry season conditions (Table 6-1; from Best et al. 2007, Table 3-3). The base MeHg

demethylation rates represent the means of the rates measured in the field in 2003-2004 in wet and dry season conditions (Table 6-1; from Best et al. 2007, Table 3-3). Demethylation rates varied from 2.8125 percent of the new MeHg pool converted per hour in the Mid Marsh to 3.5833 percent per hour in the High Marsh (Table 6-1). The base demethylation rates used in QnD:HAAF V2 are in the same range as those used in V1.

The relative effect of redox potential on demethylation follows a linearized saturation curve with a maximum of 1.0 at a redox potential more positive than 100 mV, and a minimum of 0.1 at a value more negative than -100 mV (Figure 6-7). This curve has been fitted to data of Bartlett and Craig (1981a, 1981b), modified by McFarland and Lee (2002), and fitted to field data from Best et al. (2005, Chapter 3).

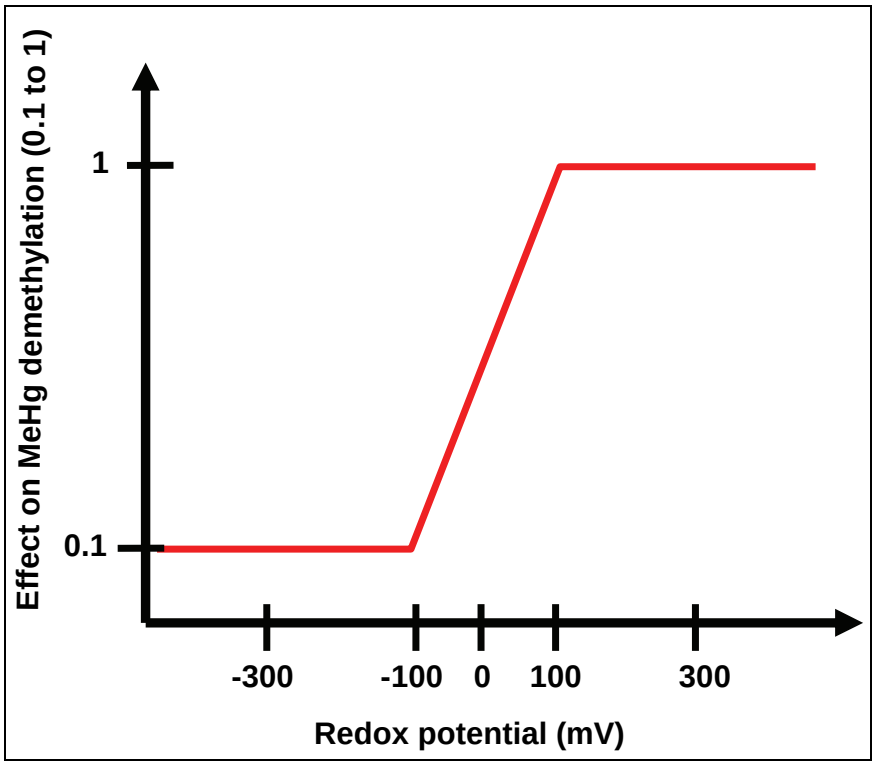

Figure 6-7. Effect of redox potential on methylmercury demethylation rate (relative).

The multiplication factors accounting for the effects of wet season on demethylation rate range from 1.1 in the High Marsh to 1.3 in the three other spatial areas. These factors have been derived from in situ determinations of methylation and demethylation rates at the China Camp marsh conducted in 2004 (Table 6-1; from Best et al. 2007, Table 3-3). In QnD:HAAF V1 no multiplication factors for demethylation were used.

Rates were generally 25% greater in light than in darkness in 2003, but the data showed a high variability (Best et al. 2005, Chapter 3). No further field data are available that would enable distinction between demethylation in darkness relative to demethylation in the light, and, therefore, in QnD:HAAF V2 factors accounting for the decreasing effect of darkness on demethylation have been included but are currently inactive (=set to 1; Table 6-1).

Export and diffusion of methylmercury from sediments

In QnD:HAAF V2, MeHg is exported by tidal resuspension from the sediments at a constant rate as described in Best et al. (2005-Chapter 3). It is assumed that 0.8 percent of the MeHg in the sediment is exported per day (i.e., 0.0333 percent per hour; Table 6-1). This amount of MeHg (*MeHgWatExportAmount*) enters a non-returnable MeHg pool that estimates the potential MeHg export to the bay. In addition, MeHg diffuses from the sediments with rates measured in the field in 2004 varying from 0.00005892 ng MeHg g^{-1} h^{-1} in bare sediments to 0.000205327 in vegetated sediments ng MeHg g^{-1} h^{-1} (Table 6-1; Best et al. 2007, Chapter 4). This amount of MeHg (*MeHgWatDiffusionAmount*) also enters the non-returnable MeHg pool that estimates the potential MeHg export to the bay.

Volatilization of mercury from wetlands

Volatilization of mercury has been shown to be a major route of export in other wetland systems, from sediments as well as from vegetation, causing significant decreases in the THg concentration and potentially depleting the reactive fraction of THg in surface sediments (Lindberg et al. 2002; Canario and Vale 2004). QnD:HAAF V2 has, therefore, been expanded with a Hg volatilization pool that is filled daily with a spatial area characteristic rate following Equation 6A.5. Hg deposition has been included in the model formulation as a process augmenting the THg pool, but has not as yet been calibrated with monitoring data.

Biota

The biota and food web relationships in QnD:HAAF V2 are the same as in V1, since new information only recently became available and is reported in Best et al. (2007) and in Chapters 4 and 5 of this report. More realistic formulations of a typical salt marsh-associated food web and MeHg

bioaccumulation from food and environment may be feasible using this new information.

Selected organisms are currently included in QnD:HAAF V2, i.e., plants, invertebrates, and one vertebrate animal (a bird). Two emergent macrophytic plant species and one microalgal group are represented. *S. virginica* and *S. foliosa* are simulated simplistically as an established standing crop with constant biomass over the two-week simulation. Plant MeHg load (ng) and its potential contribution to MeHg export from the marsh were assumed to be the primary data of interest in these simulations. Epipelon (algae living on sediments) also potentially contribute to the MeHg export. The data on plant biomass, and THg and MeHg concentrations used for model calibration were collected in 2003 at HAAF and are presented in Table 6-2 (from Best et al. 2005). Four wetland invertebrates are modeled as potentially resident in all four spatial areas, but with population size and biomass being spatial area specific: the ribbed mussel (*Geukensia demissa*), yellow shore crab (*Hemigrapsus oregonensis*), and eastern mud snail (*Ilyanassa obsoleta*). These animals were identified in HAAF field samples in 2003 and are presented in Table 6-2 (from Best et al. 2005). To explore trophic transfer and bioconcentation of MeHg up the food chain, the California clapper rail (*Rallus longirostris obsoletus*) is included as potentially resident in all four spatial areas (Evens et al. 1991; Table 6-2). For the time being, it is assumed that biota do not migrate between spatial areas.

Food web relationships

The initial MeHg pool ($MeHg_{Load}$) for each organism is calculated following Equation 6A.6. Initial population size and biomass of the biota were estimated from literature values, since this information was not available for HAAF nor for the salt marsh at China Camp, considered as a reference for the future HAAF system. Population densities were assumed to vary with spatial area, depending on identified typical behavior of the organism. The calculated loads of MeHg in the biota are presented in Table 6-2.

Table 6-2. Initial estimated population size, biomass, MeHg concentration and loads of biota in QnD:HAAF V2.

Biota	Spatial area	Population ($N\ m^{-2}$)	Indiv. weight ($g\ DW\ indiv^{-1}$)	Biomass ($g\ DW\ m^{-2}$)	MeHg ($ng\ g^{-1}\ DW$)	Load ($ng\ m^{-2}$)
S. virginica				2000.0 [a]	1.64	3280.0
S. foliosa				2000.0 [a]	2.52	5040.0
Epipelon (all areas)				286.0 [b]	1.50	429.0
Ribbed mussel	Sal-marsh	12.0 [c]	0.2 [d]	2.4	1.86	4.46
Ribbed mussel	Spar-marsh	156.0	0.2	31.2	1.86	58.0
Ribbed mussel	Mud Flat	412.0	0.2	82.4	1.86	153.3
Ribbed mussel	Sub Tidal	412.0	0.2	82.4	1.86	153.3
Eastern mud snail	Sal-marsh	1.0 [d]	0.1 [d]	0.1	7.9	0.79
Eastern mud snail	Spar-marsh	1.0	0.1	0.1	7.9	0.79
Eastern mud snail	Mud Flat	10.0	0.1	1.0	7.9	7.9
Eastern mud snail	Sub Tidal	10.0	0.1	1.0	7.9	7.9
Yellow shore crab		1.0 [d]	2.0 [d]	2.0	1.72	3.44
Clapper rail		0.000125 [e]	69.2 [f]	0.00865	0.1[g]	0.00865

Note: [a] Best et al. 2005-Tables 3-5, 3-11; [b] 130 g C m^{-2} y^{-1}, with 1 g C = 2.22 g DW (Best et al. 2005-Table 3-1; after Onuf 1987); [c] Vitaliano and Bejda (2001); [d] Best et al. 2005-Chapter 6; [e] One rail per 0.8 ha (Gill 1979); [f] Weight per rail: 346.1 g wet or 69.22 g dry (U.S. Fish and Wildlife Service 2003); [g] Assumed initial load, since no data available.

The relationships between consumers and their food sources are formulated following a predator-prey approach, depend on species-characteristic prey demand, and are proportional with the predator biomass and prey availability (Figure 6-1). The intake of prey biomass by the predator ($Intake_{pred}$) is calculated following Equation 6A.7. The prey biomass is transferred from the prey pool to the predator pool, and if the prey pool is smaller than the demand of the predator, all available prey biomass is transferred to the predator pool. The predators, their prey, and prey demand rates are listed in Table 6-3.

Long-term changes in biomass due to growth and respiration are not included in QnD:HAAF V2. Plant (*Salicornia*, *Spartina,* and epipelon) and ribbed mussel biomass is assumed to be constant within the two-week simulation period. The predator biomass, which would increase because of feeding, is kept constant by loss of a fraction (mass-loss rate) set equal to the biomass intake rate to enable simulation of MeHg bioaccumulation due to trophic transfer. Predator mass loss rates are listed in Table 6-3.

The intake of MeHg with prey biomass ($MeHgIntake_{Prey}$) by predators is calculated by transferring the MeHg contained in the consumed prey biomass to the predator pool following Equation 6A.8, formulated after Rogers (1994).

Table 6-3. Predators and estimated prey demands and predator mass loss rates.

Predator	Prey species	Prey demand (g prey-DW g^{-1}predator-DW h^{-1})	Predator mass loss rate (g lost-DW g^{-1} predator-DW h^{-1})
Eastern mud snail [a]	Epipelon	0.0042[a]	0.006[d]
Yellow shore crab[b]	Epipelon	0.0003[b]	0.006[e]
Yellow shore crab[b]	Eastern mud snail	0.0003[b]	0.006[e]
Yellow shore crab[b]	Ribbed mussel	0.0003[b]	0.006[e]
Clapper rail[c]	Eastern mud snail	0104[c]	0.021[f]
Clapper rail[c]	Ribbed mussel	0.0052[c]	0.021[f]
Clapper rail[c]	Yellow shore crab	0.0052[c]	0.021[f]

Note: [a] 10% predator-biomass per day; [b] 20% predator-biomass per day; [c] 50% predator-biomass per day, based on a diet composed for 50% by ribbed mussels, 25% by mud snails, and 25% by shore crabs (Shellhammer 2000; U.S. Fish and Wildlife Service 2003); [d] 10% predator-biomass per day; [e] 20% predator-biomass per day; [f] 50% predator-biomass per day.

Intake of methylmercury by biota from sediment

In QnD:HAAF V2, all biota have intake and loss rates that allow them to potentially bioaccumulate and release MeHg. This methodology is in agreement with DTMC/ SRWP (2002), recommending an initial simplified approach, followed by a detailed bioenergetic approach once MeHg data become available for higher trophic levels. Data on intake and bioaccumulation of MeHg from soil, sediment, and pore water are still extremely scarce in the literature, and they are, therefore, largely estimated from data published by Rogers 1994; Mason et al. 1994; Barber 2001, and Best et al. 2005. MeHg is only taken in from sediment when the organismal MeHg concentration is less than the sediment MeHg concentration, since the latter is assumed to be in equilibrium with the environment. The same potential MeHg transfer rate ($Transfer_{sed}$) of 0.14042 ng MeHg g^{-1} organism-DW from sediment into organism is used for all organisms (Table 6-1). This value was measured in preliminary Hg uptake experiments on the filter-feeding *Macoma balthica* (Best et al. 2005, Chapter 6). Intake of MeHg from sediment ($MeHgIntake_{sed}$) is calculated following Equation 6A.9, is proportional to the biomass of the organism, and is limited to 0 when the organismal MeHg concentration reaches the species-characteristic equilibrium level.

Loss of methylmercury from biota

Both macrophytes, *S. virginica* and *S. foliosa*, lose an estimated 50% of their biomass per year (Best et al. 2005, Table 3-11), and the associated MeHg fraction contained in the plant material. In QnD:HAAF V2, all plants (macrophytes and epipelon) are modeled as losing 50% of the MeHg contained in their maximum standing crop per year (i.e., 5.7078 x 10^{-3} percent h^{-1}; Table 6-1). All animals are assumed to lose 10% of their body- MeHg load per day (i.e., 0.4167 percent h^{-1}; Table 6-1), despite the fact that estimated loss rates based on diet intake are far lower (Table 6-3). The latter value is based on a study on elimination of THg and MeHg by the zooplankter *Daphnia magna* feeding on phytoplankton (Tsui and Wang 2004). This amount of MeHg lost enters a general potential MeHg export pool to the bay.

QnD:HAAF V2 Simulation Results

Two hourly time series were simulated, i.e., one scenario representing a wet season (1–14 February 2005) and one scenario representing a dry

season (1–14 June 2005). The tidal water levels relative to the elevations of the typical HAAF spatial areas are shown in Figure 6-8.

Comparison of simulated sediment MeHg concentrations and transfer rates under wet and dry season conditions

The simulation results for all spatial areas, i.e., *Salicornia* (High) Marsh, *Spartina* (Mid) Marsh, Mud Flat and Sub Tidal, are presented separately to facilitate comparison. Within the HAAF landscape, however, the spatial areas will differ in size.

The simulated sediment MeHg concentrations increased far more during the wet season than during the dry season (Figure 6-9). Increases were several orders of magnitude greater in bare than in vegetated sediments, largely because the base methylation rates used for calibration were about three times higher in bare than in vegetated sediments, while the base demethylation rates were on the same order of magnitude in all spatial areas. The simulated MeHg concentrations stabilized in the wet season at 7 ng g^{-1} in the *Salicornia* Marsh, 15 ng g^{-1} in the *Spartina* Marsh, 43 ng g^{-1} in the Mud Flat, and 27 ng g^{-1} in the Sub Tidal spatial area (Figure 6-9). The simulated MeHg concentrations stabilized in the dry season at 4 ng g^{-1}in the *Salicornia* Marsh, 5 ng g^{-1} in the *Spartina* Marsh, 18 ng g^{-1} in the Mud Flat, and 12 ng g^{-1} in the Sub Tidal spatial area (Figure 6-9). The simulated wet season MeHg concentrations in particular exceeded non-vegetated marsh sediment MeHg concentrations found during previous field studies, maximally 5.6 ng g^{-1} (Best et al. 2005, Table 3-5), indicating that simulated net MeHg production exceeded actual net MeHg production and/or substantial MeHg export from sediment leading to lesser sediment MeHg concentrations.

The simulated methylation and demethylation rates in the sediments of the four spatial areas leading to the above-mentioned MeHg concentrations are shown in Figure 6-10. Also in this case, the increasing effect of the wet relative to the dry season was apparent. The potential MeHg transfer rates in the wet season for methylation increased in the order of *Salicornia* Marsh>*Spartina* Marsh>Sub Tidal> Mud Flat up to 13,500 ng m^{-2} h^{-1}, while the demethylation rates increased in the order of *Salicornia* Marsh>*Spartina* Marsh>Sub Tidal> Mud Flat up to 5,486 ng m^{-2} h^{-1}.

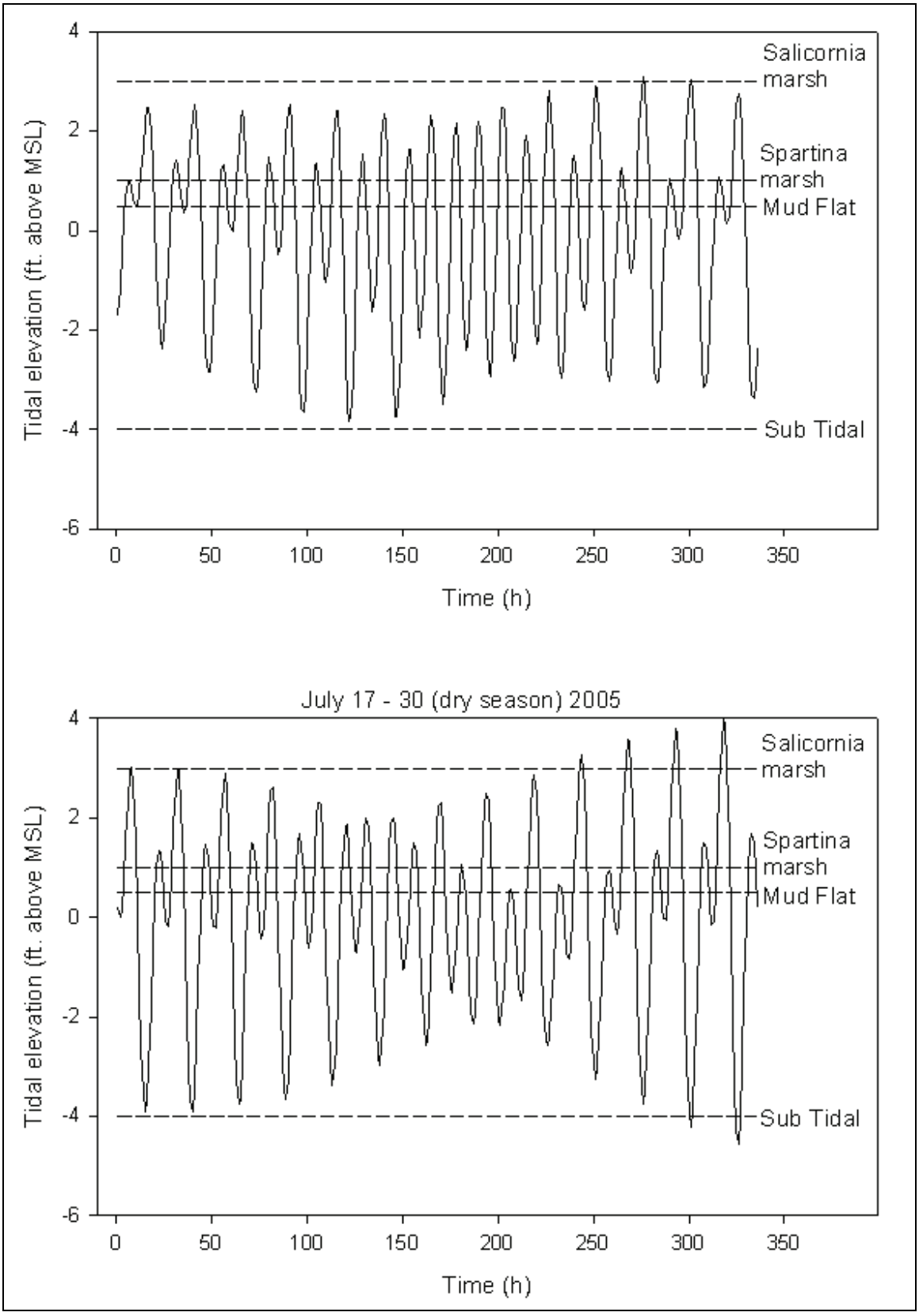

Figure 6-8. Tidal water levels in the wet and dry seasons relative to the typical elevations of the HAAF spatial areas.

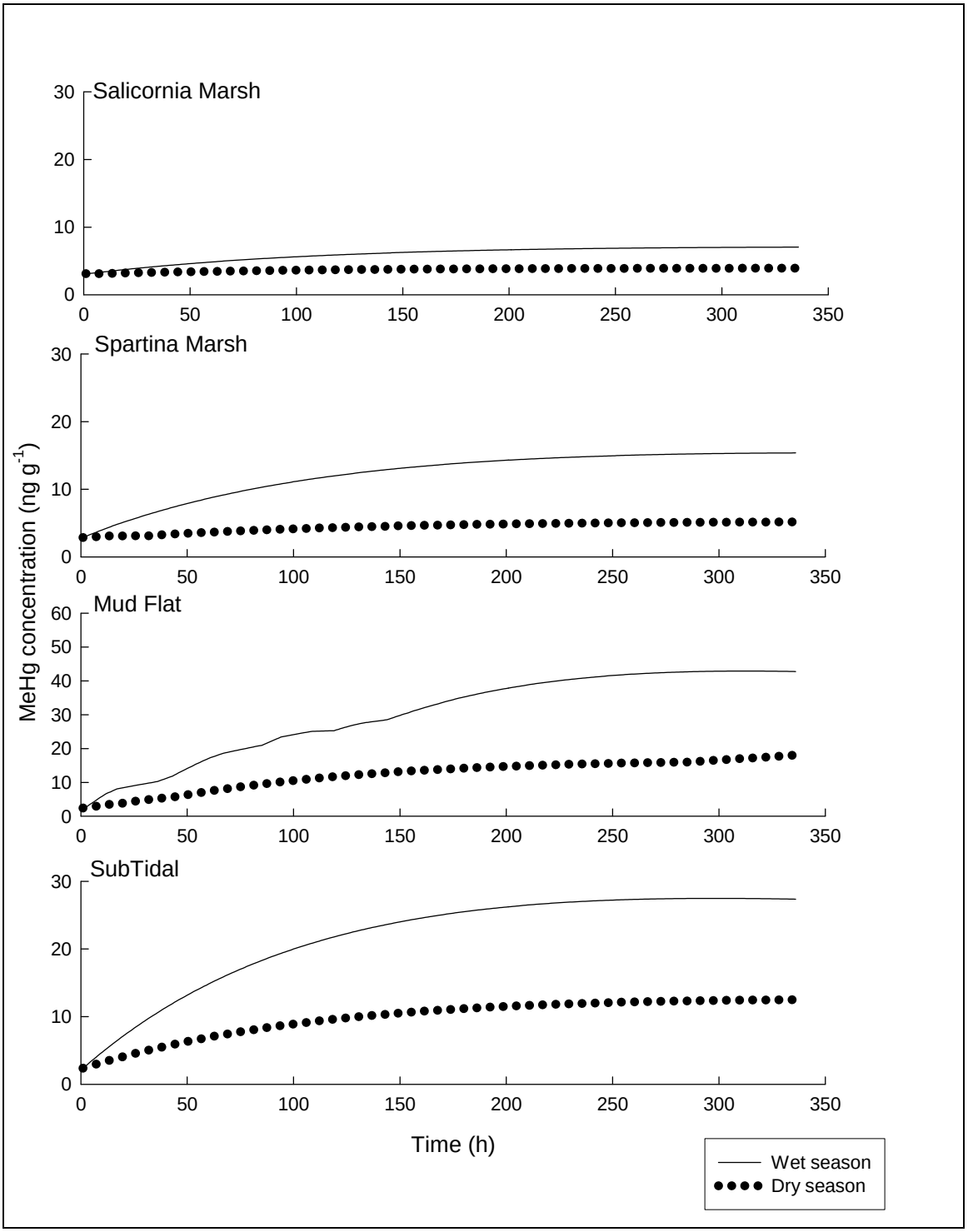

Figure 6-9. Simulated MeHg concentrations in surface sediments of the spatial areas.

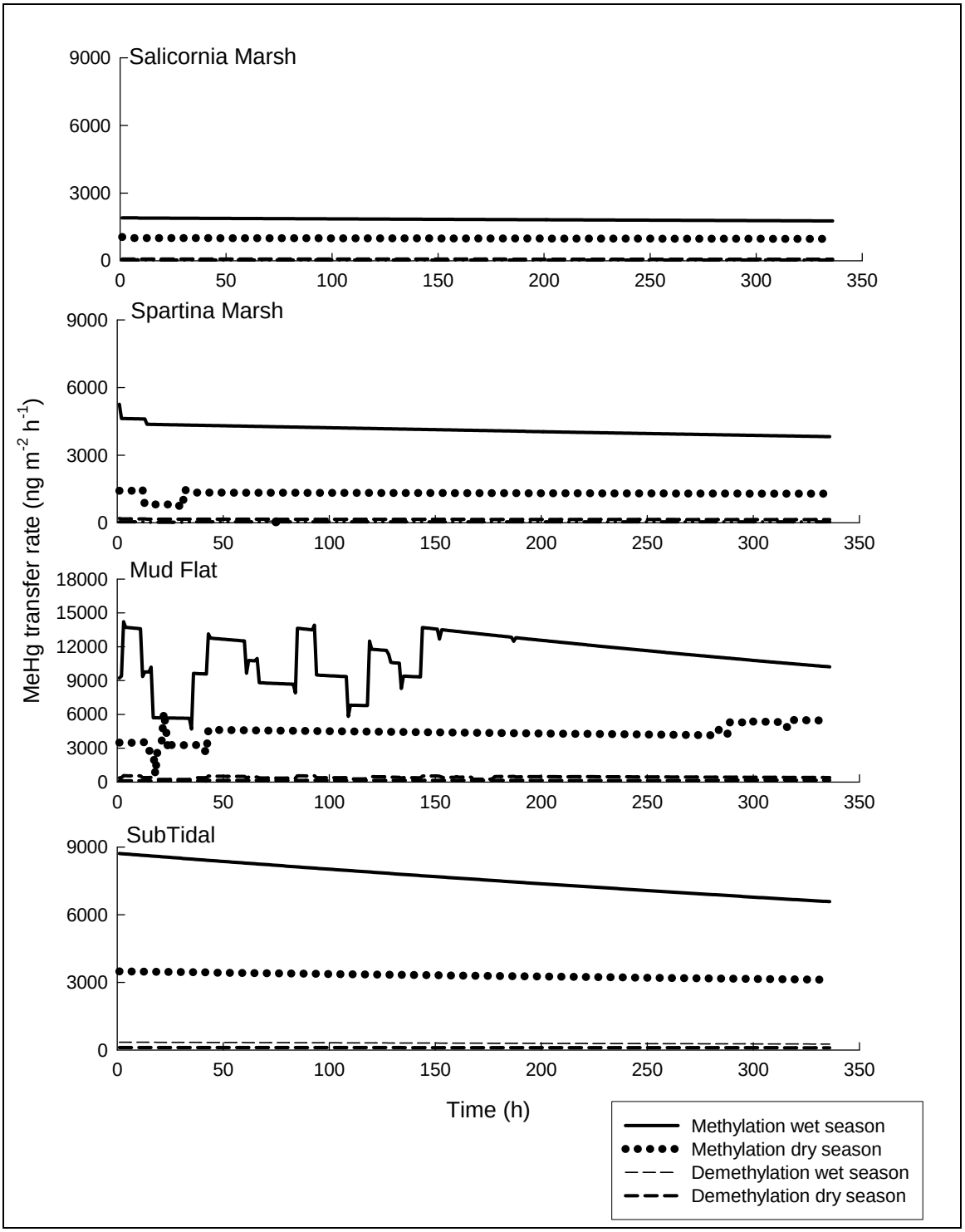

Figure 6-10. Simulated methylation and demethylation rates in surface sediments of the spatial areas.

Particularly the Mud Flats showed great and variable methylation and demethylation rates, and inherent net MeHg production, due to the tidally induced changes in redox potential. This is in agreement with observations by Gribsholt and Kristensen (2003), who found the greatest sulfate reduction (presumably with concomitant methylation) in the transition zone between marsh and mudflat. The methylation and demethylation rates did not reach equilibria during the two-week simulated period in the *Spartina* Marsh and Mud Flat spatial areas.

Methylmercury export

Potential MeHg export was considerable in all spatial areas. In QnD:HAAF, potential export encompasses export with tidal movements and by diffusion. Simulated results showed a large difference in export by spatial areas and seasons (Figure 6-11). In the wet season, export increased in the order of *Salicornia* Marsh (67 ng m^{-2} h^{-1})<*Spartina* Marsh (158 ng m^{-2} h^{-1})<Sub Tidal (292 ng m^{-2} h^{-1})< Mud Flat (440 ng m^{-2} h^{-1}). In the dry season potential export was a factor of two to three less.

By scaling the sizes of the spatial areas up to an area with the size of the future HAAF tidal wetland, i.e. 203 ha, insights were gained into the potential consequences of wetlands such as the HAAF-wetland for the MeHg TMDLs in San Pablo Bay. Export of 1 ng MeHg m^{-2} (wetland area) h^{-1} would result in an input of 17.8 g MeHg $system^{-1}$ y^{-1} in San Francisco Bay, and, therefore, MeHg export from a HAAF-size wetland would potentially range from 934 to 5718 g MeHg y^{-1} (Table 6-4). These values generated by dynamic simulation are far higher than those derived from relatively simple, back-of-the envelope, calculations using static measured values, as presented earlier (Table 6-4; from Best et al. 2005, Table 3-12). Dynamic simulations often yield higher production values for ecosystems than calculations based on values collected with a low frequency, e.g. for wetland vegetation (Morris and Haskin 1990). However, for the current HAAF case and for other wetland restoration and creation plans, it would be prudent to narrow the range of potential MeHg export and fate, effects, and consequences for the food chain of MeHg further down.

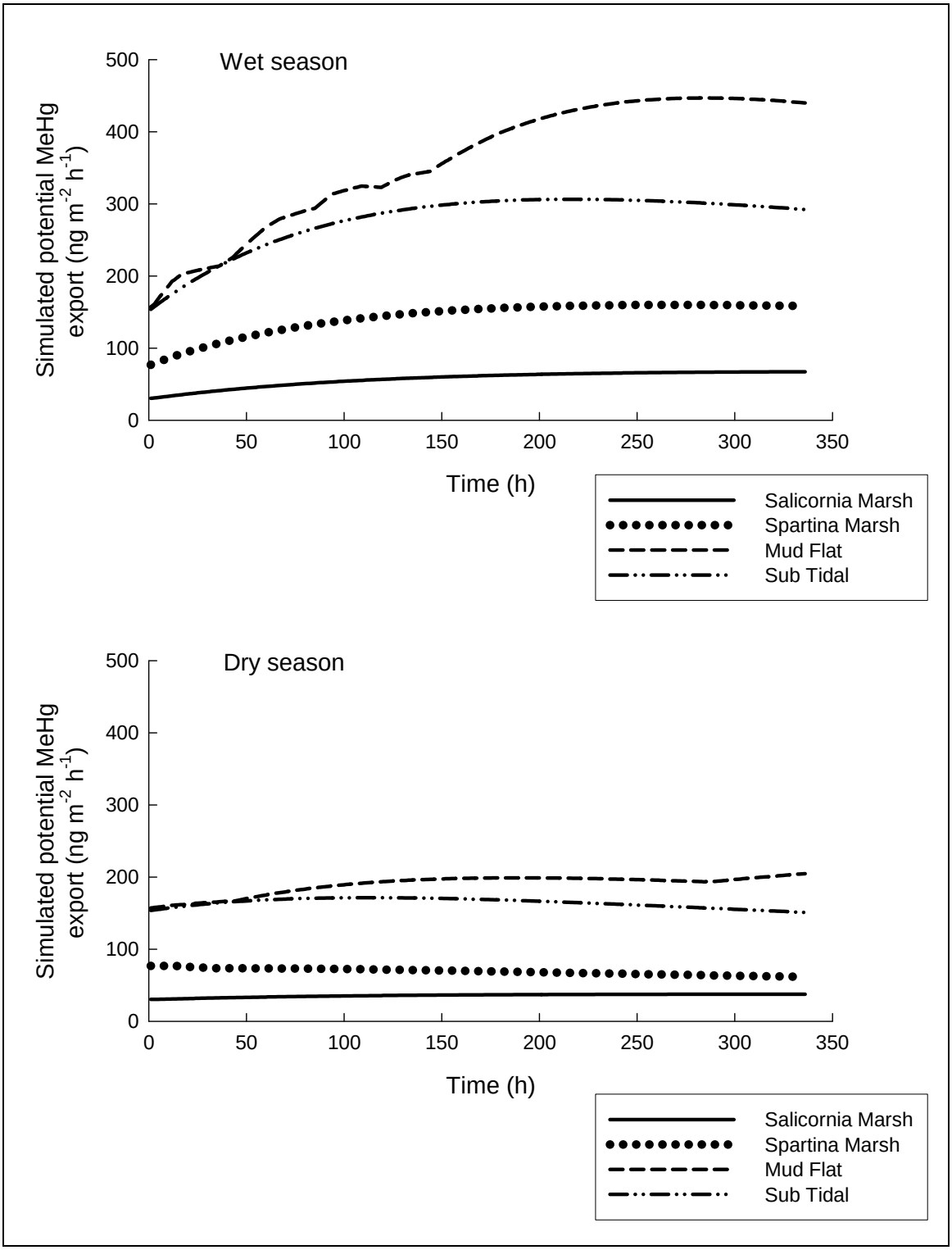

Figure 6-11. Simulated potential MeHg export rates from the surface areas of the spatial areas.

Table 6-4. Estimated potential MeHg export from tidal marsh areas in a restored HAAF wetland using the simulation approach shown in Figure 6-11 and a static approach including measured values shown in Table 3-12 from Best et al. (2005).

Marsh type	Net MeHg export (ng m^{-2} h^{-1})		Potential total MeHg export (g $system^{-1}$ y^{-1})[b]
	Wet season[a]	Dry season[a]	
Simulation approach			
Salicornia Marsh	67.4	37.7	933.7
Spartina Marsh	158.4	61.7	1954.6
Sub Tidal	439.7	204.0	5717.5
Mud Flat	292.2	151.0	3937.1
Static approach			
Salicornia Marsh	NA	NA	143
Spartina Marsh	NA	NA	89
Mud Flat	NA	NA	18

Note: [a] Wet season lasts 182 days (1 November to 30 April), dry season 183 days (1 May to 30 October)
[b] Surface area of HAAF wetland is 203 ha.

Mercury dynamics in biota

QnD:HAAF simulation results for the potential MeHg biomagnification up the food chain depend strongly on the size of the bioavailable MeHg pool in the sediment and on the MeHg body burdens in the biota of each of the four spatial areas.

Mercury dynamics in plants

At the current stage of QnD:HAAF development, biomass and initial MeHg levels in all plants were kept at levels measured in 2003 and did not change, because they were only measured at one point in time (Best et al. 2005, Chapter 3). This was done to keep initial model development simple. However, macrophytes and microalgae may play varied roles in the food webs of San Francisco Bay wetlands, as became apparent recently (Best et al. 2007, Chapter 7; Chapter 5, this report), and these relationships may serve as a basis for a more realistic model approach to food web relationships. Thus, based on this simplified assumption, *Salicornia* and *Spartina* had little influence on the overall MeHg dynamics within the sediment and in animals. Simulated uptake of MeHg by the plants was only to replace what was lost via simple export.

Mercury dynamics in animals

At the current stage of QnD:HAAF development, the simulations were started from biomass and initial MeHg levels in all animals (mussels, snails, shore crabs, and clapper rails) measured at one point in time (Best et al. 2005, Table A5-8). Simulation results conducted for the dry and wet seasons showed that the MeHg pools in the various spatial areas were large enough to allow unlimited uptake and bioaccumulation of MeHg in animals.

Simulation results on sediment-dwelling animals with a high biomass, such as the ribbed mussel in the Mud Flat and Sub Tidal spatial areas, indicated that these animals exhibit stable uptake and retention of MeHg because their biomass is high and loss from predation by clapper rails and crabs is small. This can be explained from the fact that most potential losses of MeHg from these animals, ranging from 0.43 in the High Marsh spatial area to 14.9 ng m^{-2} d^{-1} in the Sub Tidal spatial area, were regained through uptake of MeHg through the ingestion of sediment. Given the current assumptions of QnD:HAAF, ribbed mussels and epipelon may play similar roles as mid-level organisms in the food chain transfer of MeHg. These preliminary judgments are based on the assumptions of large, initial biomass levels with no short-term changes in biomass. Once biomass growth and mortality are simulated, these dynamics may result in different conclusions.

Simulation results on sediment-dwelling animals with a lower biomass than ribbed mussels, such as eastern mud snails (0.1 to 1.0 g DW m^{-2}), showed that these animals are more sensitive to predation by crabs and clapper rails, since their biomass decreased in both seasons over the two-week period. The snails are different from mussels in that they bioaccumulate MeHg directly from sediment and by consuming epipelon. Because sediment and epipelon pools are large, the uptake of MeHg by snails was unlimited. The MeHg concentration in snails remained, therefore, close to the initial level of 7.9 ng MeHg g^{-1}. In addition, because of the low biomass and MeHg body burdens, the potential loss of MeHg from these animals (0.036 to 0.36 ng m^{-2} day^{-1}) was also small compared to exports from other MeHg sources.

Yellow shore crabs have a biomass on the same order of magnitude as eastern mud snails, a relatively lower MeHg body burden at equilibrium, but provide a significant resource for predators higher up the food web.

Simulation results indicated that the biomass of the crabs decreased substantially and in all spatial areas in both seasons over the two-week period due to the assumed biomass loss and predation by clapper rails. The MeHg concentration in crabs decreased slightly, i.e., 1.72 to 1.68-ng-g^{-1}, over the simulation period since the MeHg loss rate decreased the MeHg loads of the crabs. In exploratory sensitivity analysis simulations, biomass and MeHg concentrations of the crabs were more sensitive to assumed biomass loss than to direct MeHg loss from biomass- probably since the MeHg concentration at equilibrium was extremely low.

The clapper rail is considered as a 'capstone' species. It has the lowest biomass of all animals considered in HAAF-QnD, and the initial MeHg concentration was intentionally set low to explore the bioaccumulation of MeHg. Simulated results indicated that under the initial diet and MeHg assumptions, clapper rails may bioaccumulate MeHg to substantial levels within an ecosystem such as HAAF. All clapper rail MeHg concentrations increased from 0.3 to 12 ng g^{-1} almost entirely through their diet of snails, crabs, and mussels.

Addressing Questions Raised at the CALFED Stakeholders Workshop 8-9 October 2002 at the Moss Landing Marine Laboratories Using QnD:HAAF V2

What are the present levels of MeHg in San Francisco Bay wetlands with respect to biota, sub-habitats, and location within the Bay?

MeHg levels in biota were simulated in such a way that they could not exceed the equilibrium concentrations measured in the field samples collected in 2003. The QnD:HAAF simulation results indicated a significant bioaccumulation potential of MeHg from lower to higher trophic levels, regardless of season. Simulations were greatly inhibited by the lack of available data on food chain structure, components, and MeHg accumulated in the biota. However, new data have recently become available and may be used as a basis for further model development (Best et al. 2007, Chapter 7; 2008; 2009, Chapters 4 and 5 of this report).

The initial sediment MeHg levels used in the simulations for the four sub-habitats, represented by the spatial zones in QnD:HAAF, ranged from 2.38 ng MeHg g^{-1} DW in the Sub Tidal area to 3.15 ng MeHg g^{-1} DW in the *Salicornia* Marsh, and were derived from measured levels in 2004 (Best et al. 2007, Table 3-3, reference site China Camp). The simulated MeHg

levels in the four sub-habitats showed dynamics that depended on season and redox levels. MeHg concentrations increased over the two-week simulation period in all areas and both seasons to levels vastly exceeding the measured levels. Simulations for sites other than the HAAF wetland have not as yet been conducted.

What are the rates of MeHg production?

The simulated methylation and demethylation rates ranged from 35 ng m^{-2} h^{-1} (demethylation *Salicornia* Marsh, dry season) to 13,510 ng m^{-2} h^{-1}(methylation Sub Tidal, wet season) depending on environmental conditions. Measured field data and estimated effects of daylight, redox potential via tidal movements, and season were used as a basis for these simulations. The fluctuations in methylation and demethylation due to the effect of time of day (being light or dark) found in earlier simulations presented in Best et al. (2005, Chapter 5) did not show, because the recalibration was based on daily values without distinction between light and darkness. Within areas that were frequently flooded and exposed to air, the redox potential became an important driver. The four spatial zones exhibited methylation rates that varied considerably with the tidal movements, because of the assumed 90-percent decreased methylation under air-exposed conditions. Methylation was assumed to be increased maximally by a factor of 2.5 during the wet season compared to methylation in the dry season, and, this, therefore, directly affected net MeHg production and pool size. The first simulation results compare favorably with the scarce values published for similar marsh areas. However, more monitoring data are required on the variation in net MeHg production in spatial zones and locations within the bay, for higher confidence in the potential of the QnD:HAAF model results.

What factors control MeHg production? Can these be managed?

Of the three environmental drivers included in QnD:HAAF V2, tidal action, wet/dry season, and daylight, it was tidal action that had the greatest influence on net MeHg production. This factor is not easily managed, and the only management option available to minimize net MeHg production by minimizing sediment exposure to tides would be to create a wetland with a high proportion of high marsh. Because these drivers are confounded with other factors affecting net MeHg production, a more detailed discussion of mercury cycling controlling factors and

options to minimize meHg impacts of wetlands restoration and management in San Francisco Bay is presented below.

Are some wetlands larger mercury exporters than others?

Potential export in QnD:HAAF V2 includes THg and MeHg export and MeHg diffusion. The exported Hg species are deposited into separate 'potential export' pools, one for THg and one for MeHg. How export takes place is not specified, and, thus, movement with tides is not specifically described. Export by volatilization of THg from sediment is considered as a separate process. Simulated potential export from the spatial zones proved to be vastly different, and based on these simulations it is to be expected that wetlands predominated by a relatively large share of mudflats may produce a relatively high contribution to the MeHg TMDL in the Bay. The latter is in contrast to earlier simulation results (Best et al. 2005, Chapter 5) where calibration was based on initial values of methylation and demethylation measured in 2003 (Best et al. 2005, Chapter 3), which indicated a greater net MeHg production in vegetated wetlands than in mudflats and subtidal areas. Simulated potential export greatly exceeded the export estimated from simple calculations using static values measured in the dry season (Table 6-4). Although dynamic simulations often yield greater production values for ecosystems than calculations based on values collected with a low frequency, it would be prudent to reach a better understanding of the discrepancy between simulated and measured export before using these model outcomes as a guide for the current HAAF case and for other wetland restoration and creation plans.

Can we model/predict the effects of wetland restoration on MeHg production and export?

Models exist as testing platforms of concepts and measured data. The predictive power of models usually grows with the confidence of the users in the concepts and data on which the models are based, and in the model results that reflect phenomena users can observe. QnD:HAAF V2 is based largely on field data on methylation and demethylation rates in 2003 and 2004-5, and on field data on Hg species in biota in 2003. Most data on local and regional environmental conditions, and on biota have not yet been incorporated into the model. However, with this still limited data set, the model results have generated several interesting points for discussion and further exploration.

General Discussion of Mercury Cycling and Options to Minimize MeHg Impacts of Wetland Restoration and Management in San Francisco Bay

Mercury

Hg is a metal of concern. One of the methylated forms of Hg, MeHg, is far more toxic than Hg and has great biomagnification potential. The Hg concentrations in the majority of the San Francisco Bay sediments are 300 ng g^{-1} dry weight, with MeHg typically being 1% or less of total Hg.

Sources and transport of mercury

Although the dominant global transport mechanism for Hg is through atmospheric dispersion (Mason et al. 1994), other mechanisms become relatively more important within coastal zones. Through runoff from mining areas, erosion of floodplain soils and traditional waterfront siting of industrial facilities, rivers may serve as major transport conduits for particulates. The potential delivery of river-borne contaminants to the coastal part of the ocean is further mediated via the chemical, physical, and biological interactions in estuaries such as San Francisco Bay. Studies of Hg transport across the estuaries of large, industrial rivers have demonstrated that while fluvial Hg transport may be significant, Hg is effectively trapped and recycled within the estuarine zone (Turner et al. 2001; Stordal et al. 1996). In stressing the storage potential of estuaries, it is important to consider whether these environments ultimately serve as long-term sinks or sources of Hg contamination. Specifically, it is important to assess the extent to which estuarine storage may affect the speciation and bioavailability of the introduced Hg pool. It has been demonstrated that estuary sediments may act as a net sink for particulate Hg inputs, but also function as a source of dissolved, ligand-mediated, Hg for a considerable period of time (Penobscott River estuary, ME; Merritt 2007; Merritt and Amirbahman 2007).

Mercury species transformation processes

MeHg production is the net result of methylation and demethylation rates, and input/output processes. In surface sediments methylation has been shown to dominate over the other two processes (Hintelmann et al. 2000; Drott et al. 2007, 2008). Biotic methylation occurs predominantly in the sediment; however, because the water column is by volume far larger, water column methylation is also important.

Mainly sulfate-reducing bacteria (SRB), but iron-reducing bacteria (FeRB) as well, methylate inorganic Hg (Compeau and Bartha 1985; Kerin et al. 2006).

Methylation and demethylation are influenced by both the speciation and bioavailability of the metal/metalloid, the microbial community, and a large number of environmental factors, many of which are interrelated. Trends of environmental factors affecting methylation/demethylation rates are presented in Table 6-5 (after USEPA 2007). Maximum methylation rates typically occur at the redox boundary, which may vary seasonally and tidally and frequently coincides with the sediment-water interface (Ulrich et al. 2001). Methylation rate decreases with sediment depth. Bacteria may also demethylate MeHg. Microbial populations usually increase with the amount of organic material in a system. High temperatures and anaerobic conditions favor methylation, and low temperatures and/or aerobic conditions favor demethylation. pH does not appear to directly influence methylation/demethylation processes, but indirectly affects solubility and electron donor and acceptor concentrations. In reducing environments, increasing sulfide concentration decreases methylation rates.

Table 6-5. General trends of environmental factors affecting rates of methylation and demethylation.

Organometallic transformation	Temperature		pH		SO_4^{2-}	Organic matter	Redox		Salinity
	High	Low	High	Low	High		Oxic	Anoxic	High
Net methylation	↑	↓	?	?	?	?	↓	↑	↓
Methylation aq	↑	↓	↓?	↑?	↓	↑↓	↓	↑	↓
Methylation sed	↑	?	↑	↓	↓	?	?	?	?
Demethylation	↓	↑		↑	?	?	↑	↓	?

Note: ↑ indicates an increase in rate.
↓ indicates a decrease in rate.
? indicates conflicting data or insufficient data to indicate a likely trend.

Net MeHg production reaches an optimum under suboxic and low anoxic conditions, with sulfide concentrations below ~10-50uM (Gilmour et al. 1998). The methylating process is believed to take place within bacterial cells. Because of this, the methylating activity of bacteria is controlled by the availability of electron-donors, electron-acceptors, and bioavailable forms of inorganic Hg. The neutral form $HgCl_2^0$ is preferentially taken up

over negatively charged $HgCl_3^-$ and Hg-DOC complexes (Barkay et al. 1997).

The chemical composition of bioavailable forms of Hg, for methylating bacteria, and of MeHg, for demethylation reactions, is of major importance for the production and bioaccumulation of MeHg in food webs. The bioavailable forms of Hg and MeHg are determined by the competition among dissolved thiols, inorganic monosulfides, bisulfides and polysulfides, as well as their competition with organic and inorganic particle surfaces and solid phases. Several computational approaches to estimating Hg and MeHg species bioavailabilities have recently been published (Skyllberg 2008).

Within non-vegetated sediments, the greatest MeHg production occurs at shallow sediment depths, with a sharp decrease in pore water MeHg concentration near the sediment-water interface likely explained by demethylation. With ponding overlying water, the redoxcline moves upwards and, thus, greatest net methylation moves closer to the sediment surface. In contrast, with shoaling, overlying water the MeHg efflux from the sediment-water interface increases (Merritt 2007).

Within vegetated sediments of salt marshes, methylation rates of cores exposed to ambient light exceeded those kept in darkness, illustrating the stimulating effect of root-DOC during periods of high photosynthesis of *Salicornia* and *Spartina* in June. Methylation rates exceeded demethylation rates as well when exposed to ambient light (Best et al. 2005). Sites with Hg that exhibit sulfate reduction are likely to exhibit methylation, because most methylating bacteria are SRBs. Therefore, the results of Best et al. (2005) agree with those of Hines et al. (1989) indicating that sulfate reduction in a *Spartina* marsh increased greatly with rapid plant growth in spring (high delivery of DOC via roots) and decreased with scenescing plants in late summer (low delivery of DOC via roots). Observations on another *Spartina* marsh tied plant activity directly to redox potential and sulfate reduction, indicating that oxidizing activity of roots with its inhibitory effect on sulfate reduction decreased with decreasing tidal elevation, with the greatest sulfate reduction occurring in the transition zone between marsh and mudflat (Gribsholt and Kristensen 2003). The greatly increased activity in the latter zone was explained by receipt of substantial seepage of DOC-poor and HCO_3-rich pore water from the marsh during low tide, followed by massive release of HCO_3 during high

tide stimulating sulfate reduction. Because the latter studies were conducted in August-September, when plant activity decreases, it is feasible that this phenomenon typical for the marsh transition zone occurs year-round.

Options to minimize MeHg impacts of wetland restoration and management in San Francisco Bay

Wetlands restoration in and around San Francisco Bay requires large quantities of sediment to elevate the subsided land to an elevation suitable for colonization by wetland vegetation. Coastal wetlands are typically exposed to tidal waters and vegetated by wetland plants. Coastal wetlands serve as habitat for certain organisms and as feeding area for others.

- Sediment quality. Most surface sediments in and around San Francisco Bay contain 300 ng g^{-1} Hg. When used for wetlands restoration, these sediments form a potential source for methylation. Use of deeper sediments and sediments from other areas less rich in Hg may form a smaller Hg source.

- Methylation controlling factors. Methylation is controlled by the availability of electron donors, electron acceptors, and bioavailable forms of inorganic Hg. Methylation can be constrained by limiting the wetland portions with optimum conditions for methylation. This can be done by designing coastal wetlands with a relatively large zone at high elevation and keeping the 'edge' surface area as small as possible (e.g., by limiting the number of creeks and designing/ maintaining regular wetland-mudflat transition zones with a relatively steep slope). Methylation can also be limited by decreasing the amount of sulfate for SRB by facilitating precipitation and adsorption reactions."

- Organisms with potential for MeHg bioaccumulation. The major pathway for MeHg bioaccumulation is via the ingestion of food. Aquatic systems have more complex food webs and more trophic levels, and the primary producers from aquatic systems may accumulate more Hg from water and sediment than do soil-based primary producers in terrestrial systems. Therefore, top predators in aquatic systems are at greatest risk from MeHg bioaccumulation. The compositions of aquatic, semi-aquatic, and high marsh food chains are not fully known, and, therefore, management measures targeted at minimizing MeHg levels in selected species are not yet feasible. However, for now it may

be possible to minimize access to identified hotspots of methylation by the creation of (physical) barriers for the organisms of interest.

Conclusions and Recommendations for Research

1. QnD:HAAF Version 2 (QnD:HAAF V2) was developed in 2006-2007, based on QnD :HAAF V1.

2. QnD:HAAF V2 differs from V1 by inclusion of:
   a. A HAAF base map containing 100- x 100-m grid cells and digital elevation information.
   b. Verified, realistic elevation assignments to the spatial areas and tidal movements pertaining to 2005.
   c. Revised formulation of net methylmercury production matching field data collected after 2003.
   d. MeHg diffusion from sediments.
   e. Hg deposition and volatilization from wetlands module.

3. From comparisons of simulated and measured data, it appears that:
   a. Simulated MeHg concentrations in sediments of the spatial areas exceeded measured MeHg concentrations, potentially indicating either limitations to solubilities of Hg species and, therefore, limited export, or considerable transport with tidal waters. A data gap exists on the concentrations of Hg species and important electron donors and acceptors in sediments of various locations within the Bay and adjacent wetlands.
   b. Simulated potential export of MeHg from wetlands exceeded MeHg export calculated from measured values, causing uncertainties in the contribution of wetlands to the MeHg TMDL of the Bay.
   c. A data gap exists on food chain structure, components, bioaugmentation mechanisms and MeHg accumulated in the biota associated with San Francisco Bay wetlands.

4. The following actions are recommended:
   a. Expand QnD:HAAF with descriptions of factors controlling methylation in coastal wetlands (temperature, sulfate reduction, salinity).
   b. Explore the speciation of Hg species for the San Francisco Bay wetland situation following existing modeling approaches describing competition among organic matter and sulfurous compounds for Hg and MeHg, using existing environmental data; include new insights in QnD:HAAF.

c. Include better descriptions of selected San Francisco Bay marsh-associated food webs in QnD:HAAF, e.g., as presented in Chapter 4, and conduct simulations.
d. Explore monitoring data associated with San Francisco Bay wetlands mercury Cycling, e.g., RMP 2006, for use in QnD:HAAF (validation, exploration).
e. Identify crucial data gaps and formulate projects to collect this information.

Equations

$$WaterDepth = TidalDepth - Elev_{base} \quad (6A.1)$$

$$Load = Conc \times Depth \times BD \times 1000 \quad (6A.2)$$

$$MeHgn = ((BaseRate_{meth} \times TotalHg) - (BaseRatede_{meth} \times new\ MeHg)) \times Season(month) \times \mathrm{Re}\, dox_m(hours) \times Light_m(daylight) \quad (6A.3)$$

$$DemethHg_t = BaseRate_{Demeth} \times \mathrm{Re}\, dox_d(hours) \times Light_d(daylight) \times new\ MeHg_t \quad (6A.4)$$

$$THgAirVol = TotalHg \times VolRate_{Marshtype} \quad (6A.5)$$

$$MeHg_{Load} = Org_{biom} \times Conc_{MeHg} \quad (6A.6)$$

$$Intake_{pred} = Biom_{pred} \times DemandRate_{prey} \quad (6A.7)$$

$$MeHgIntake_{prey} = Biomass_{pred} \times \mathrm{Pr}\, eyConsumed \times MeHg_{prey} \quad (6A.8)$$

$$MeHgIntake_{sed} = Biomass \times Transfer_{sed} \times Sat(MeHg_{conc}) \quad (6A.9)$$

References

American Society for Testing and Materials (ASTM). 2008. Standard guide for conducting acute toxicity tests on aqueous ambient samples and effluents with fishes, macroinvertebrates and amphibians. ASTM E1192-97.

Barber, M. C. 2001. *Bioaccumulation and Aquatic System Simulator (BASS) User's Manual Beta Test Version 2.1*. USEPA Report No. 600/R-01/035. http://www.epa.gov/AthensR/staff/members/barbermahlonc/bass21_manual.pdf

Barkay, T., M. Gillman, and R. R. Turner. 1997. Effects of dissolved organic carbon and salinity on bioavailability of mercury. *Applied and Environmental Microbiology* 63: 4267-4271.

Bartlett, P. D., and P. J. Craig. 1981a. Total mercury and methylmercury levels in British estuarine sediments. *Applied and Environmental Microbiology* 63: 37-47.

Bartlett, P. D., and P. J. Craig. 1981b. Total mercury levels in British estuarine sediments-II. *Water Research* 15: 37-47.

Beijer, K., and A. Jernelow. 1979. Methylation of mercury in aquatic environments. In The biogeochemistry of mercury in the environment. *Topics in Environmental Health, Volume 3*, ed. J. O. Nriagu , 203-210. New York: Elsevier/North-Holland.

Benoit, D. A., F. A. Puglisi, and D. L. Olson. 1982. A fathead minnow *Pimephales promelas* early life stage toxicity test method evaluation and exposure to four organic chemicals. *Environmental Pollution Series A* 8: 189–98.

Benoit, J. M., C. C. Gilmour, R. P. Mason, and A. Heyes 1999. Sulfide controls on mercury speciation and bioavailability to methylating bacteria in sediment and pore waters. *Environmental Science and Technol*ogy 33: 951-957.

Berner, R. A. 1971. *Principles of chemical sedimentology*. New York: McGraw-Hill.

Berner, R. A. 1980. *Early diagenesis: A theoretical approach*. Princeton, NJ: Princeton University Press.

Best, E. P. H., A. J. Bednar, H. Hintelmann, and B. Dimock. 2008. Natural cycles and transfer of mercury through Pacific coastal marsh vegetation by dominated by *Spartina foliosa* and *Salicornia virginica*. *Estuaries and Coasts* 31: 1072-1088.

Best, E. P. H., H. L. Fredrickson, H. Hintelmann, O. Clarisse, B. Dimock, C. H. Lutz, G. R. Lotufo, R. N. Millward, A. J. Bednar, and J. Furey. 2007. *Pre-construction bio-geochemical analysis of mercury in wetlands bordering the Hamilton Army Airfield (HAAF) wetlands restoration site; Part 2*. ERDC/EL TR-07-21. Vicksburg, MS: U.S. Army Engineer Research and Development Center.

Best, E. P. H., H. L. Fredrickson, V. A. McFarland, R. P. Jones, C. H. Lutz, G. A. Kiker, A. J. Bednar, R. A. Price, G. R. Lotufo, G. A. Ray, H. Hintelmann, and R. N. Millward. 2005. *Pre-construction biogeochemical analysis of mercury in wetlands bordering the Hamilton Army Airfield (HAAF) wetlands restoration site*. ERDC/EL Technical Report TR-05-15. Vicksburg, MS: U.S. Army Engineer Research and Development Center.

Bjerregaard, P., and M. H. Depledge. 1994. Cadmium accumulation in *Littorina littorea*, *Mytilus edulis* and *Carcinus maenas*: The influence of salinity and calcium ion concentrations. *Marine Biol*ogy 119:385-395.

Black, L. F. 1980. The biodepositional cycle of a surface deposit-feeding bivalve, *Macoma balthica* (L.). In *Estuarine Perspectives*, ed. V. S. Kennedy, 389-402. New York: Academic Press.

Bloom, N. S, G. A. Gill, S. Cappellino, C. Dobbs, L. McShea, C. Driscoll, R. Mason, and J. Rudd. 1999. Speciation and cycling of mercury in Lavaca Bay, Texas, sediments. *Environmental Science and Technology* 33: 7–13.

Boisson, F., M. G. J. Hartl, S. W. Fowler, and C. Amiard-Triquet. 1998. Influence of chronic exposure to silver and mercury in the field on the bioaccumulation potential of the bivalve *Macoma balthica*. *Marine Environmental Research* 45: 325–340.

Cabana, G., and J. B. Rasmussen. 1994. Modelling food chain structure and contaminant bioaccumulation using stable nitrogen isotopes. *Nature* 372: 255-257.

Campbell, P. G. C. 1995. Interaction between trace metals and organisms: A critique of the free ion model. In *Metal Speciation and aquatic systems*, ed. A. Tessier and D. R. Turner, 45-102. New York: John Wiley & Sons Ltd.

Canario, J., and C. Vale. 2004. Rapid release of mercury from intertidal sediments exposed to solar radiation: A field experiment. *Environmental Science and Technology* 38: 3901-3907.

Carlton, J. T. 1979. *History, biogeography, and ecology of the introduced marine and estuarine invertebrates of the Pacific coast of North America*. PhD diss., University of California, Davis.

Carlton, J. T., J. K. Thompson, L. E. Schemel, and F. H. Nichols. 1990. Remarkable invasion of San Francisco Bay (California, USA) by the Asian clam *Potamocorbula amurensis*. I. Introduction and dispersal. *Marine Ecology Progress Series* 66: 81-94.

Cifuentes, L. A., J. H. Sharp, and M. L. Fogel. 1988. Stable carbon and nitrogen bio-chemistry in the Delaware estuary. *Limnology and Oceanography* 33:1102-1115.

Cloern, J. E. 1987. Turbidity as a control on phytoplankton biomass and productivity in estuaries. *Continental Shelf Research* 7: 1367-1381.

Cloern, J. E., E. A. Canuel, and D. Harris. 2002. Stable carbon and nitrogen isotope composition of aquatic and terrestrial plants of the San Francisco Bay estuarine system. *Limnology and Oceanography* 47: 713-729.

Cohen, A. N., and J. T. Carlton. 1995. *Biological study. Nonindigenous aquatic species in a United States estuary: A case study of the biological invasions of the San Francisco Bay and Delta*. A Report for the U.S. Fish and Wildlife Service, Washington D.C., and the National Sea Grant College Program, Connecticut Sea Grant. NOAA Grant No NA36RG0467.

Cohen, A. N., J. T. Carlton, and M. C. Fountain. 1995. Introduction, dispersal, and potential impacts of the green crab *Carcinus maenas* in San Francisco Bay, California. *Marine Biology* 122: 225-237.

Cole, B. E., and J. E. Cloern. 1987. An empirical model for estimating phytoplankton productivity in estuaries. *Marine Ecology Progress Series* 36: 299-305.

Compeau, G. C., and R. Bartha. 1985. Sulfate-reducing bacteria: Principal methylators of mercury in anoxic estuarine sediment. *Applied and Environmental Microbiology* 50: 498-502.

Davison, W., and H. Zhang. 1994. In situ speciation measurements of trace components in natural waters using thin film gels. *Nature* 367: 546-548.

Delta Tributaries Mercury Council (DTMC) and Sacramento River Watershed Program (SRWP). 2002. *Final strategic plan for the reduction of mercury-related risk in the Sacramento River Watershed: Appendices 1 and 4*. (http://www.sacriver.org/subcommittees/dtmc/documents.html)

Devlin, E. W., J. D. Brammer, and R. L. Puyear. 1982. Acute toxicity of toluene to three age groups of fathead minnows (*Pimephales promelas*). *Bulletin of Environmental Contamination and Toxicology* 29: 7–12.

Divis, P., M. Leermakers, H. Docekalova, and Y. Gao. 2005. Mercury depth profiles in river and marine sediments measured by the diffusive gradients in thin films technique with two different specific resins. *Analytical and Bioanalytical Chemistry* 382: 1715-1719.

Drevnick, P. E., and M. B. Sandheinrich. 2003. Effects of dietary methylmercury on reproductive endocrinology of fathead minnows. *Environmental Science and Technol*ogy 37: 4390-4396.

Drott, A., L. Lambertsson, E. Bjorn, and U. Skyllberg. 2007. Importance of dissolved neutral Hg-sulfides for methyl mercury production in contaminated sediments. *Environmental Science and Technology* 41: 2270-2276.

Drott, A., L. Lambertsson, E. Bjorn, and U. Skyllberg. 2008. Do potential methylation rates reflect accumulated methyl mercury in contaminated sediments? *Environmental Science and Technology* 42: 153-158.

Evens, J., G. W. Page, S. A. Laimon, and R. W. Stallcup. 1991. Distribution and relative abundance and status of the California black rail in Western North America. *Condor* 93: 952-966.

Fisler, G. F. 1965. Effects of salt water on food and water consumption and weight of harvest mice. *Ecology* 44: 604-608.

Fry, B. 1988. Food web structure on Georges Bank from stable C, N, and S isotopic compositions. *Limnology and Oceanography* 33: 1182-1190.

Fry, B. 1991. Stable isotope diagrams of freshwater food webs. *Ecology* 72: 2292-2297.

Gill, R. G. 1979. Status and distribution of the California clapper rail (*Rallus longirostris obsoletus). California Fish and Game* 65: 36-49.

Gilmour, C. C., G. S. Riedel, M. C. Elderington, J. T. Bell, J. M. Benoit, G. A. Gill, and M. C. Stordal. 1998. Methylmercury concentrations and production rates across a trophic gradient in northern Everglades. *Biogeochemistry* 40: 327-345.

Goals Project. 1999. *Baylands Ecosystem Habitat Goals. A report of habitat recommendations prepared by the San Francisco Bay Area Wetlands Ecosystem Goals Project.* First Reprint. U.S. Environmental Protection Agency, San Francisco, CA, San Francisco Bay Regional Water Quality Control Board, Oakland, CA.

Greenberg, R. 1990. Feeding neophobia and ecological plasticity: A test of the hypothesis with captive sparrows. *Animal Behaviour* 39: 375-379.

Grenier, J. L., J. N. Collins, J. A. Davis, and B. K. Greenfield. 2002. *Preliminary Report: The tidal marsh food web.* Report to the San Francisco Bay Fund for the grant: Food pathways of bird contamination in Bay Area tidal marshes.

Gribsholt, B., and E. Kristensen. 2003. Benthic metabolism and sulfur cycling along an inundation gradient in a tidal *Spartina anglica* salt marsh. *Limnology and Oceanography* 48: 2151-2162.

Grippo, M. A., and A. G. Heath 2003. The effect of mercury on the feeding behavior of fathead minnows (*Pimephales promelas*). *Ecotoxicology and Environmental Safety* 55: 187–98.

Hall, B. D., R. A. Bodaly, R. J Fudge, J. W. Rudd, and D. M. Rosenberg. 1997. Food as the dominant pathway of methylmercury uptake by fish. *Water, Air, Soil Pollution* 100: 13-24.

Hammerschmidt, C. R., M. B. Sandheinrich, J. G. Wiener, and R. G. Rada. 2002. Effects of dietary methylmercury on reproduction of fathead minnows. *Environmental Science and Technology* 36: 877–83.

Hammerschmidt, C. R., W. F. Fitzgerald, C. H. Lamborg, P. H. Balcom, and P. T. Visscher. 2004. Biogeochemistry of methylmercury in sediments of Long Island Sound. *Marine Chemistry* 90: 31-52.

Harper, M., W. Davison, H. Zhang, and W. Tych. 1998. Solid phase to solution kinetics in sediments and soils interpreted from DGT measured fluxes. *Geochimica Cosmochimica Acta* 62: 2757-2770.

Hieb, K. A. 2000. Arrow goby. Clevelandia ios. In: *Goals project. Baylands Ecosystem Species and Community Profiles. Life histories and environmental requirements of key plants, fish and wildlife,* ed. P. R. Olofson, 136-138. Oakland, CA: San Francisco Bay Area Wetlands Ecosystem Goals Project, San Francisco Bay Regional Water Quality Control Board.

Hieb, K. A. 2006. Common shrimp of the San Francisco Estuary: 2004 Status and Trends Report. *IEP (Interagency Ecological Program for the San Francisco Estuary) Newsletter* 19 (3), Summer/Fall 2006: 7.

Hillier, F. S., and G. J. Lieberman. 1990. *Introduction to linear programming*. *Introduction to Operations Research,* 5th ed, 29-57. New York: McGraw-Hill.

Hines, M. E., S. L. Knollmeye, and J. B. Tugel. 1989. Sulfate reduction and other sedimentary biogeochemistry in a northern New England salt marsh. *Limnology and Oceanography* 34: 578-590.

Hintelmann, H., P. M. Welbourn, and R. D. Evans. 1997. Measurement of complexation of methylmercury(II) compounds by freshwater humic substances using equilibrium dialysis. *Environmental Science and Technol*ogy 31: 489-95.

Hintelmann, H. and N. Ogrinc. 2003. Determination of stable mercury isotopes by ICP/MS and their application in environmental studies. In *Biogeochemistry of environmentally important trace elements,* ed. Y. Cai and C. O. Braids, 321-338. Washington, D.C.: ACS Symposium Series 835.

Hintelmann, H., and H. T. Nguyen. 2005. Extraction of methylmercury from tissue and plant samples using acid leaching. *Analytical and Bioanalytical Chemistry* 381: 360-365.

Hintelmann, H., and R. D. Evans. 1997. Application of stable isotopes in environmental tracer studies – Measurements of monomethylmercury (CH_3Hg^+) by isotope dilution ICP-MS and detection of species transformation. *Fresenius Journal of Analytical Chemistry* 358: 378-385.

Hintelmann, H., K. Keppel-Jones, and R. D. Evans. 2000. Constants of mercury methylation and demethylation rates in sediments and comparison of tracer and ambient mercury availability. *Environmental Toxicology and Chem*istry 19: 2204-2211.

Hopkins, D. R., and V. T. Parker. 1984. A study of the seed bank of a salt marsh in northern San Francisco Bay. *American Journal of Botany* 71: 348-355.

Hudson, R. J. M., S. A. Gherini, C. J. Watras, and D. B. Porcella. 1994. Modeling the biogeochemical cycle of mercury in lakes: The mercury cycling model (MCM) and its application to the MTL Study Lakes. In *Mercury pollution: integration and synthesis*, ed. C. J. Watras, and J. W. Huckabee, 473-523. Lewis Publishers.

Jensen, G. C., P. S. McDonald, and D. A. Armstrong. 2007. Biotic resistance to green crab, *Carcinus maenas*, in California bays. *Marine Biology* 151: 2231-2243.

Jonsson, G., R. K. Bechmann, S. D. Bamber, and T. Baussant. 2004. Bioconcentration, biotransformation, and elimination of polycyclic aromatic hydrocarbons in sheepshead minnows (*Cyprinodon variegatus*) exposed to contaminated seawater. *Environmental Toxicology and Chemistry* 23: 1538-1548.

Kerin, E. J., C. C. Gilmour, E. Roden, M. T. Suzuki, and J. D. Coates, and R. P. Mason. 2006. Mercury methylation by dissimilatory iron-reducing bacteria. *Applied and Environmental Microbiology* 72: 7919-7921.

Kiker, G. A., N. A. Rivers-Moore, M. K. Kiker, and I. Linkov. 2006. QnD: A scenario-based gaming system for modeling environmental processes and management decisions. In *Environmental Security and Environmental Management: The Role of Risk Assessment*, ed. B. Morel, and I. Linkov, 151-185. The Netherlands: Springer Verlag.

Kimmerer, W. J., and J. J. Orsi. 1996. Changes in the zooplankton of the San Francisco Bay estuary since the introduction of the clam *Potamocorbula amurensis*. In *San Francisco Bay: The Ecosystem*, ed. J. T. Hollibaugh, 403-425. San Francisco, CA: American Association for the Advancement of Science.

Klerks, P. L., and C. J. Moreau. 2001. Heritability of resistance to individual contaminants and to contaminant mixtures in the sheepshead minnow (*Cyprinodon vairegatus*). *Environmental Toxicology and Chemistry* 20: 1746-1751.

Kline, K. F. 2000. Starry flounder. Platichthys stellatus. In *Goals project. Baylands Ecosystem Species and Community Profiles. Life histories and environmental requirements of key plants, fish and wildlife*, ed. P. R. Olofson, 148-150. Oakland, CA: San Francisco Bay Area Wetlands Ecosystem Goals Project, San Francisco Bay Regional Water Quality Control Board.

Kljakovic-Gaspic, Z., N. Odzak, I. Ujevic, T. Zvonaric, M. Horvat, and A. Baric. 2006. Biomonitoring of mercury in polluted coastal area using transplanted mussels. *The Science of Total Environment* 368: 199-209.

Kozloff, E., and L. H. Price. 1996. *Marine invertebrates of the Pacific Northwest*. Field Guide. Longitude.

Kwak, T. J., and J. B. Zedler. 1997. Food web analysis of southern California coastal wetlands using multiple stable isotopes. *Oecologia* 110:262-277.

Leaner, J. J., and R. P. Mason. 2001. The effect of thiolate organic compounds on methylmercury accumulation and redistribution in sheepshead minnows, *Cyprinodon variegatus*. *Environmental Toxicology and Chemistry* 20: 1557-63.

Leaner, J. J., and R. P. Mason. 2004. Methylmercury uptake and distribution kinetics in sheepshead minnows, *C. variegatus*, after exposure to CH3Hg-spiked food. *Environmental Toxicology and Chemistry* 23: 2138-2146

Lee, B. G., W. G. Wallace, and S. N. Luoma. 1998. Uptake and loss kinetics of Cd, Cr, and Zn in the bivalves *Potamocorbula amurensis* and *Macoma balthica*: Effects of size and salinity. *Marine Ecology Progress Series* 175: 177-189.

Lidicker, W. Z. Jr. 2000. California vole. Microtus californicus. In *Goals project. Baylands Ecosystem Species and Community Profiles. Life histories and environmental requirements of key plants, fish and wildlife*, ed. P. R. Olofson, 229-231. Oakland, CA: San Francisco Bay Area Wetlands Ecosystem Goals Project, San Francisco Bay Regional Water Quality Control Board.

Lindberg, S. E., W. Dong, and T. Meyers. 2002. Transpiration of gaseous elemental mercury through vegetation in a subtropical wetland in Florida. *Atmospheric Environment* 36: 5207-5219.

Lopez, G. R., J. S. Levinton, and L. B. Slobodkin. 1977. The effect of grazing by the detritivore Orchestia grillus on Spartina litter and its associated microbial community. *Oecologia* 30: 111-127.

Lubetkin, S. C. 1997. *Multi-source mixing models: Food web determination using stable isotopic tracers*. MS thesis, University of Washington, Seattle, WA.

Lubetkin, S. C., and C. A. Simenstad. 2004. Multi-source mixing models to quantify food web sources and pathways. *Journal of Applied Ecology* 41: 996-1008.

Lytle, T. F., C. S. Manning, W. W. Walker, J. S. Lytle, and D. S. Page. 2003. Life-cycle toxicity of dibutyltin to the sheepshead minnow (*Cyprinodon variegatus*) and implications of the ubiquitous tributyltin impurity in test material. *Applied Organometallics Chemistry* 17: 653-661.

Macko, S. A., W. Y. Lee, and P. L. Parker. 1982. Nitrogen and carbon isotope fractionation by two species of marine amphipods: Laboratory and field studies. *Journal of Experimental and Marine Biology and Ecology* 63: 145-149.

Maffei, W. A. 2000a. A note on the invertebrate populations of the San Francisco Estuary. In *Goals project. Baylands Ecosystem Species and Community Profiles. Life histories and environmental requirements of key plants, fish and wildlife,* ed. P. R. Olofson, 184-192. Oakland, CA: San Francisco Bay Area Wetlands Ecosystem Goals Project, San Francisco Bay Regional Water Quality Control Board.

Maffei, W. A. 2000b. Tiger beetles. *Cicindela senilis senilis, C. oregona,* and *C. hemorrhagica*. In *Goals project. Baylands Ecosystem Species and Community Profiles. Life histories and environmental requirements of key plants, fish and wildlife*, ed. P. R. Olofson, 156-161. Oakland, CA: San Francisco Bay Area Wetlands Ecosystem Goals Project, San Francisco Bay Regional Water Quality Control Board.

Maginnis, T. L. 2006. The costs of autonomy and regeneration in animals: A review and framework for future research. Review. *Behavioral Ecology* 17: 857-872.

Manning, C. S., T. F. Lytle, W. W. Walker, and J. S. Lytle. 1999. Life-cycle toxicity of bis(tributyltin) oxide to the sheepshead minnow (*Cyprinodon variegatus*). *Archives Environmental Contamination and Toxicology* 37: 258-266.

Mason, R., N. Bloom, S. Cappellino, G. Gill, J. Benoit, and C. Dobbs. 1998. Investigation of porewater sampling methods for mercury and methylmercury. *Environmental Science and Technol*ogy 32: 4031-4040.

Mason, R., W. Fitzgerald, and F. Morel. 1994. The biogeochemical cycling of elemental mercury: Anthropogenic influences. *Geochimica Cosmochimica Acta* 58:3191-3198.

McCutchan, J. H., W. M. Lewis, Jr., C. Kendall, and C. C. McGrath. 2003. Variable in trophic shift for stable isotope ratios of carbon, nitrogen, and sulfur. *Oikos* 102: 378-390.

McFarland, V. A., and C. R. Lee. 2002. *Dredging-related mercury issues in the San Francisco Bay-Delta region*. White Paper prepared for the USACE District, San Francisco. Vicksburg, MS: U.S. Army Engineer Research and Development Center.

McFarland, V. A., C. Lutz, J. U. Clarke, and D. K. MacMillan. 2003. *Mercury concentrations bordering the Hamilton Army Air Field Remediation Site: February, 2003: Wet Season - Dry Season Contrast*. Report to USACE District, San Francisco. Vicksburg, MS: U.S. Army Engineer Research and Development Center.

Merritt, K. A. 2007. Mercury dynamics in sulfide-rich sediments: Geochemical influence on contaminant mobilization and methylation within the Penobscot River estuary, Maine, USA. PhD diss., University of Maine, Orono.

Merritt, K. A., and A. Amirbahman. 2007. Mercury dynamics in sulfide-rich sediments: Geochemical influence on contaminant mobilization within the Penobscot River estuary, Maine, USA. *Geochimica Cosmochimica Acta* 71: 929-941.

Meyer, J. J. 2003. Sublethal fish predation on one native and two non-native bivalves. *Proceedings of the Third International Conference on Marine Bioinvasions, La Jolla, California, March 16-19, 2003*: 90.

Michener, R. H, and D. M. Schell. 1994. Stable isotope ratios as tracers in marine aquatic food webs. In *Stable isotopes in ecology and environmental science*, eds. K. Lajtha, and R. H. Michener, 138-157. Oxford, Great Britain: Blackwell Scientific Publishers.

Morris, J. T., and B. Haskin. 1990. A 5-y record of aerial primary production and stand characteristics of *Spartina alterniflora*. *Ecology* 71: 2209-2217.

Mouneyrac, C., A. Geffard, J. C. Amiard, and C. Amiard-Triquet. 2000. Metallothionein-like proteins in *Macoma balthica*: Effects of metal exposure and natural factors. *Canadian Journal of Fisheries and Aquatic Sciences* 57: 34–42.

National Introduced Marine Pest Information System (NIMPIS). 2002. *Potamocorbula amurensis* species summary. National Introduced Marine Pest Information System, ed. C. L. Hewitt, R. B. Martin, C. Sliwa, F. R. McEnnulty, N. E. Murphy, T. Jones, and S. Cooper. http://crimp.marine.csiro.au/nimpis, accessed 10 July 2009.

National Oceanic and Atmospheric Administration (NOAA). 2006. Website http://www.sailingsource.com/weather/tides.html. Accessed 26 July 2006.

Nichols, F. H. H., J. K. Thompson, and L. E. Schemel. 1990. Remarkable invasion of San Francisco Bay (California, USA) by the Asian clam *Potamocorbula amurensis*. 2. Displacement of a former community. *Marine Ecology Progress Series* 66: 95-101.

Odzak, N., T. Zvonaric, Z. Kljakovic Gaspic, M. Horvat, and A. Baric. 2000. Biomonitoring of mercury in the Kastela Bay using transplanted mussels. *The Science of Total Environment* 261: 61-68.

Olafsson, E. B. 1986. Density dependence in suspension-feeding and deposit-feeding populations of the bivalve *Macoma balthica*: A field experiment. *Journal of Animal Ecology* 55: 517-526.

Olive, P. J. W., J. K. Pinnegar, N. V. C. Polunin, G. Richards, and R. Welch. 2003. Isotopic trophic-step fractionation: A dynamic equilibrium model. *Journal of Animal Ecology* 72: 608-617.

Olivier, M., G. Desrosiers, A. Caron, C. Retiere, and A. Caillou.1996. Juvenile growth of *Nereis diversicolor* (O. G. Muller) feeding on a range of marine vascular and macroalgal plant sources under experimental conditions. *Journal of Experimental Marine Biology and Ecology* 208: 1-12.

Onuf, C. P. 1987. *The ecology of Mugu Lagoon, California: An estuarine profile*. U.S. Fish and Wildlife Service Biological Report 85.

Peterson, B. J., and B. Fry. 1987. Stable isotopes in ecosystem studies. *Annual Review of Ecology and Systematics* 18: 293-320.

Peterson, B. J., R. W. Howarth, and R. H. Garritt. 1986. Sulfur and carbon isotopes as tracers of salt-marsh organic matter flow. *Ecology* 67: 865-874.

Peterson, B., and R. W. Howarth. 1987. Sulfur, carbon and nitrogen isotopes used to trace organic matter flow in the salt-marsh estuaries of Sapelo Island, Georgia. *Limnology and Oceanography* 32: 1195-1213.

Peterson, H.1997. Clam stuffed sturgeon. *IEP (Interagency Ecological Program) for the San Francisco Estuary Newsletter* 9: 19.

Post, D. M. 2002. Using stable isotopes to estimate trophic position: Models, methods and assumptions. *Ecology* 83: 703-718.

Post, J. R., and R. Vandenbos, and D.J. McQueen. 1996. Uptake rates of food-chain and waterborne mercury by fish: Field measurements, a mechanistic model, and an assessment of uncertainties. *Canadian Journal of Fisheries and Aquatic Sciences* 53: 395-407.

Poulton, V. K., J. R. Lovvorn, and J. Y. Takekawa. 2002. Clam density and scaup feeding behavior in San Pablo Bay, California. *The Condor* 104: 518-527.

Richman, S. E., and J. R. Lovvorn. 2004. Relative foraging value to lesser scaup ducks of native and exotic clams from San Francisco Bay. *Ecological Applications* 14: 1217-1231.

Riisgard, H. U., T. Kiorboe, F. Mohlenberg, I. Drabaek, and P. P. Madsen. 1985. Accumulation, elimination and chemical speciation of mercury in the bivalves *Mytilus edulis* and *Macoma balthica*. *Marine Biology* 86: 55-62.

Regional Monitoring Program (RMP). 2006. RMP Status and Trends Monitoring Data. http://www.sfei.org/RMP/report: Sediment mercury values San Pablo Bay.

Roe, P. 1975. Aspects of the life history and of territorial behavior in young individuals of *Platynereis bicanaliculta* and *Nereis vexillosa* (Annelida, Polychaeta). *Pacific Science* 29: 341-348.

Rogers, D. W. 1994. You are what you eat and a little bit more: Bioenergetics-based models of methylmercury accumulation in fish revisited. In *Mercury Pollution: Integration and Synthesis*, ed. C. J. Watras, and J. W. Huckabee, 473-523. Lewis Publishers.

Rosing, M. M., M. Ben-David, and R. R. Perry. 1998. Analysis of stable isotope data: a K nearest neighbors randomization test. *Journal of Wildlife Management* 62: 380-388.

Sackett, W. M. 1989. Stable isotope studies on organic matter in the marine environment. In *Handbook of Environmental Isotope Geochemistry*, ed. P. Fritz and J. C. Fontes, 139-170. The Netherlands: Elsevier, Amsterdam.

Shellhammer, H. 1998. A marsh is a marsh is a marsh...but not always to a salt marsh harvest mouse. *Tideline* 18(4): 1-3.

Shellhammer, H. S. 2000. Salt marsh harvest mouse. *Reithrodontomys raviventris*. In *Goals Project. Baylands Ecosystem Species and Community Profiles: Life histories and environmental requirements of key plants, fish and wildlife*, ed. P. R. Olofson, 219-228. Oakland, CA: San Francisco Bay Area Wetlands Ecosystem Goals Project, San Francisco Bay Regional Water Quality Control Board.

Simstead, C. A., B. Miller, C. F. Nyblarde, K. Thronburgh, and L. J. Lewis. 1979. *Food web relationships of northern Puget Sound and the Strait of Juan de Fuca. A synthesis of the available knowledge*. Report EPA-600/7-79-259.

Sitts, R. M., and A. W. Knight. 1979. Predation by the estuarine shrimps *Crangon franciscorum* Stimpson and *Palaemon macrodactylus* Rathbun. *Biological Bulletin* 156: 356-368.

Skyllberg, U. 2008. Competition among thiols and inorganic sulfides and polysulfides for Hg and MeHg in wetland soils and sediments under suboxic conditions: Illumination of controversies and implications for MeHg net production. *Journal of Geophysical Research* 113: G00C03.

Smith, J. N. M., P. Arcese, and I. G. McLean. 1984. Age, experience, and enemy recognition by wild song sparrows. *Behavioral Ecology and Sociobiology* 14: 101-106.

Stordal, M. C., G. A. Gill, L. S. Wen, and P. H. Santschi. 1996. Mercury phase speciation in the surface waters of three Texas estuaries: Importance of colloidal forms. *Limnology and Oceanography* 41: 52-61.

Svensson, O., and C. Karnemo. 2007. Parasitic spawning in sand gobies: An experimental assessment of nest-opening size, sneaker male cues, paternity, and filial cannibalism. *Behavioral Ecology* 18: 410-419.

Svensson, O., C. Magnhagen, E. Forsgren, and C. Karnemo. 1998. Parental behaviour in relation to the occurrence of sneaking in the common goby. *Animal Behaviour* 56: 175-179.

Takekawa, J. Y., M. A. Bias, I. Woo, S. A. Demers, and G. T. Downard. 2002. *Restoration research and monitoring in Bayland wetlands of the San Francisco Bay Estuary: The Tolay Creek Project*. U.S. Geological Survey, Unpublished Progress Report. Vallejo, CA.

Tasto, R. N. 2000. Pacific staghorn sculpin. *Leptocottus armatus armatus*. In *Goals project. Baylands Ecosystem Species and Community Profiles. Life histories and environmental requirements of key plants, fish and wildlife*, ed. P. R. Olofson, 123-126. Oakland, CA: San Francisco Bay Area Wetlands Ecosystem Goals Project, San Francisco Bay Regional Water Quality Control Board.

Trulio, L. A., and J. G. Evens. 2000. California black rail. Laterallus *jamaicensis coturniculus*. In *Goals project. Baylands Ecosystem Species and Community Profiles. Life histories and environmental requirements of key plants, fish and wildlife*. ed. P. R. Olofson, 341-345. Oakland, CA: San Francisco Bay Area Wetlands Ecosystem Goals Project, San Francisco Bay Regional Water Quality Control Board.

Tsui, M. T. K., and W. Wang. 2004. Uptake and elimination routes of inorganic mercury and methylmercury in *Daphnia magna*. *Environmental Science and Technol*ogy 38: 808-816.

Turner, A., G. E. Millward, and S. M. Roux. 2001. Sediment-water partitioning of inorganic mercury in estuaries. *Environmental Science and Technology* 35: 4648-4654.

U.S. Environmental Protection Agency (USEPA). 2007. *Framework for metals risk assessment*. EPA 120/R-07/001. Washington, DC: U.S. Environmental Protection Agency Office of the Science Advisor. Risk Assessment Forum.

U.S. Fish and Wildlife Service. 2003. *Evaluation of the Clean Water Act Section 304(a) human health criterion for methylmercury: Protectiveness for threatened and endangered wildlife in California*. Sacramento, CA: U.S. Fish and Wildlife Service, Sacramento Fish and Wildlife Office, Environmental Contaminants Division.

U.S. Geological Survey (USGS) 2002.
http://sfbay.wr.usgs.gov/access/IntegratedScience/IntSci.html

U. S. Geological Survey (USGS). 2006. http://seamless.usgs.gov/. NED shaded relief (resolution = 1 arc second or approximately 30 m). Elevation data pertaining to 1999. Accessed 18 September 2006.

Ulrich, S. M., T. W. Tanton, and S. A. Abdrahitova. 2001. Mercury in the aquatic environment: a review of factors affecting methylation. *Critical Reviews in Environmental Science and Technology* 31: 241B293.

Valiela, I, D. Rutecki, and S. Fox. 2004. Salt marshes: Biological controls in food webs in a diminishing environment. *Journal of Experimental Marine Biology and Ecology* 300: 131-159.

Vitaliano, J. J, and A. J. Bejda. 2001. Age, growth, and allometric relationships of ribbed mussels (*Geuken demissa*). *NOAA Technical Memo 167*.
(http://nefsc.noaa.gov/nefsc/publications/tm/tm167/tm167p5.htm)

Washington Department of Fish and Wildlife (WDFW). 2009. Invasive species fact sheet. *Carcinus maenas* (European green crab). http://wdfw.wa.gov/fish/ans/identify/html/index.php?species=carcinus_maenas#feeding. Accessed 10 July 2009.

Wiener, J. G., C. G. Gilmour, and D. P. Krabbenhoft. 2003. *Mercury strategy for the Bay-Delta ecosystem: A unifying framework for science, adaptive management, and ecological restoration*. Final Report to the California Bay Delta Authority for Contract 4600001642 between the Association of Bay Area Governments and the University of Wisconsin- La Crosse, December 31, 2003.

Williams, J. 2004. Impact of green crab (*Carcinus maenas* L.) predation on a population of soft-shell clams (*Mya arenaria* L.) in the Southern Gulf of St. Lawrence. *Journal of Shellfish Research 1CNOV*, August 1.

Wright, D. A. 1995. Trace metal and major ion interactions in aquatic animals. *Marine Pollution Bulletin* 31: 8-18.

Zhang, H., and W. Davison. 1995. Performance characteristics of diffusion gradients in thin films for the in situ measurement of trace metals in aqueous solution. *Analytical Chemistry* 67: 3391-3400.

Zhang, H., W. Davison, B. Knight, and S. McGrath. 1998. In situ measurements of solution concentrations and fluxes of trace metals in soils using DGT. *Environmental Science and Technol*ogy 32: 704 -710.

Zhang, H., W. Davison, S. Miller, and W. Tych. 1995. In situ high resolution measurements of fluxes of Ni, Cu, Fe, and Mn and concentrations of Zn and Cd in porewaters by DGT. *Geochimica Cosmochimica Acta* 59: 4181-4192.

REPORT DOCUMENTATION PAGE

Form Approved
OMB No. 0704-0188

1. REPORT DATE *(DD-MM-YYYY)*	2. REPORT TYPE	3. DATES COVERED *(From - To)*
December 2009	Final report	

4. TITLE AND SUBTITLE

Preconstruction Biogeochemical Analysis of Mercury in Wetlands Bordering the Hamilton Army Airfield (HAAF) Wetlands Restoration Site; Part 3

5a. CONTRACT NUMBER

5b. GRANT NUMBER

5c. PROGRAM ELEMENT NUMBER

6. AUTHOR(S)

E. P. H. Best, H. L. Fredrickson, H. Hintelmann, O. Clarisse, B. Dimock, G. R. Lotufo, W. A. Boyd, and G. A. Kiker

5d. PROJECT NUMBER

5e. TASK NUMBER

5f. WORK UNIT NUMBER

7. PERFORMING ORGANIZATION NAME(S) AND ADDRESS(ES)

U.S. Army Engineer Research and Development Center, Environmental Laboratory
3909 Halls Ferry Road, Vicksburg, MS 39180-6199;
Trent University, 1600 West Bank Drive, Peterborough, ON K9J 7B8, Canada;
U.S. Environmental Protection Agency, National Risk Management Research Laboratory,
26 West Martin Luther King Blvd., Cincinnati, OH 45268;
University of Florida, Agricultural and Biological Engineering Department
PO Box 110570, Gainesville, FL 32611

8. PERFORMING ORGANIZATION REPORT NUMBER

ERDC/EL TR-09-21

9. SPONSORING / MONITORING AGENCY NAME(S) AND ADDRESS(ES)

U.S. Army Corps of Engineers
Washington, DC 20314-1000;
U.S. Army Engineer Research and Development Center
3909 Halls Ferry Road, Vicksburg, MS 39180-6199

10. SPONSOR/MONITOR'S ACRONYM(S)

11. SPONSOR/MONITOR'S REPORT NUMBER(S)

12. DISTRIBUTION / AVAILABILITY STATEMENT

Approved for public release; distribution is unlimited.

13. SUPPLEMENTARY NOTES

14. ABSTRACT

The U.S. Army Corps of Engineers (USACE) is working to reconstruct wetlands at the former Hamilton Army Airfield (HAAF) on San Pablo Bay (SPB). This 203-ha site will provide tidal habitat to endangered species such as the clapper rail and the saltmarsh harvest mouse. Means to mitigate MeHg magnification in bay aquatic food webs are needed not only for HAAF but for other Bay restoration sites as well. This interim technical report describes studies primarily performed in 2006.

A field study was conducted in San Pablo Bay focusing on site-specific rates of mercury methylation and demethylation, and biogeochemical parameters related to the mercury cycle as measured by both conventional and emerging methods, including Diffusive Gradient in Thin Film (DGT) and Diffusional Equilibration in Thin Film (DET) techniques. Experiments on MeHg accumulation by clams, fish, and DGTs were conducted under laboratory conditions to test the ability of the DGT technique to mimic MeHg bioaccumulation.

(Continued)

15. SUBJECT TERMS

Coastal wetlands restoration	Management	Monitoring
Food Chain	Mass balance	Stable isotopes
	Mercury model	Sediment

16. SECURITY CLASSIFICATION OF:			17. LIMITATION OF ABSTRACT	18. NUMBER OF PAGES	19a. NAME OF RESPONSIBLE PERSON
a. REPORT	b. ABSTRACT	c. THIS PAGE			19b. TELEPHONE NUMBER *(include area code)*
UNCLASSIFIED	UNCLASSIFIED	UNCLASSIFIED		145	

14. ABSTRACT (concluded)

The multiple source mixing models SOURCE and STEP were used to quantify food web sources and trophic structure using multiple stable isotopes, and, thus, contribute to elucidating the trophic relationships leading to MeHg bioaccumulation. Use of these models showed that macrophytic primary producers of the salt marsh formed important food sources of consumers. Consumers in the nearshore bay were found to be largely benthivorous and fed partly on higher plant fragments and/or bay-POM, of which the relative contributions decreased with increasing trophic level.

The Questions and Decisions ™ (QnD) screening model system was developed as a framework to evaluate consequences of wetland restoration for MeHg emissions at the former Hamilton Army Air Field (HAAF).

A data gap exists on food chain structure, components, bioaugmentation mechanisms and MeHg accumulated in the biota associated with San Francisco Bay wetlands. Additional field, experimental, and modeling research was recommended to decrease the uncertainty of these early model outcomes.